_____

Organic solid-solid wetting in water:
Probing nonenzymatic formation of RNA, influencing molecular self-assembly and doping of graphene

_____

_____

Organic solid-solid wetting in water:
Probing nonenzymatic formation of RNA, influencing molecular self-assembly and doping of graphene

_____

L'acqua è la forza trainante della natura

Water is the driving force of nature

Leonardo da Vinci

Contents

List of Abbreviations

ADP	adenosine-diphosphate
AMP	adenosine-monophosphate
AMP acid	adenosine-monophosphoric acid
cAMP	cyclic adenosine-monophosphate
ATP	adenosine-triphosphate
CMP	cytidine-monophosphate
CV	cyclic voltammetry
dmQAC	dimethyl-quinacridone
DNA	deoxyribonucleic acid
FAD	flavin adenine dinucleotide
FVT	flavanthrone
GMP	guanosine-monophosphate
HOPG	highly oriented pyrolytic graphite
MEP	molecular electrostatic potential
miRNA	microRNA, micro nucleic acid
NAD	nicotinamide adenine dinucleotide
Nd:YAG	neodym yttrium-aluminium-garnet
NMPs	nucleotide monophosphates
nt	nucleotide(s)
OSWDorganic	solid/solid wetting deposition
PHA	polycyclic heteroaromatics
Phth	Phthalocyanine
PMMA	Poly(methyl methacrylate)
QAC	quinacridone
RNA	ribonucleic acid
RT	room temperature
RT-qPCR	reverse transcription polymerase quantitative chain reaction
SAM	self-assembled monolayer
SEM	standard error of the mean

STM	scanning tunnelling microscopy
TS	tunnelling spectroscopy
UHV	ultra-high vacuum
UMP	uridine-monophosphate

Abstract

H_2O, known as water in its liquid phase, is one of the most studied molecules in many scientific disciplines, such as chemistry, physics and biology. For terrestrial ecosystems, the supply of water is harmless in the chemical sense. This harmlessness of water could also be a consequence of how life on earth originated, namely - according to many theories of origin - in water.

Its harmlessness and its low price are reasons why water, as a polar or protic solvent and suspending agent, is preferable to other substances, provided that several solvents are suitable for the respective process. For reasons of environmental protection and economics, it is also worthwhile to optimize work processes in such a way that the respective solvent can be replaced by water, even in processes in which non-polar solvents are necessary.

So, how can we use the properties of water for new technologies, such as semiconductor technology? And vice versa, how can we explain natural phenomena with the knowledge of technical approaches?

In this thesis, two scientific fields - semiconductor research and the explanation of an essential biochemical phenomenon - are linked by studying and applying the same physico-chemical process.

In this thesis, organic solid/solid wetting deposition (OSWD) is used as a physico-chemical process. With it, it will be demonstrated how the properties of water can be used for nanotechnology. Organic solid/solid wetting deposition (OSWD) is a method of forming a monomolecular layer (monolayer) of organic semiconductor molecules on crystal surfaces, such as graphite or graphene. Organic semiconductor molecules are widely used as industrial organic pigments and components for optical storage and organic electronics. By definition, these pigment molecules are not soluble in polar solvents such as water. This has been problematic when using current thin-film technology techniques, since molecular deposition and monolayer formation required non-polar solvents, which are more environmentally harmful than using water as the liquid medium. In order to circumvent this limitation, technically very complex approaches or expensive chemical modifications are required.

One aim of this study is to investigate whether OSWD can be used to establish a new method for doping graphene with water-insoluble organic semiconductors in aqueous environments. This would open new prospects for the environmentally friendly manufacturing of

semiconductor systems, which is of great importance as this kind of technology will be indispensable in the future, to support environmental protection.

In order to make this environmentally friendly technology operational, it is important to generate the necessary amount of monolayers on the graphene surface. This is necessary to achieve efficient doping of graphene. Therefore, this work investigates whether and how this OSWD can be optimized by adding selected biomolecules to the pigment-water suspension. As a result, the system is optimized using only environmentally friendly components. By screening 20 different candidates and mixtures thereof, mostly biomolecules, especially nucleotides, the addition of adenosine monophosphate (AMP) showed a significant increase in coverage, i.e. the percentage of the substrate surface covered by organic semiconductor monolayers. Therefore, in this work, the role of AMP in the OSWD system was further investigated to find possible reasons for the strong increase in the coverage of the organic molecule monolayers.

Finally, the OSWD process was used as a method to study the influence of nano-fluidic phenomena on nucleotides. The idea came up that a nano-fluid environment could also explain the enzyme-free condensation reaction (reaction with the elimination of a low-molecular substance such as H_2O) from nucleotides to RNA - as it must have taken place when the first RNA molecules were formed. This was inspired on the one hand by the strong influence of AMP on the suspended particles in the OSWD system and on the other hand by the significant role of AMP in biological processes that are crucial for the existence of life on this planet. RNA macromolecules can be formed in water without the need for enzymes by condensation reactions in a nano-fluid environment, which is per se an unresolved contradiction in current theories on the origin of life (water paradox). The OSWD system can be used as a reference method to test hypotheses about the reaction behaviour with regard to the condensation reaction of certain combinations of substances.

The new explanatory model shown in this work solves numerous contradictions that previous theories cannot yet clarify: The use of a nano-constrained environment as a prebiotic reaction vessel makes an important contribution to solving the water paradox in theories on the origin of life in water, although water inhibits the condensation reaction of nucleotides. The theoretical model of prebiotic reaction vessels does not need wet-dry cycles, spark discharges, or molecular species that probably did not even exist on Earth at that time. Instead, this study shows a simple, geochemically very common and therefore very probable situation in which macromolecules such as RNA can be formed. The situation shown is even compatible with the conservative nature of evolution - a principle that states that evolutionary developments in biology always

build on existing solutions. The model presented can plausibly explain how the first RNA molecules could have arisen without the presence of enzymes.

Zusammenfassung

H_2O, in seiner flüssigen Phase als Wasser bekannt, ist eines der am besten untersuchten Moleküle in vielen naturwissenschaftlichen Disziplinen, wie der Chemie, der Physik und der Biologie. Für irdische Ökosysteme ist die Zufuhr von Wasser, im chemischen Sinne, unschädlich. Diese Unschädlichkeit des Wassers könnte auch eine Folge dessen sein, wie das Leben auf der Erde entstanden ist, nämlich - laut vieler Entstehungstheorien - im Wasser.

Seine Unschädlichkeit und auch sein geringer Preis, sind Gründe, weswegen Wasser als polares bzw. protisches Lösungs- und Suspensionsmittel anderen Substanzen vorzuziehen ist, sofern mehrere Lösungsmittel für den jeweiligen Prozess geeignet sind. Wegen des Umweltschutzes und der Wirtschaftlichkeit ist es ebenso erstrebenswert, selbst bei den Prozessen, bei denen unpolare Lösungsmittel nötig sind, die Arbeitsabläufe so zu optimieren, dass das jeweilige Lösungsmittel durch Wasser ersetzt werden kann.

Wie können wir die Eigenschaften des Wassers für neue Technologien, wie z.B. Halbleitertechnologie nutzen? Und umgekehrt, wie können wir Naturphänomene mit den Erkenntnissen technischer Ansätze erklären?

In dieser Arbeit werden zwei wissenschaftliche Gebiete - die Halbleiterforschung und die Erklärung eines essenziellen biochemischen Phänomens - miteinander verbunden, indem der gleiche physikalisch-chemische Prozesses untersucht und angewandt wird.

Als physikalisch-chemisches Verfahren wird in dieser Arbeit die organische Festphasenbenetzung (engl. Organic Solid/Solid Wetting Deposition (OSWD)) verwendet. Damit wird gezeigt, wie die Eigenschaften des Wassers für die Nanotechnologie eingesetzt werden können. Die organische Festphasenbenetzung (OSWD) ist ein Verfahren zur Bildung einer monomolekularen Schicht (Monoschicht) organischer Halbleitermoleküle auf Kristalloberflächen, wie Graphit oder Graphen. Organische Halbleitermoleküle werden häufig als industrielle organische Pigmente und Komponenten für optische Speicher und organische Elektronik verwendet. In polaren Lösungsmitteln wie Wasser sind diese Pigment-Moleküle, laut Definition, nicht löslich. Dies war bisher bei der Anwendung gängiger Techniken der Dünnschichttechnologie problematisch, da molekulare Abscheidung und Monolagenbildung unpolare Lösungsmittel erforderten, welche für die Umwelt schädlicher sind als der Einsatz von Wasser als flüssiges Medium. Um diese Einschränkung zu umgehen, sind technisch sehr aufwendige Ansätze oder teure chemische Modifikationen erforderlich.

Ziel dieser Studie ist es unter anderem zu untersuchen, ob mit OSWD eine neue Methode zur Dotierung von Graphen mit wasser-unlöslichen organischen Halbleitern in wässrigen Umgebungen etabliert werden kann. Dies würde neue Perspektiven für die umweltfreundliche Herstellung von Halbleitersystemen eröffnen, was von großer Bedeutung ist, da diese Art von Technologie in Zukunft unverzichtbar sein wird, um dem Umweltschutz gerecht zu werden.

Um diese umweltschonende Technologie einsatzbereit zu machen, ist es wichtig, die nötige Menge von Monoschichten auf der Graphen-Oberfläche zu erzeugen. Nur dadurch kann eine effiziente Dotierung von Graphen erzielt werden. Daher wird in dieser Arbeit untersucht, ob und wie diese OSWD, durch Zugabe ausgewählter Biomoleküle zur Pigment-Wasser-Suspension, optimiert werden kann. Dadurch erfolgt die Optimierung des Systems nur unter Verwendung umweltfreundlicher Komponenten. Durch das Screening von 20 verschiedenen Kandidaten und Mischungen derselben, meist Biomoleküle, vor allem Nukleotide, zeigte die Zugabe von Adenosin-Monophosphat (AMP) eine signifikante Erhöhung der Bedeckung, d.h. des prozentualen Anteils der Substratoberfläche, der von organischen Halbleiter-Monoschichten bedeckt wurde. Daher wurde in dieser Arbeit die Rolle von AMP im OSWD-System weiter untersucht, um mögliche Gründe für die starke Erhöhung der Bedeckung der organischen Molekülmonoschichten zu finden.

Schließlich wurde der OSWD-Prozess als Methode verwendet, um den Einfluss nano-fluider Phänomene auf Nukleotide, zu untersuchen. Die Idee, kam auf, dass eine nano-fluide Umgebung auch die enzymfreie Kondensationsreaktion (Reaktion unter Abspaltung eines niedermolekularen Stoffes wie z.B. H_2O) von Nukleotiden zu RNA - wie sie bei der Entstehung der ersten RNA-Moleküle stattgefunden haben muss - erklären könnte. Dazu inspiriert hat zum einen der starke Einfluss von AMP auf die suspendierten Partikel im OSWD-System und zum anderen die signifikante Rolle von AMP in biologischen Prozessen, die für die Existenz des Lebens auf diesem Planeten entscheidend sind. Durch Kondensationsreaktionen in nano-fluider Umgebung können RNA-Makromoleküle ohne die Notwendigkeit von Enzymen in Wasser gebildet werden, was bisher per se ein ungeklärter Widerspruch in den gängigen Theorien zum Ursprung des Lebens ist (Wasser-Paradoxon). Dabei kann das OSWD-System als Referenzmethode verwendet werden, um Hypothesen über das Reaktionsverhalten, hinsichtlich der Kondensationsreaktion, bestimmter Kombinationen von Stoffen zu testen.

Das in dieser Arbeit gezeigte neue Erklärungsmodell löst zahlreiche Widersprüche, die bisherige Theorien noch nicht klären können: Die Verwendung einer nano-beschränkten (engl. nanoconfined) Umgebung als präbiotisches Reaktionsgefäß liefert einen wichtigen Beitrag zur

Lösung des Wasser-Paradoxons in Theorien zum Ursprung des Lebens im Wasser, obwohl Wasser die Kondensationsreaktion von Nukleotiden hemmt. Das theoretische Modell der präbiotischen Reaktionsgefäße braucht weder Nass-Trocken-Zyklen noch Funkenentladungen oder Molekülarten, die wahrscheinlich nicht einmal auf der Erde zu diesem Zeitpunkt vorkamen. Stattdessen zeigt diese Studie eine einfache, geochemisch sehr häufige und damit sehr wahrscheinliche Situation, wie Makromoleküle wie RNA gebildet werden können. Dabei ist die gezeigte Situation sogar mit der konservativen Natur der Evolution vereinbar – ein Prinzip, das besagt, dass evolutorische Entwicklungen in der Biologie immer auf vorhandenen Lösungen aufbauen. Das vorgestellte Modell kann plausibel erklären, wie die ersten RNA-Moleküle ohne die Anwesenheit von Enzymen entstanden sein können.

1.   Introduction

1.1.   Water

Without water, life as we know it today would not exist. It may have played a fundamental role in the origin of life as a solvent and reactant and further as a medium which enabled the basic (bio-) molecules to react with each other[1], so that they could react and form more complex molecules, like amino acids, peptides, carbohydrates, lipids and nucleic acids. For this evolutionary reason, every cell contains water, accounting for 70 % or more of the total cell mass, what makes water being the most abundant molecule in cells[2] and therefore essential for species (actively) living on Earth. Furthermore, the consumption of undistilled water is not toxic, at least in appropriate amounts.

Water has an ambivalent role in basic and applied sciences: Due to its non-toxicity, ubiquity and low cost it is desirable to use water as an agent in physicochemical processes. Nevertheless, in applied sciences, such as semiconductor technologies, the water insolubility of industrial produced organic semiconductors hampers their sustainable processing. And also, regarding the research on life's origins, water generates a paradox by preventing the formation of key biopolymers such as RNA: Though many theories of the origin of RNA assume, that the first polymers of the nucleic acid was formed in an aqueous environment[3], the condensation reaction to form RNA out of single nucleotides needs to take place in the absence of water.

1.2.   Semiconductor technologies

1.2.1.   Technologization and environment protection

Over the last decade and still ongoing, one of the most growing technologies is the semiconductor technology. Semiconductors are used, whenever miniaturized switches – transistors - are needed, e.g., to construct microchips for any kind of computer system but also for communication engineering and power electronics[4]. Therefore, it is especially important for the well-being of our environment and nature in general, that the semiconductor industry becomes more environment friendly.

Though environment protection becomes increasingly important, so far, semiconductor technology approaches still use deposition methods that either use toxic, rare or expensive

chemicals, are highly energy consumptive and/or need special instruments and skills of the operators.

With the advancement of the industrialization and technologization, made by humas, it is also our responsibility to focus on technologies and production methods that are as less harmful for the organisms in our environment as possible. Though or especially because there are a lot of technical workflows, that do use alcoholic or organic solvents, with many of them being indeed toxic for our environment, new methods need to be explored and applied to make industrialization and technologization more environment friendly. As a possible solution for this problem, water-based workflows show up to be a promising possibility. Due to its in-toxicity, as mentioned before, water is an optimal solvent and dispersion agent to design environment friendly workflows.

Furthermore, by taking advantage of its outstanding properties, new possibilities of physico chemical processes can and should be explored and transferred to other scientific fields. For example, a possible approach for water-based workflows for the semiconductor industry, that also can be used as a probe to examine phenomena in other scientific fields is the organic solid/solid wetting deposition (OSWD)

1.2.2. Organic Solid/Solid Wetting Deposition (OSWD) for possible semiconductor technology approaches

OSWD is a deposition method to generate monolayers of polycyclic heteroaromatics (PHA), e.g. organic semiconductors, on crystal surfaces, graphite (highly oriented pyrolytic graphite, HOPG) (Fig. 1), graphene and others[5,6] . The PHAs may form regular patterns on the crystal surface by molecular self-assembly, as shown in Fig. 1.
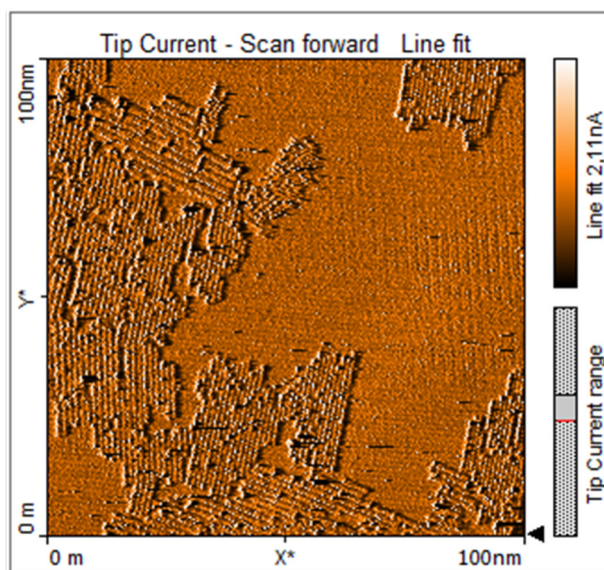
Figure 1: HOPG substrate covered with SAM domains of dimethyl-quinacridone (dmQAC), scanning tunnelling microscopy.

With the OSWD method there is no need of a PHAs-containing solution, but monolayer formation happens out of the solid state of the PHA crystal, which can be dispersed in a dispersion agent, for easier handling, such as propanol, anisole, acetone, and many others. As mentioned before even water can be used as a suspension agent. Further it was also shown by Eberle et al. that OSWD is even possible by applying the PHAs as a powder on the crystal surface and by heating it up to 240 °C, monolayer domains will form on top of the substrate, in a remarkable high amount[6].

The high coverage of the substrate surface with the mentioned semiconductor monolayer is crucial when it comes to applications in the semiconductor and thin-film electronics industry. Here, it usually is necessary that a high percentage of the substrate surface is covered with the favored semiconductor monolayer. As shown before, with the example of dimethyl-QAC (dmQAC), OSWD is a suitable method to dope graphene by organic material coating[7,8]. However, to achieve a suitable doping effect, for later applications in the semiconductor technology, a high percentage of the graphene´s surface needs to be covered with the organic monolayers.

However, heating up the material to 240 °C brings at least two disadvantages: first heating up requires high amount of energy and therefore shows up to not be efficient regarding environmental friendliness. Second those high temperatures restrict the selection of materials that can be used applying this method, as the material might melt (e.g., plastic electronics).

Though Eberle et al. showed that OSWD in water and under ambient conditions is indeed possible, the amount of covered graphene surface with PHA domains remained small and therefore not enough sufficient when it comes to application possibilities.

1.3.   The water problem in origin of life theories

As mentioned before, the OSWD is not only suitable as a possible approach for green chemistry in the semiconductor industry but can also be used as a probe to explore and explain phenomena in other scientific fields. One of this fields, in which water also plays a central role, represent the origin of life theories and the herein constantly occurring water paradox. So far, the most discussed origin of life theories deal with wetting-drying cycles, lighting strikes, or extraordinary and rare molecule species, or species that do not play a functional role in modern biochemistry, to explain the paradox of the course of hydrolysis sensitive reactions, necessary to build oligonucleotides like ribonucleic acids (RNAs) or deoxyribonucleic acids (DNAs), though they assume, that oligonucleotides must have developed in water[1] .

Though, as mentioned before, the total cell mass consists out of 70 % and more water, the liquid plays an ambivalent role within the cells, life, and the origin of life: water can function as a solvent and reactant on the one hand, but also promotes hydrolysis on the other hand, which prevents the emergence of the essential organic molecules (Fig. 2). This mystery represents one of the central issues in origin of life[9].
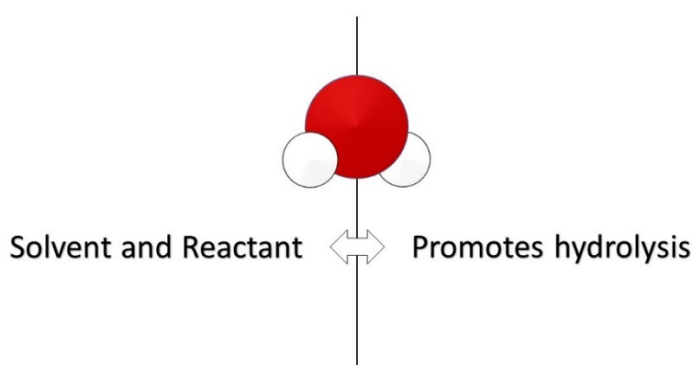

Solvent and Reactant ⇄ Promotes hydrolysis

Figure 2: Water can function as solvent and reactant on the one hand but promotes hydrolysis on the other.

However, to overcome this paradox existing in most origin of life theories[9–11], an environment which consists of water but wherein the activity of water is reduced, is needed.

"Living cells contain an intracellular aqueous fluid that is crowded with large, complex biomolecules. In this environment, virtually all water exists as interfacial water[…][8]. When viewing this dense mixture from the perspective of materials science, it is describable as an aqueous suspension of highly concentrated nanoparticles. In the vicinity of such particles, various nanofluid phenomena emerge in interfacial and nanoconfined water[…][9,10]. Consequently, such water differs significantly compared to bulk in terms of properties such as, flow behaviour, reactivity, H-bonding network dynamics, density, dielectric constant, or the quantum state of protons[…][11–13]. From a geochemical point of view, aqueous suspensions of mineral particles of micro-and nanoscopic size can be regarded as a comparable environment that generate nanofluid effects."[14]

Specialisation of science often makes us think insularly, though there are several phenomena that can be explained applying the same basic principles. By connecting the findings made during the elaboration of this thesis, working on a water based OSWD approach, applicable for semiconductor technologies, it was achieved to create a new theory to overcome the water paradox in prebiotic RNA formation, as well. This crucial point of the origin of life, so far existing theories were not able to explain in a that straight forward chemo evolutionary consensus as it can our here shown new concept.

1.4.   Aim and structure of this thesis

1.4.1.   Enhancement of OSWD using (bio-)molecules

It can be stated that an environmentally friendly method to generate monolayers of PHA dopants on graphene, using a cheap and easy to handle deposition method, applicable for virtually insoluble and hardly processable molecules such as PHAs, with sufficiently high efficiency was not available so far. Nevertheless, as mentioned before, the progress of the industrialization and technologization, made by humas, entails also a growing responsibility to advance technologies and production methods that are as less harmful for organisms as possible.

Present established methods require at least either heat, harmful chemicals, specific skills of the operator or complex instruments. For this reason, in this thesis it was examined how OSWD at

room temperature can be influenced in terms of efficacy, using only non-harmful substances, such as water as a dispersion agent and dissolved biomolecules acting as OSWD influencing agents.

Therefore, a screening of different samples was performed and will be analysed regarding their influence on the OSWD in Chapter 4.1.. Extensive STM imaging was performed with subsequent analysis of the amount of substrate area covered my domains. As an exemplary PHA, quinacridone (QAC), a red/pink pigment, insoluble in water and a p-type dopant[15,16] was used.

Since the results showed an outstanding increase of monolayer formation on the substrate, when AMP was added to the sample, further analysis about the chemical and physical properties of AMP and their possible influence on the OSWD rate, in comparison to the other monophosphate nucleotides will be shown in the same chapter. Several aspects were examined:

- The pH value of the sample (e.g., mixture of QAC, Water, AMP), as high pH can increase the percentage of covered substrate area by OSWD, whereas low pH decreases it[13]. The aim was to analyse whether the mixture of AMP with QAC, and water shows an unexpected pH.

- The zeta potential of the sample, as it was shown that the z33 value (the value where 33 % of the distribution is more negative and 66 % more positive) of the zetapotential is indirectly proportional with the coverage of OSWD in many cases[13]. The aim was to examine if this was the case with AMP.

- The molecular electrostatic potential of different nucleotides to analyse differences in the functional, chemical structure.

- Stacking possibilities and stacking constants of AMP, cytidine-monophosphate (CMP), guanosine-monophosphate (GMP) and uridine-monophosphate (UMP) to examine further intermolecular interactions.

1.4.2.   Doping of graphene at room temperature

As shown in a proof-of-concept study by Eberle et al. graphene can be doped by OSWD using dmQAC[7], yet it was not demonstrated if this method is also applicable using other PHAs. However, this would be important to gather further information about the applicability of the

OSWD for semiconductor technologies and offer different options of possible dopants, making the application more flexible regarding its raw materials. Therefore, in a second part of this thesis, it was examined if doping of graphene by monolayer formation of semiconductive PHAs on the graphene surface, also is possible by using another dopant and by applying OSWD at room temperature and in water.

To analyse this, in chapter 4.2. the results of different spectroscopy analysis will be shown. DmQAC and flavanthrone were chosen as model PHAs, to compare the results with earlier results of our group. Three different methods were performed to achieve reliable results: Tunnelling spectroscopy, Raman spectroscopy and Dirac peak measurements.

1.4.3.   Condensation of RNA in aqueous particle suspensions

To examine if OSWD-generating environments also influence the behaviour of biomolecules vice versa, aqueous OSWD-like samples, containing substrate powder and/or pigment powder as well as RNA nucleotides of different species, were analysed regarding possible oligo nucleotide formation after incubation.

This examination was done, using biochemical approaches: ethanol precipitation, reverse transcription polymerase quantitative chain reaction (RT-qPCR) and fluorescence spectroscopy.

Using the OSWD system as a probe, it will be further shown, how hypothetical assumptions about the influences of the here shown new theory of the possible origin of life in water can be proven. Predictions of the outcoming yield of oligo nucleotides in distinct samples were made and controlled, using the efficiency of the OSWD using the same sample composition.

"Inspired by […] [the idea that "from a geochemical point of view, aqueous suspensions of mineral particles of micro-and nanoscopic size can be regarded as a comparable environment which generate nanofluid effects[14]"], we designed experiments to test the potential of nanofluid environments within aqueous suspensions of particles for inducing key biochemical reactions in a possibly prebiotic context. As various prebiotic synthesis pathways of nucleosides […][17] and nucleotides[…][18] have been proposed and because the abiotic condensation of nucleotides into RNA within water is a common goal of prebiotic chemistry[…][19,20], we chose the polymerisation of nucleotides into RNA as an example reaction. The focus was set on the

formation of a pure adenosine-based RNA (poly(A) RNA) since adenosine monophosphate (AMP) is the most common nucleotide in living cells[…][21]. Furthermore, poly(A) RNAs are common RNAs in cells in the form of poly-A-tails of messenger RNAs during protein biosynthesis. Thus, we first prepared samples which contained dissolved AMP. In order to create a nanofluid environment for AMP solutions we selected quinacridone (QAC) as an example of polyaromatic heterocycle particles and graphite as an inorganic suspended particle species as both compounds have well been characterized in terms of inducing nanofluid phenomena in aqueous suspensions[…][13]."[14]

2. Basics

2.1. Organic Solid/Solid Wetting Deposition

Organic Solid/Solid Wetting Deposition (OSWD) is a deposition method to generate monolayers of organic semiconductors on substrates, out of the solid phase of the insoluble particles under ambient conditions[5,6,12,13,22].

So far, OSWD was studied in the context of two-dimensional crystal engineering and organic semiconductor device development using various substrates, like highly oriented pyrolytic graphite (HOPG), graphene, carbon nanotubes, and molybdenum disulphide (MoS2). Further, there are several organic substances, that are known to form monolayers in OSWD application, like quinacridone (QAC) and its various derivatives, phtalocyanine (Phth), flavanthrone (FVT) and many others[5,6,12,13,22].

Understanding the physical principles behind this deposition method, but also gaining technical experience using different substrates, semiconductors, dispersion agents and further conditions might help to find innovative solutions for semiconductor production. Further, the OSWD can not only be used as a technical approach, but also as a probe to examine and explain natural phenomena.

2.1.1. Practical principle

To generate monolayer formation of the mentioned pigments on a substrate using OSWD, pigment powder can be mixed with a suitable dispersion agent of choice and drop casted on the substrate. On the substrate, supramolecular, two-dimensional adsorbates form directly from the three-dimensional, insoluble solid pigment particle without further handling steps being required. Previous investigations on OSWD have shown that with respect to upper solubility limits and STM observations of monolayer coverage, distinct domain formation and the possibility of single molecule extraction via nanomanipulation, adsorbate formation from solution can be excluded[11]. This process has been shown to take only a few seconds[13] and can be handled under ambient conditions. Neither high or low temperature, nor vacuum, ultra clean environments, or time-consuming processes to manipulate the organic molecule of interest to turn them soluble, are needed. Moreover, the OSWD method can also be handled using water as a dispersion agent (Fig. 3). After drying the samples, e.g., by evaporation, a covering using

dodecane enables scanning tunnelling microscopy (STM) to examine the deposition further[22]. It needs to be ensured, that the used pigment is not soluble in dodecane.

Another approach to generate monolayer adsorbates as described above, is heating up the pigment powder on a substrate to minimum 240 °C, without using dispersion agents. With this method one can achieve very high adsorbate coverages, of substrate surface area[22]. Nevertheless, high heat energy is required.
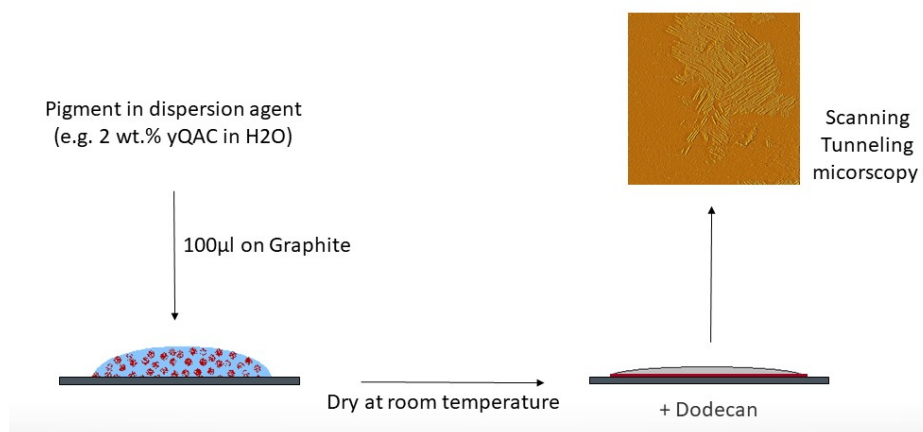

Figure 3: Graphical abstract of the basic method, used to generate OSWD.

Up-scaling is only limited to the size of the substrate. Furthermore, pigments are available in enormous amounts due to their widespread use in industrial applications but applying the OSWD method, only very small amounts in the order of mg or even less, are needed in the end to form the monolayers on the substrate.

2.1.2.   Physical Principle

Besides of the knowledge of different technical methods, Eberle et al. proposed a fundamental model of the OSWD process, being able to explain the significance of different forces at different distanced between the semiconductor particle and the crystal-surface (Fig. 4):

Distance of about 100 nm and below: particles approaching the substrate surface actually undergo a repulsive force generated by electrical double layers that encircle any object in contact with a dispersing agent. However, refined DLVO calculations suggest that for particles with strong negative zeta potential this barrier is lower. If the zeta potential is sufficiently

low the particles can negotiate the barrier and draw nearer to the substrate surface. The attraction as a result of the sum of Poisson-Boltzmann, Van-der-Waals and Casimir-like fluctuation-induced interactions lead to further increasing attraction the more the distance gets lower.

Distance of < 10 nm: the molecules of the liquid-phase, the weakly bonded ionic species as well as the solvated ions forming the outer Helmholtz planes get rejected by the hydrophobic dewetting effects[23,24], which were shown to appear in such system with two hydrophobic partners, here the semiconductor particle and the substrate surface[25–29].

Distance of < 1nm: between the substrate surface and the semiconductor crystal a steric barrier is induced by the remaining, insolvent ionic adsorbates. In water, this barrier is affected by ice-like structured water molecules and selectively adsorbed hydroxyl ions[30–32]. The formation of ice-like orientations minimizes the number of unsaturated hydrogen bonds and thus reduces the energetic penalty[33].

Summing up all forces in this system, the attractive forces are that predominant that the steric barrier finally gets eliminated by expelling the inner Helmholtz planes[25,26]. A direct contact between the semiconductor crystal and the substrate surface happens and the OSWD takes place, as far as the binding energy between the molecules themselves inside the semiconductor crystal is lower than the binding energy between the semiconductor molecule and the substrate surface.
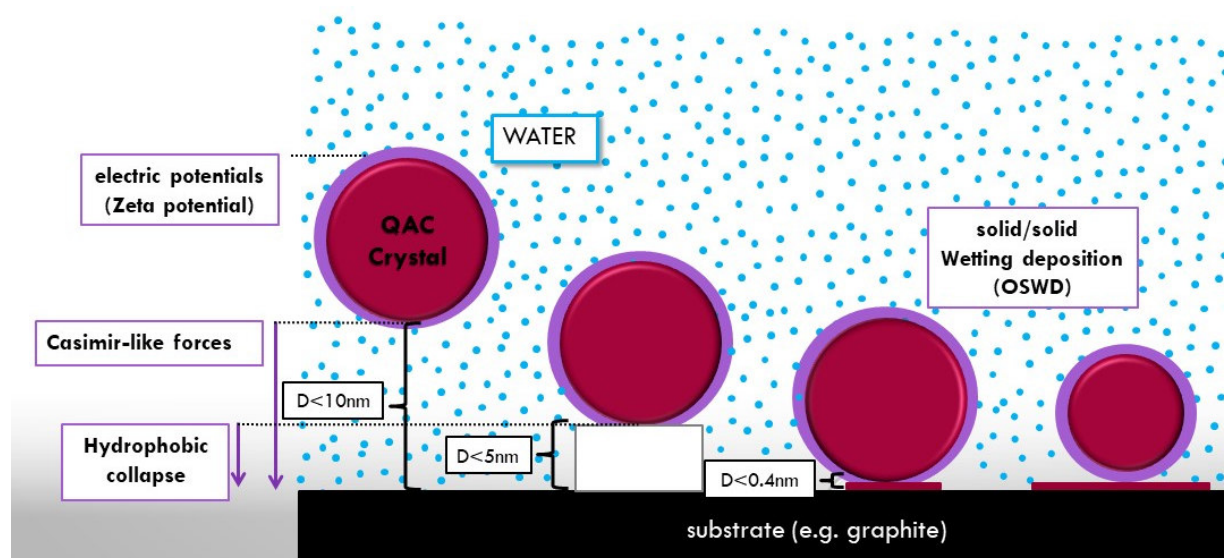

Figure 4: Graphical overview of successive stations of distances and the regarding acting forces during the approach of the pigment crystal to the substrate surface.

2.2. Organic semiconductors

2.2.1. Physical principle

Organic semiconductors are semiconductive materials with carbon-based (organic) molecular structure. Hereby, an organic semiconductor molecule consists out of various benzol rings and can contain further atoms, like nitrogen, oxygen or others[34].

Responsible for the electric conductivity in organic semiconductors is the sp2-hybridization of carbon due to its four valence electrons. By the hybridization of one 2s orbital and two 2p orbitals in bonded atoms, three equivalent sp2 hybrid orbitals are created. All three lie in one plane and form an angle of 120°. The bond between two of these atoms takes place via σ-bonds (sigma-bonds). The third p-orbital (2pz) is perpendicular to the plane and does not form a hybrid orbital itself. Between two neighboring 2pz orbitals, π-bonds (pi-bonds) can be formed by the overlap of the p orbitals. Both σ-bonds and π-bonds can occur between two neighboring atoms and therefore doble bound positions are formed between two carbon atoms (if not bound to a heteroatom).

Which of the three hybrid orbitals of carbon overlies a π-bond and thus defines a double bond position is not specified and can therefore only be described by three different structural formulas (mesomeric boundary structures)[35]. It must be supposed that none of these boundary structures is realized alone, but an overlay of all boundary structures must be assumed. This superposition of single and double bonds is called conjugated double bonds, wherein the π-bonds cannot longer be localized, so that it comes to a delocalized π-electron system, which is the reason for the conductivity of condensed carbon ring systems, such as graphite, graphene and organic semiconductors.

Further, the intermolecular conductivity in crystalline association can be described by a band-like transport, as HOMO and LUMO orbitals interact and split into the corresponding valence and conduction bands[36].

Due to their conjugated π-electron systems, organic semiconductors can work as chromophore systems, wherefore many of them also function as organic pigments[37].

2.2.2. Applications

Besides of their classical use in printing inks, car paint or for coloring plastics[37] organic semiconductors are used in molecular and organic electronics. That is because of the low production costs and the possibility of generating extremely small and thin components for electronic circuits, which becomes increasingly important also for micro- or even nanoelectronics. Further, with organic semiconductors electronic components and tracks could easily be printed on a carrier material, that even can be flexible[38–40]. Possible applications are besides of electronic paper and flatscreens also photovoltaic systems, chip cards and other sensors[38].

2.3. Biomolecules, used in this thesis

Biomolecules are molecules that are produced by living organisms to fulfil biological functions. Biomolecules classically can be divided in four groups: carbohydrates, amino acids & proteins, lipids and nucleic acids (Fig. 5)[41,42].
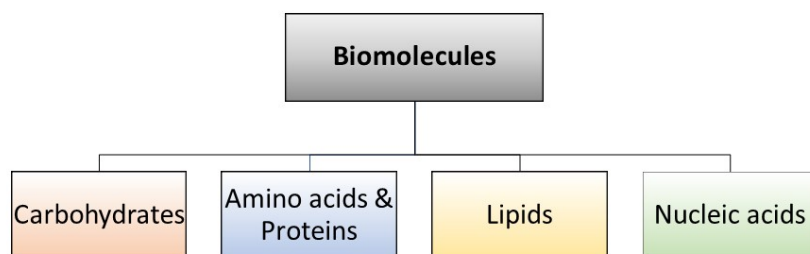
Figure 5: Overview of subgroups of biomolecules.

In this study mainly nucleic acids and their derivates were used. However also an amino acid and a phospholipid were added to the screening sample set.

2.3.1. RNA nucleotides

RNA nucleotides can be classified into the group of nucleic acids. So far, there are two classes of nucleotides known: ribonucleic acid nucleotides (RNA nucleotides) and deoxyribonucleic acid nucleotides (DNA nucleotides). The basic different between both groups of molecules is the basic sugar, which is a ribose in RNA nucleotides and a deoxyribose in DNA nucleotides.

Since only RNA nucleotides were used in this study, DNA nucleotides will not be further discussed here.

In the group of RNA nucleotides, there are four different molecules known:

- adenosine-monophosphate (AMP)
- cytidine-monophosphate (CMP)
- guanosine-monophosphate (GMP)
- uridine-monophosphate (UMP)[41–43]
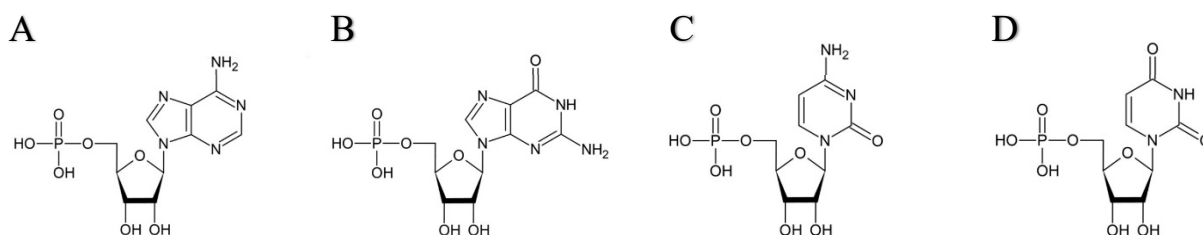
Figure 6: Chemical structure of RNA nucleoside monophosphates. Chemical structure of RNA nucleoside monophosphates. **(A)** Adenosine Monophosphate, **(B)** Guanosine Monophosphate, **(C)** Cytidine Monophosphate and **(D)** Uridine Monophosphate.

As shown in Fig. 6 RNA nucleotides (nt) always consist of a base (adenine, cytosine, guanine, or uridine) a ribose and a phosphate group. The phosphate group can consist of one (as shown in Fig. 6), two or three phosphates, what can be recognized by the respective name mono-, di or triphosphate. If the phosphate group is absent, ribose and base form a nucleoside.

RNA nucleotides can further be classified regarding their base: AMP and GMP contain purine bases, whereby CMP and UMP contain pyrimidine bases (Fig. 7)[41–43].
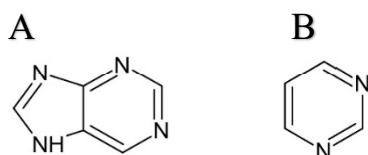
Figure 7: Chemical structures of (A) Purine and (B) Pyrimidine.

Several nucleotides of AMP, CMP, GMP and UMP together can form RNA strands by condensation reactions, forming a phosphate diester bound between the ribose of the one and the phosphate group of the other nucleotide, which itself is also connected by an ester bound to its own ribose (Fig. 8)[41–43].
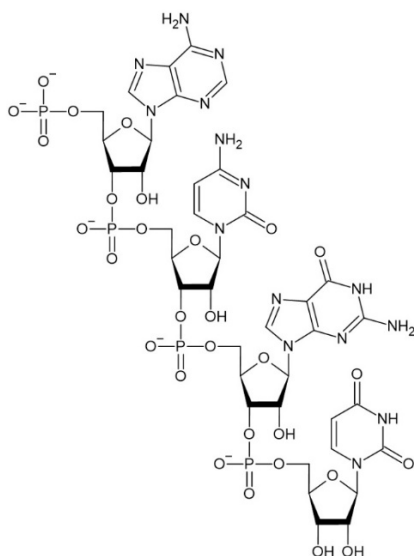

Figure 8: Chemical, primary structure of an oligo-RNA-nucleotide. Between each ribose and phosphate groups, diester bonds are formed.

By connecting more nucleotides, the RNA strand can be elongated, forming dinucleotides, oligonucleotides, and further polynucleotides. In living cells this reaction is catalyzed by enzymes, like RNA polymerases. RNA molecules can further form secondary structures, like loops and hairpins, whereby small parts of the RNA undergo complementary base pairing (adenine with uracil and cytosine with guanine)[41–43].

The central aspect of the so-called "RNA hypothesis" assumes that life on Earth must have started with RNA as a first kind of genetic information, whereas DNA developed later, as an information storage of the organism[3,44]. One of the reasons therefore is, that the functions of RNA are directly connected to the protein biosynthesis, the biological process inside cells to generate proteins. Hereby the RNA has two basic tasks: First the messengerRNA (mRNA) carries die information of the order in which the amino acids will be connected to form a specific protein; second the transferRNA (tRNA) delivers the correct amino acid to the protein factory, the ribosomes, where the amino acids are connected to peptides (later proteins) by a peptide bound[3,41].

2.3.2.   Adenosine-monophosphate (AMP) derivates

Interestingly within the group of RNA monophosphate nucleotides there is one nucleotide which can be found on the one hand in high amount within RNA macromolecules [3,41] and on the other hand also is part of various other biomolecules, which are essential for different metabolism pathways.

- AMP forms the poly-A-tail of mRNA molecules, a 100 - 250 nt long chain consisting only of AMPs (Fig. 9A).
- AMP is the basic building block of the flavin-adenine-dinucleotide (FAD/ $FADH_2$) and of the nicotinamid adenine dinucleotide (NAD^+/NADH or $NADP^+$/NADPH (plant cells)) which both are essential co-enzymes needed for the Krebs-Cycle, the central energy metabolism pathway of cells (Fig. 9B and 9C).
- AMP obviously also is the basic building block of ATP, which is the currency of the energy of the cell, as it is needed for the muscle contraction in the interaction of the actine and myosin filaments (Fig. 9D).
- AMP further is the basic building block of cyclic AMP (cAMP), which is a second messenger in several signaling pathways and further regulates several metabolism pathways, muscle contraction, secretion, calcium homeostasis, gene transcription and cell fate (Fig. 9E).
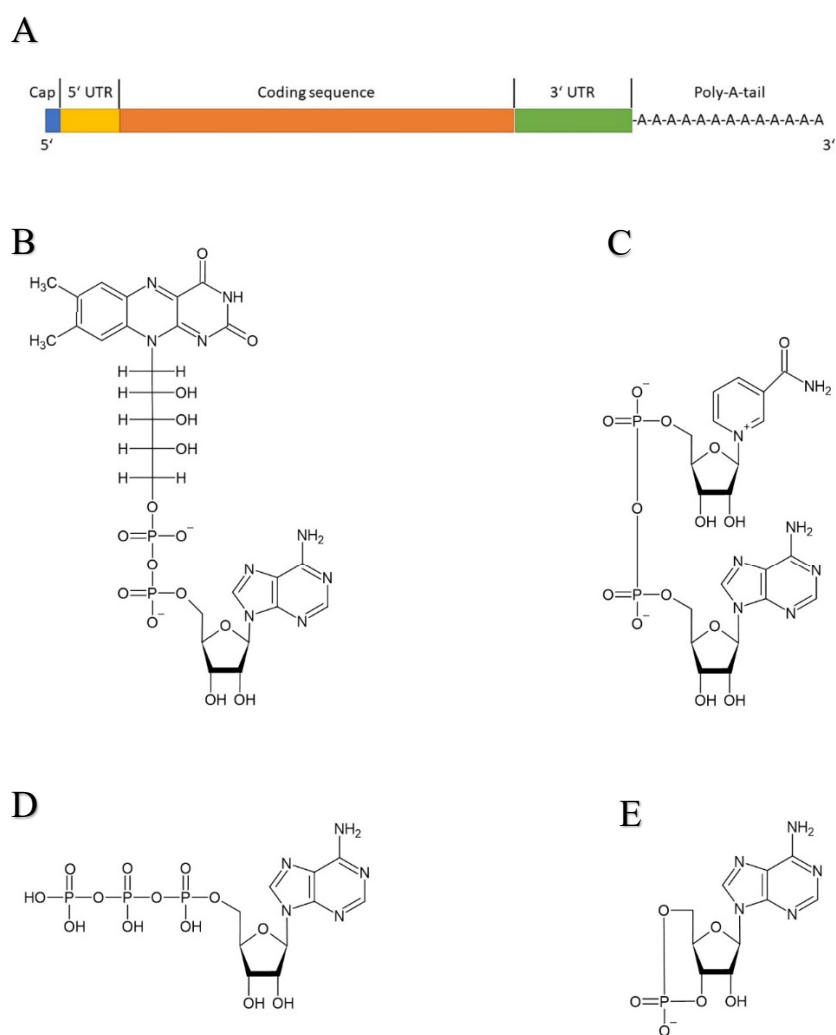
Figure 9: Derivates of AMP in living cells. **(A)** scheme of mRNA with Cap, 5' Untranslated region (UTR), Coding sequence, 3' Untranslated region (UTR) and Poly-A-tail. **(B-E)** chemical structure of **(B)** FAD, **(C)** NAD, **(D)** AMP and **(E)** cAMP.

Neither CMP, GMP nor UMP show this brought spectrum of derivates and applications within the cell. Only AMP does. This might be for different outstanding chemical characteristics, as they will be shown in the discussion section.

2.3.3.   Further biomolecules used in this study

Besides nucleotides, RNA and the derivates of AMP (NAD, FAD, cAMP) in this study also the amino acid L-arginine was used.

Arginine is an α-amino acid that contains a hydrophilic, basic guanidino group in its side chain (Fig. 10). Arginine belongs to the group of basic amino acids, together with lysine and histidine.

The guanidino group is a very strong base because it has delocalized π electrons in its protonated form as a guanidinium ion. Most of it is only deprotonated above a pH value of 12.1[45]. The isoelectric point at which arginine has no net charge and therefore does not migrate in the electric field is pH 10.8. At this pH value, arginine also has its lowest solubility in water[45].
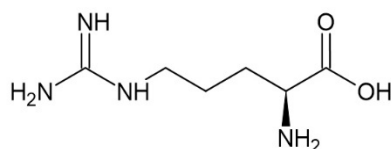
Figure 10: Chemical structure of arginine.

3. Material & Methods

3.1. List of chemicals

ADP disodium salt	Alfa Aesar, CAS-Nr. 16178-48-6, p. grade: 96%
Alloxacine	Sigma Aldrich, Cas-Nr. 490-59-5
AMP disodium salt	Sigma Aldrich, CAS-Nr. 61-19-8, p. grade: 97%
AMP acid	Alfa Aesar, CAS-Nr. 61-19-8, p. grade: 99%
Anthraquinone	Fluka, CAS-Nr. 84-65-1
L-Arginine	Alfa Aesar, CAS-Nr. 74-79-3, p. grade: 98+%
ATP disodium salt	Sigma Aldrich, CAS-Nr. 34369-07-8, p. grade: $\geq$ 99%
Carbon nanopowder	Sigma Aldrich, CAS-Nr. 7440-44-0; <100 nm particle size
Carbon	Sigma Aldrich, CAS-Nr. 1333-86-4
cAMP sodium salt	Alfa Aesar, CAS-Nr. 37839-81-9, p. grade: 99%
CMP disodium salt	Sigma Aldrich, CAS-Nr. 6757-06-8, p. grade: $\geq$ 99%
dmQAC (2,9-Dimethylquinacridone)	Clariant, CAS-Nr. 980-26-7 Hostaperm PinkE, av. particle size: 65 nm
HOPG	NT-MDT, item no. GRBS/1.0
Indigo	Sigma Aldrich, Cas-Nr. 482-89-3, p. grade: 95%
nuclease-free water	Sigma Aldrich, W4502
Dodecane	Sigma Aldrich, D221104
FAD disodium salt	Sigma Aldrich, CAS-Nr. 84366-81-4;p. grade: $\geq$95%
Flavanthrone	ABCR GmbH& Co. KG, CAS-Nr. 475-71-8
GMP disodium salt	Sigma Aldrich, CAS-Nr. 85-32-5, p. grade: $\geq$95%
Graphene on copper foil	Graphenea
Graphene on silicon	Graphenea
Iron (II, III) oxide	Sigma Aldrich, CAS-Nr. 1317-61-9
miRNA-34	eurofins, (CAAUCAGCAAGUAUACUGCCCU)
β-NAD sodium salt	Sigma Aldrich, CAS-Nr. 20111-18-6
Phospholipids (mixture)	Sigma Aldrich, PH9-1KT
Phthalocyanine	Sigma Aldrich, Cas-Nr. 574-93-6
Polyethylene (<400 micron)	Alfa Aesar, CAS-Nr. 9002-88-4

γQAC (gamma-Quinacridone)   Clariant, CAS-Nr. 1047-16-1, Hostaperm Red E5 B02, av. particle size: 65nm

Silicon dioxide (325mesh)   Sigma Aldrich, CAS-Nr. 60676-86-0; amorph

UMP disodium salt   Alfa Aesar, CAS-Nr. 3387-36-8; purity grade: ≥99%

Water, nuclease free   Sigma Aldrich, CAS-Nr. 7732-18-5

3.2. Quinacridone and Flavanthrone

In this study basically two semiconductor substances were used: quinacridone (QAC, 5,12-Dihydroquinolino[2,3-b]acridine-7,14-dione, pigment violet 19; here used as 3,9-dimethylquinacridone and gamma-quinacridone) (Fig. 11A) and flavanthrone (Benzo[*h*]benzo[6,7]acridino[2,1,10,9-*klmna*]acridine-8,16-dione, vat yellow 1, pigment yellow 24) (Fig. 11B). Both substances are cheap and highly available pigments. QAC powder is pink or red, whereas flavanthrone is orange. Both pigments are known to be produced for and used in the paint industry. They are mainly non-toxic and virtually insoluble in water[15,16], as it was also practically shown for QAC by Eberle et al.[22], and also specified as such by different data bases, like the Hazardous Substances Data Bank (HSDB)[46].

Further, both semiconductor substances show electron-acceptor properties[47,48]. Their structure is planar, without any atom reaching out in the z-plane. Due to this chemical and geometric structure, they are predestined to undergo pi-pi-stacking on benzol based substrates, like graphite and graphene. Consistently, each pigment forms a characteristic monolayer pattern on these substrates.
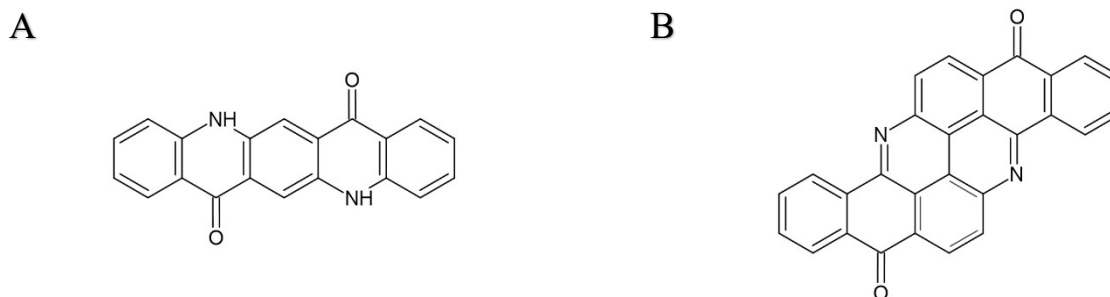
Figure 11: Chemical structures of the two main pigments used in this study. **(A)** Chemical structure of QAC. **(B)** Chemical structure of flavanthrone.

3.3. Physical and chemical analysis

3.3.1. Scanning tunneling microscopy

Sample preparation:

If not differently indicated, nuclease-free water was used (free of nucleases, DNase, protease, RNase) for all samples.

For pigment-only samples, 67 mM aqueous pigment dispersions were used. This concentration was chosen to be able to compare the results with earlier studies, like of Eberle et al..

For pigment-biomolecule samples, aqueous dispersions with a final concentration of 67 mM pigment and 26.8 mM biomolecule were used.

Prepared mixtures were thoroughly mixed by using a small shaker (Vortex), until the mixture appeared to be uniform.

150 µl of the regarding dispersion was applied to a one cm^2 graphite or graphene sample (both purchased, see list of chemicals), and dried over night at room temperature. This volume was chosen so that the surface area was covered as much as possible, without dispersion flowing off the substrate. Applied dispersions form a dome-like drop on the substrate´s surface.

Samples were each time freshly prepared and remaining dispersions were discarded.

For the coverage screening section, each dispersion was made in three replicates and from each replicate two samples on graphite were prepared.

To perform scanning tunneling microscopy (STM) measurements under ambient conditions, samples were covered with 3 µl dodecane. Dodecane itself was shown to not from supramolecular assemblies at room temperature[13] but generates a hydrophobic film on the sample, so that condensation water cannot disturb the measurements.

Measurements:

For STM measurements for coverage analysis, a home built STM with a SPM 100 control system (RHK Technology) was used, with tungsten wire tips. Tips were produced by etching, using 1 M KOH and 20 V dc.

The bias of the STM was set to 1 V, the tunnel current to 300 pA and the line time to 50 ms. Voltage pulses were set to 2.4 V. These settings were equal for all samples to receive best possible comparable results.

For the coverage screening section, from each prepared sample minimum three different regions were measured.

For split images of flavanthrone and imaging of samples for tunnelling spectroscopy an Easy Scan NaioSTM (Nanosurf) was used, with platinum/iridium (Pt/Ir) wire tips. Tips were produced by tearing of the tip end with pliers.

The basic STM settings were set to bias = 1.2 V, tunnel current = 300 pA and the line time to 100ms. Voltage pulses were set to 1 V. As above these initial settings were equal for all samples to receive best possible comparable results.

To generate split images the tip voltage was gradually reduced to 0.1 V and the setpoint gradually increased to 1 nA while measuring.

3.3.2. Coverage measurements

To calculate the fraction of surface, which is covered with monolayer domains of PHAs, images were analyzed using the Image J software. Hereby, domains were masked in white by hand (Fig. 12B) and the background was set to black (Fig. 12C). Subsequently the black/white ratio was determined using the histogram function of the software. Values were then set in ratio to a negative sample without domains (100 % black).
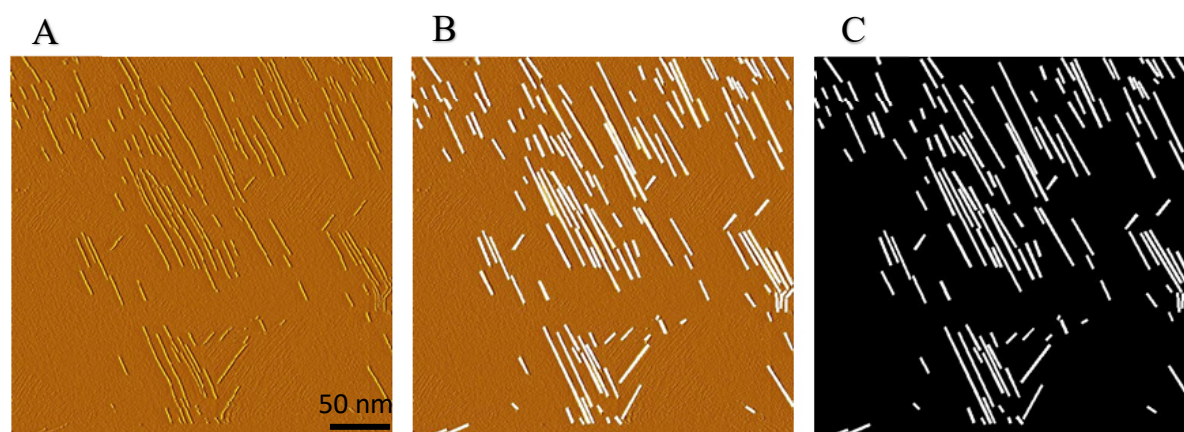
Fig. 12: will be continued on next page

D
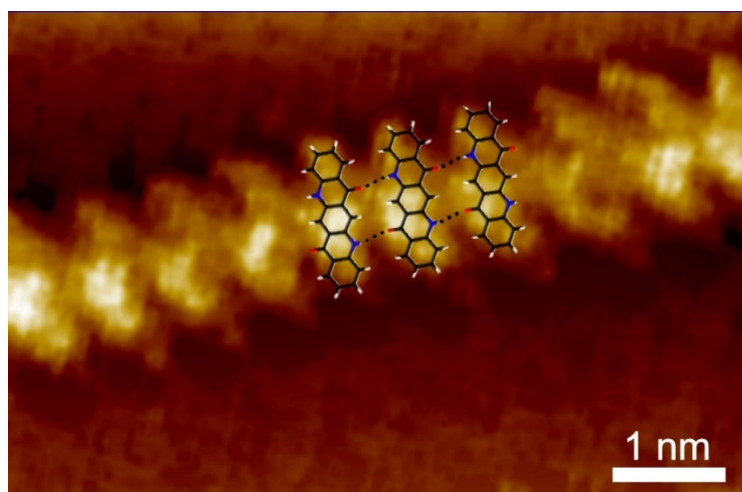
Figure 12: Image Processing for histogram analysis. **(A)** Raw image; here QAC on graphite. **(B)** White masking of QAC domains. **(C)** Background set to black to enable black/white ratio measurement. **(D)** STM image of a supramolecular chain of QAC molecules adsorbed on graphite. Deviating from measurement settings given above, this image was generated with I = 250 pA and U = 0.9 V. A force field calculated energy minimized adsorbate structure of QAC on graphite was overlayed on the image. Adapted from[5].

3.3.3. Zeta potential measurements

Zeta (ζ) potential measurements were performed by the Papiertechnische Stiftung (PtS), Germany. There, a Zetasizer Nano ZS ZEN 3600 system (Malvern) was used. Samples were prepared with the same concentrations as mentioned in chapter 3.3.1.. In case of samples that contained nucleoside monophosphates, stock solutions with double the concentration were mixed only directly before the measurement, in a ratio of 50:50, to achieve the same final sample concentration as mentioned in chapter 3.3.1..

Three measuring replicates were performed per sample, with a potential range of -150 mV to +150 mV, with 80 measurement points distributed equally over the potential range.

Data evaluation and calculation were performed by linear interpolation. Both,

- z50, the median value of the cumulative zeta potential distribution and
- z33, the value where 33 % of the distribution is more negative and 66 % more positive

were calculated using

$$zNN(I) = z_{i-1} + \frac{z_i - z_{i-1}}{I_i - I_{i-1}} (I - I_{i-1})$$

With *zNN* being the zeta potential of interest (z33 or z50), *I* the corresponding value of the cumulative distribution, index *i* indicating the upper value of the respective interval and index *i-1* indicating the lower value of the respective interval.

3.3.4.   pH measurements

pH measurements were performed on samples contained the same concentrations as mentioned in chapter 3.3.1.. pH measurements were performed using a Voltcraft pH-100 ATC pH-meter. The pH-meter was calibrated with purchased calibration solutions with pH 4 and pH 10. Each sample was prepared and measured three times. Between each measurement pH-meter was washed with H2O ddest. and stored in electrolytic solution.

3.3.5.   Spectroscopies

3.3.5.1.   Tunnelling spectroscopy

<u>Sample preparation:</u>

Sample preparation for tunnelling spectroscopy was carried out at room temperature, without using vacuum. From flavanthrone, 0.03 mM suspensions in water were prepared and mixed thoroughly using a small shaker (Vortex). Subsequently the suspensions were applied by pipetting to purchased graphene substrates on copper foil and immediately taken off again, also pipetting. To achieve a higher number of self-assembled monolayer SAM-domains and to enable easier downstream measurements, this step was repeated five times. Thereafter the substrates were rinsed with water to get rid of residual pigment crystals, which might disturb the following measurements. Therefore, the substrate was hold in a ~ 45° angle and 2 ml of water (see material list) was run over the surface using a pipet. To enable Tunnelling spectroscopy (TS) measurements without vacuum, the pigment coated graphene was covered with dodecane.

Measurements:

Tunnelling spectroscopy (TS) measurements were performed with an Easy Scan NaioSTM (Nanosurf). Directly before to the spectroscopy measurements, an image of the area of interest was taken, using the same settings as described in chapter 2.3.1.. Immediately afterwards spectroscopy measurements were performed.

TS measurements were conducted performing a tip current – tip voltage curve with a range from -3.0 V to +3.0 V of several single points with different distances to the domains.

From each distance (measuring point – SAM domain of flavanthrone) ten measurements of tip current – tip voltage curves were performed. The trend line was applied as a smoothed medium line of each ten measurements. The band gap size was finally determined by measuring the length of the section of the trend line, where dI < 0.7 nA was given, presuming a differential conductance of dI < 0.7 nA to be zero[7].

3.3.5.2. Raman spectroscopy

Sample preparation:

For Raman spectroscopy samples were prepared as mentioned in chapter 3.3.5.1. but applied to graphene on a $1cm^2$ silicon substrate instead of copper foil.

Measurements

Raman measurements were performed using a LabRAM HR Evolution Raman System (HORIBA Scientific) with LabSpec 6 software and frequency-doubled Nd:YAG laser (neodym yttrium-aluminium-garnet), with a wavelength length of 532 nm and a laser power output of 0.84 mW on the sample. Before determining the peaks and peak-shifts, measurements were adjusted by baseline correction, applying a polynomial of the sixth degree.

To enable a statistical analysis, of each sample 10 measurements were performed and peak intensity maxima and the regarding peak shift were seek out using the LabSpec 6 peak finding tool. Statistical analysis was performed by t-testing.

3.3.5.3. Dirac peak measurements

Dirac peak measurements were performed with the support of Lucas Hille at the Faculty of Physics, Ludwig-Maximilians-Universität München, Working group of Prof. Weitz.

Sample preparation:

The following steps were prepared previously by colleagues of the Prof. Weitz group.

Graphene substrates were prepared via mechanically exfoliating flakes from a block of graphite and subsequent transfer of the flakes onto the surface of a SiO_2 (300nm)/Si substrate. To determine the number of layers in the flakes, optical microscopy (contrast) as well as Raman spectroscopy (peak definition) was applied. Subsequently, after structuring a spin-on Poly(methyl methacrylate) (PMMA) layer with electron beam lithography (E-Line, Raith) gold contacts were deposited. For this deposition an ultra-high-vacuum (UHV) evaporation chamber was used.

The following steps were performed by the author:

0.03 mM water pigment samples were applied to the substrates as described in chapter 3.3.5.1. and samples were dried with compressed air.

Measurements:

Electrical measurements were performed using source-measure units (Keithley 2450, Tektronix) whereby two needle probes were connected to two gold pads, respectively. Furthermore, for each measurement an island of graphene including the two gold pads with the needle probes were created by scratching the graphene surface with the needle probs before locating them on the gold pads. From each sample 15 measurements were performed on three different single-layer graphene flakes. For the sample covered with dmQAC only two measurements could be used for the analysis, as the bigger dmQAC particles disenabled the before described isolation of the graphene islands by creating unwanted bridges to the residual graphene surface.

3.4. Molecular biological analysis

3.4.1. Sample preparation

"Three millilitre of aqueous suspension was made of each 0.1 g/ml inorganic substrate (e.g., graphite powder) and/or organic pigment with a total nucleoside monophosphate concentration of 50 mM. Samples were incubated overnight at 60 °C while mixed horizontally at 300 rpm, to avoid sedimentation of substrates and pigment. After incubation, samples were centrifuged at 8000 × g for 1 min at room temperature (RT). The supernatant was transferred to a new collection tube."[14]

3.4.2. Precipitation

"If not differently indicated, precipitation was carried out with 0.2 M NaCl and 3.5 volumes of EtOH. One sample was precipitated with 0.3 M NaOAc (pH 5.2) and 0.7 volumes of isopropanol to test the efficacy of a different precipitation method. After the addition of the appropriate amount of salt solution and alcohol, samples were mixed by inverting the tubes 5 times, and precipitation reactions were incubated 24 h at −20 °C. Afterwards the samples were subsequently centrifuged at 14,000 × g, for 1 h without cooling (room temperature between 20 and 25 °C). The supernatant was discarded, leaving ~20 μl of it inside the reaction tube, in addition to any formed gel pellet. Formed gel pellets were dried at 37 °C for 20 min and resuspended in an appropriate amount of nuclease free water, as little as possible needed to dissolve the gel pellet. Depending on the volume of the gel pellet, more or less volume of water was added. Final RNA concentrations were then normalised to a uniform volume of 200 μl, using the total RNA amount measured and the final volume."[14]

3.4.3. RNA concentration measurements

"Concentrations of […] RNA suspensions were measured using a Qubit™ 3 Fluorometer (Invitrogen™), and the Qubit® microRNA Assay Kit (Invitrogen™) due to its high specificity and reliability: >The assay is highly selective for small RNA over rRNA or large mRNA (>1000 nt) (...), and tolerant of common contaminants such as salts, free nucleotides, solvents, detergents, or protein (...).<[…][49]. Concentrations were calculated by the chosen microRNA

(miRNA) or RNA program of the Qubit® 3 Fluorometer. Standard curves and samples were prepared, following the manuals[…][50]."[14] :

The Qubit™ working solution was prepared by diluting the Qubit™ microRNA reagent 1:200 in the Qubit™ microRNA buffer.

The Fluorometer was calibrated with the standard samples (0 ng/µl and 10 ng/µl) provided by the Assay Kit. Following the instructions, 10 µl of each standard sample were added to each 190 µl of working solution. The so diluted standard samples were mixed 5 s using a small shaker (Vortex) and after incubation at room temperature for 2 min., standards were read in the Qubit™ Fluorometer.

For the RNA samples, 5 µl of each sample was added to 195 µl working solution, mixed, incubated and read as described above.

"Concentrations were calculated and normalized regarding the respective volume of each sample."[14]

3.4.4. Quantitative Polymerase Chain Reaction after reverse transcription (RT-qPCR)

"For RT-qPCR selected samples were reverse transcribed using the TaqMan™ Advanced miRNA cDNA Synthesis Kit (Thermo Fisher) following the manual:

As a positive control the synthetic miRNA hsa-miR-134-3p (5´-phosphorylated) (eurofins) with an oligonucleotide length of 23 nt was used. As a negative control nuclease-free water was used."[14]

Samples were diluted with RNase-free water of the Kit to 5 ng/µl. A master mix was prepared using for each sample 0.5 µl 10X Poly(A) Buffer, 0.5 µl ATP, 0.3 µl Poly(A) Enzyme, 1.7 µl RNase-free water. The Poly(A) Reaction Mix was mixed 3 s with a small shaker (Vortex) and centrifuged for 5 s to spin down the contents. 2 µl of each sample were added to 3 µl of Poly(A) Reaction Mix. Samples mixtures were centrifuged for 5 s to spin down the contents. Subsequently, samples were incubated 45 min at 37°C for polyadenylation, followed by 10 min at 65°C to stop the reaction. Samples were then cooled down to 4°C.

A Ligation Reaction Mix master mix was prepared containing for each sample 3 µl 5X DNA Ligase Buffer, 4.5 µl 50 % PEG 8000, 0.6 µl 25X Ligation Adaptor, 1.5 µl RNA Ligase and 0.4 µl RNase-free water. The Ligation Reaction Mix was mixed 3 s with a small shaker (Vortex) and centrifuged for 5 s to spin down the contents. To each polyadenylated sample from the previous step 10 µl of Ligation Reaction Mix was added. These mixtures were mixed 3 s with a small shaker (Vortex) and centrifuged for 5 s to spin down the contents. Mixtures were then incubated 60 min at 16°C to perform the ligation of the ligation adaptor to the polyadenylated samples and cooled to 4°C afterwards.

A RT Reaction Mix, to perform reverse transcription, was prepared containing for each sample 6 µl 5X RT Buffer, 1.2 µl dNTP Mix (25 mM each), 1.5 µl 20X Universal RT Primer, 3 µl 10X RT Enzyme Mix, 3.3 µl RNase-free water. The RT Reaction Mix was mixed 3 s with a small shaker (Vortex) and centrifuged for 5 s to spin down the contents. 15 µl of RT Reaction Mix were added to each ligation reaction product from the previous step. Mixtures were mixed 3 s with a small shaker (Vortex) and centrifuged for 5 s to spin down the contents. Finally, the new mixtures were incubated 15 min at 42°C for the reverse transcription, followed by 5 min at 85°C to stop the reaction and subsequently cooled down to 4°C.

Next, a miR-Amp Reaction Mix to amplify the product was prepared containing for each sample 25 µl 2X miR-Amp Master Mix, 2.5 µl 20X miR-Amp Primer Mix and 17.5 µl RNase-free water. The miR-Amp Reaction Mix was mixed 3 s with a small shaker (Vortex) and centrifuged for 5 s to spin down the contents. 5 µl of RT reaction product from previous step were mixed with 45 µl miR-Amp Master Mix, mixed 3 s with a small shaker (Vortex) and centrifuged for 5 s to spin down the contents. miR-Amp mixtures were incubated 5 min at 95°C for enzyme activation, 14 x {3 s at 95° C for denaturing followed by 30 s at 60 °C for annealing} and finally 10 min at 99°C to stop the reaction. Mixtures were then cooled down to 4°C.

So generated cDNAs were diluted 1:10 using the RNase-free water of the Kit.

"For qPCR the Master Mix reaction was composed of 10 µl QuantiTect SYBR® Green (Qiagen), 2 µl amplification primer mix from the TaqMan™ Advanced miRNA cDNA Synthesis Kit (Thermo Fisher), and 8 µl of diluted sample. qPCR, including a melting curve of the formed amplicons after the last cycle, was run on a LightCycler® 480 Instrument II with the following settings: 15min 95 °C, 40 x: 15 s 94 °C – 30 s 60 °C – 30 s 72 °C – Single Data Acquisition, 2 min 72 °C, Melting curve."[14]

C_t-values were generated by the LightCycler® 480 Software.

3.4.5.   Capillary gel electrophoresis

"For RNA gel electrophoresis the Agilent RNA 6000 Nano Kit was used, and the gel setting was prepared following the manual:

In a first step the gel matrix was equilibrated to room temperature and filtered by centrifuging through the provided spin filter, 10 min at 1,500 x g. Next the dye concentrate was mixed thoroughly for 10 sec on a small mixer (Vortex) and spined down briefly. 1 µl of the dye concentrate was added to 65 µl gel matrix. The mixture was mixed thoroughly and spined 10 min at 13,000 x g. A RNA Nano Chip, provided within the kit, was put on the chip priming station. 9 µl of gel-dye mix was pipetted on the bottom of the well marked with "(G)". The plunger of the syringe of the priming station was pressed down until was held by the clip. After exactly 30 sec the plunger was released and after further 5 sec the priming station was opened. Subsequently the 9 µl of the gel-dye mix was added to each well marked with "G". Then 5 µl of the marker was added to each sample well and to the well marked with the ladder symbol. Finally 1 µl of heat denatured ladder (2 min at 72 °C) was added to the well marked with the ladder symbol and 1 µl of each sample was added to its regarding well. The chip was then mixed 60 sec at 2400 rpm using the provided vortex shaker with the chip adaptor.

The chip was immediately run "on a 2100 Bioanalyzer Instrument with the 2100 Expert Software (Agilent) and the total RNA Nano program. Samples were applied in triplicates. As a negative control a particle suspension based sample was used that resulted in a "too low" signal in the Qubit® concentration measurement, to identify possible background noises that might have been generated by residual nanoparticles leftover in the samples after precipitation, like those of inorganic substrates or organic pigments."[14]

3.5. Computational analysis of the molecular electrostatic potential

To visualize the differences of the molecular electrostatic potential (MEP) of each nucleotide, molecules of interest were drawn using Materials Studio (Biovia). On drawn molecules electron density and the MEP were applied using the VAMP tool of the software. From these results a MEP torque (Fig. 13) was calculated. Therefore, first the distance D_a between the C_1-atom of the ribose and the outer atoms of the base (without the nearest nitrogen), were measured. Second

the mean value of the electrostatic potential φ_a around each outer atom of the base was measured. From this data the sum of all MEP torques of each base b was calculated as $M_b = \sum D_a \times \varphi_a$
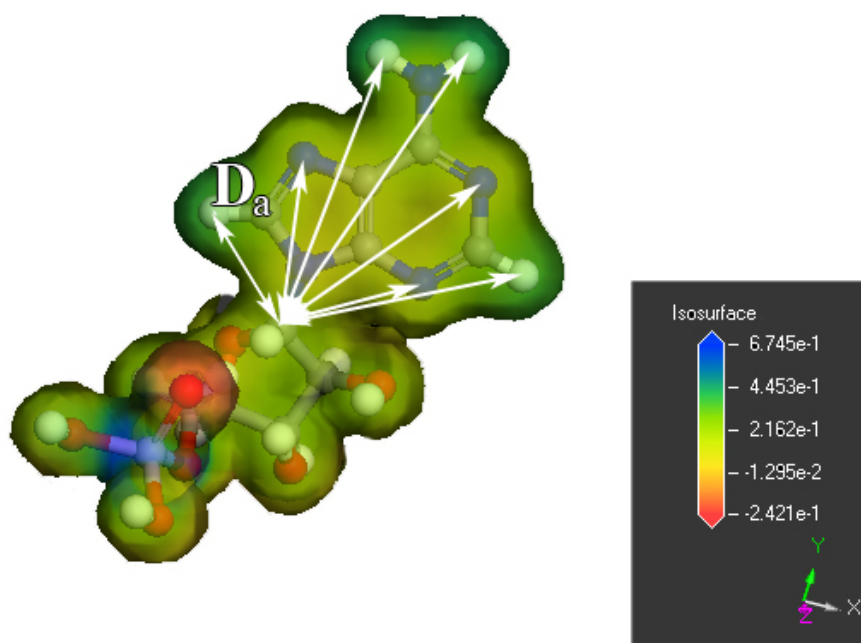
Figure 13: MEP torque calculation of AMP. In white depicted are the distances between the outer atoms of the base and the C_1-atom. The isosurface scale indicates the measured MEPs regarding the color of the cloud at a certain location of the molecule.

4. Results and Discussion

4.1. Influence of selected biomolecules on the OSWD in water

4.1.1. Scanning tunnelling microscopy and coverage measurements

To explore environment friendly possibilities to improve SAM formation of organic pigments on graphite by OSWD in water, a STM screening of 20 different samples that differ in the added (bio-)molecules, including the control sample (no added (bio-)molecule, only pigment in H_2O) was performed (Fig. 14), with γQAC as the SAM generating organic pigment. From each 30 STM images with 222 nm x 222 nm size were analyzed, as described above.

The H_2O- γQAC control sample was taken as a reference value ((11.6 +/- 1.5) % coverage with SAM of γQAC) for comparative studies. If not differently indicated, results are given as Mean +/- SEM for a more straightforward comparison of the mean.
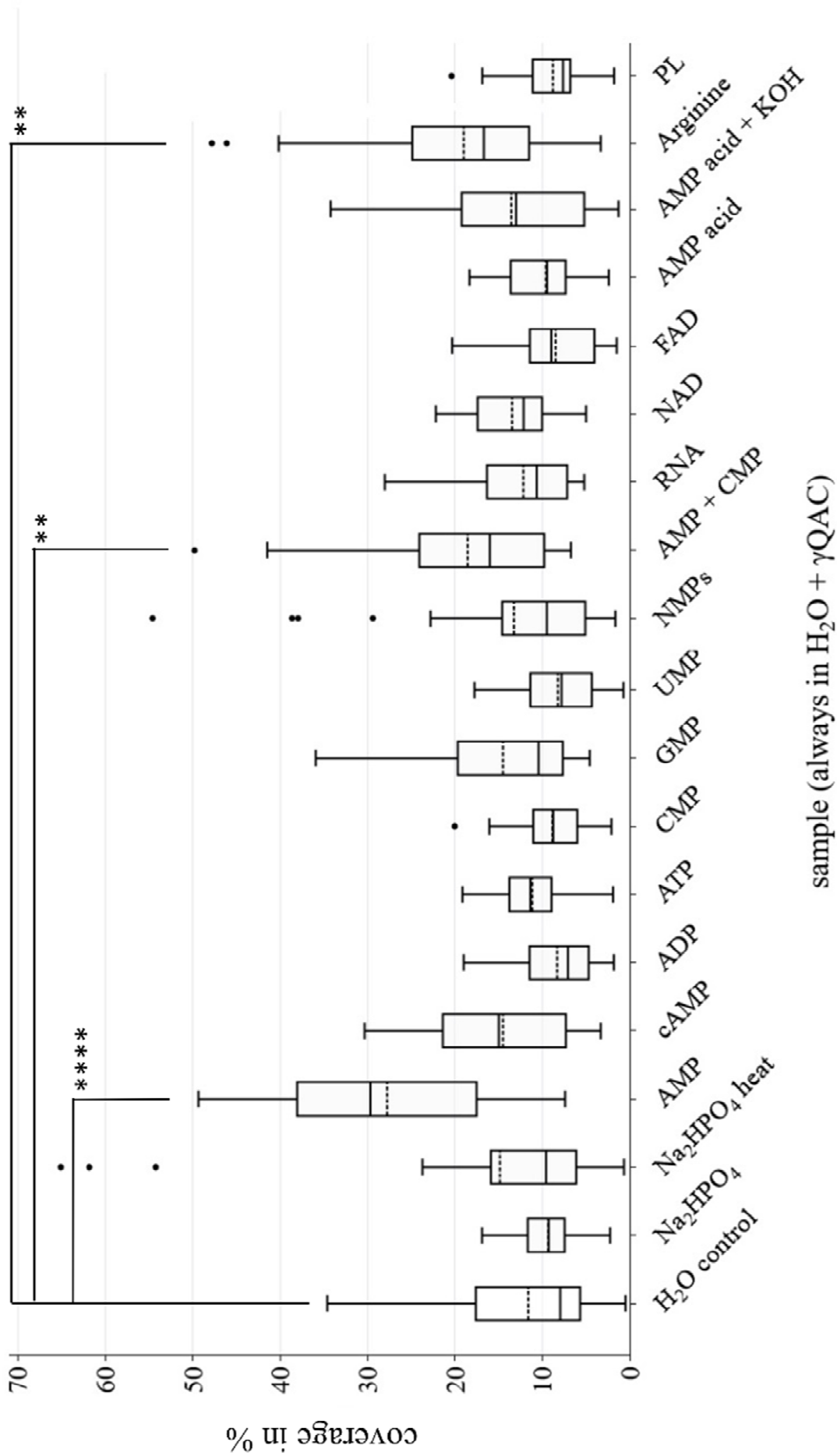
Fig. 14: see next page.

Figure 14: Boxplots of coverage rates in % of all measured samples with 5 measurements of each of the six replicates (n = 30) of each sample. The dotted line within the box is the mean value auf each dataset. The solid line inside the box represents the median, that means where 50 % of all datapoints of this dataset are lower than this value and 50 % are higher. The lower and upper endings of the box represent the first and the third quartile, where 25 % of all datapoints are lower than the median and 25 % are higher, respectively. The ends of the whiskers indicate the minimum and the maximum of the dataset, excluding any outliers. The outliers that differ significantly from the dataset are plotted as single spots, above or underneath the whiskers. Boxplots were chosen in this thesis to represent both the distribution of the datapoints, and the statistic mean. Statistical analysis: Samples were analysed using t-test with Welch´s correction with the "H_2O control"-sample used as the reference. p-values: *: $p < 0.05$; **: $p < 0.01$; ***: $p < 0.001$; ****: $p < 0.0001$.

Before analyzing different biomolecules, two mixtures of γQAC with Na_2HPO_4 were examined, one applied and dried at room temperature, the other one applied and dried at 60 °C, as the later was the method so far used in our working group. Though the heated-up sample showed a high coverage in three of 30 samples, a significant overall increase of SAM formation could not be confirmed (Fig. 14; H_2O and Na_2HPO_4) in contrast to earlier studies by Eberle et al.[13].

As AMP plays an extraordinary number of central roles in biological systems and therefore seemed to be an interesting candidate as a possible bimolecular enhancer of OSWD in water, a sample containing γQAC and AMP was analyzed. AMP showed a significant, more than a double higher amount ((27.7 +/- 2.3) % average coverage) (Fig. 14; AMP) of SAM formation of γQAC as the H_2O-control sample with a p-value of $3.13 * 10^{-7}$.

In order to conclude from comparative results, which are the crucial properties needed for biomolecules to enhance the coverage, further AMP derivates and RNA nucleotide monophosphates were included in the screening.

Hereby no significant increase of SAM formation of γQAC could be found. Adding cyclic AMP (cAMP) to the aqueous γQAC suspension leaded to an average coverage of (14.50 +/- 1.4) %. Adenosine diphosphate (ADP) and adenosine triphosphate (ATP), neither showed a significant increase with (8.3 +/- 0.9) % coverage in case of ADP and (11.1 +/. 0.8) % coverage in case of ATP (Fig 14; cAMP, ADP, ATP).

Analyzing the coverage of the γQAC-samples containing each one of the other three RNA nucleotide monophosphates CMP, GMP and UMP, also did not present significant increase of SAM formation of γQAC, with average coverages of (8.8 +/- 0.7) % (CMP), (14.5 +/- 1.7) % (GMP) and (8.2 +/- 0.9) % (UMP) (Fig. 14; CMP, GMP, UMP).

To test if the combination of the nucleotide monophosphates (NMPs), containing AMP will influence the coverage, samples containing mixtures of NMPs were included into the screening. A mixture of all four NMPs (AMP, CMP, GMP and UMP) was analyzed. Though this sample showed some regions with high coverage, the total average coverage came to (13.2 +/- 2.3) % and did not show a significant difference (Fig. 14; NMPs). In contrast to a mixture only containing AMP and CMP, that equally showed some regions with relatively very high coverage, totaling in an average coverage of (18.1 +/. 1.9) % and a significant increase with a p-value of 0.01 (Fig. 14; AMP + CMP).

As the mixture of NMPs did not show a significant increase of SAM covered surface area, but the mixture of AMP and CMP does, and to see if AMP as a part of a macromolecule will influence the OSWD rate, a γQAC sample containing a microRNA (miRNA-34) was analyzed. However, this sample did not show significant difference. The average amount of coverage was (12.1 +/- 1.1) % (Fig. 14, RNA).

As AMP is the basic chemical structure of many other biomolecules with central roles in biomolecular pathways and showed the extraordinary increase of the coverage, a sample containing NAD and a sample containing FAD, both being chemical structure relatives to AMP, were included in the sample set. NAD showed an average coverage of (13.4 +/- 0.8) % and FAD of (8.4 +/- 0.8) %. None of both showed a significant difference (Fig. 14; NAD, FAD).

To get further overview, what might be the reason of the extraordinary increase of coverage when adding AMP, a sample containing adenosine-monophosphoric acid (AMP acid) (Fig. 14, AMP acid) was examined, as higher pH showed to enhance SAM formation by OSWD[13] and therefore lower pH should inhibit SAM formation by OSWD. Indeed, no increase of the average coverage in this sample could be found. It showed an average coverage of (9.6 +/- 0.8) %. Interestingly, adding KOH to the AMP acid sample could not recuperate a higher coverage as this sample showed an average coverage of (13.5 +/- 1.6) without significance (Fig. 14, AMP acid + KOH). This result leads to the assumption that the sequence of adding ions like Na^+ or K^+ might play a crucial role regarding their effect on the OSWD coverage ("effect of sequence"). The AMP containing sample contains Na^+ from the beginning of the sample preparation process on, as part of the used AMP salt. Thus, Na^+ is already involved when AMP

comes in contact with the suspended QAC particles. It showed a significant increase of the coverage compared to the water control sample. The AMP acid containing sample on the other hand does not contain cations when coming in contact to the particle surfaces in the beginning. The powder is first mixed with aqueous solution of AMP and then KOH-solution is added. These findings offer interesting indications for further research, using the "effects of sequence" of the addition of reagents as a probe for further analysis of the interaction between AMP and QAC and other effects shown in this thesis. To understand this effect however, more experimental analysis is necessary and would go beyond the scope of this thesis.

Furthermore, two biomolecules of other molecular species were included in the screening: the amino acid arginine and a mixture of phospholipids. According to the known stacking capabilities of arginine with carbon ring systems[51] it may be possible that the coverage gets enhanced by the addition of this amino acid, as it will be discussed later (Chapter 4.3). Indeed, the sample containing arginine showed a significant increase of the average coverage with (18.8 +/- 2.2) % and a p-value of 0.008 (Fig. 14, Arginine). On the other hand, phospholipids act like liquid crystals, which enhance Casmir-like fluctuation-induced forces within the OSDW system[52]. Furthermore, phospholipids represent a further group of biomolecules containing phosphates besides to the nucleotides, tested before. However, the sample containing the phospholipids mixture did not show a significant change, its average coverage was (8.8 +/- 0.7) % (Fig. 14, PL). Likely, the dissolved phospholipids form micelles in a rapid way, and therefore their liquid crystal characteristics as well as others get lost regarding the entire system and are no longer operational for the OSWD.

In addition to the shown samples in Fig. 14 also a sample containing adenine was included. It resulted that adenine, as it is soluble in water, covers the surface area by itself (Fig. 15) and no SAMs of QAC could have been found.
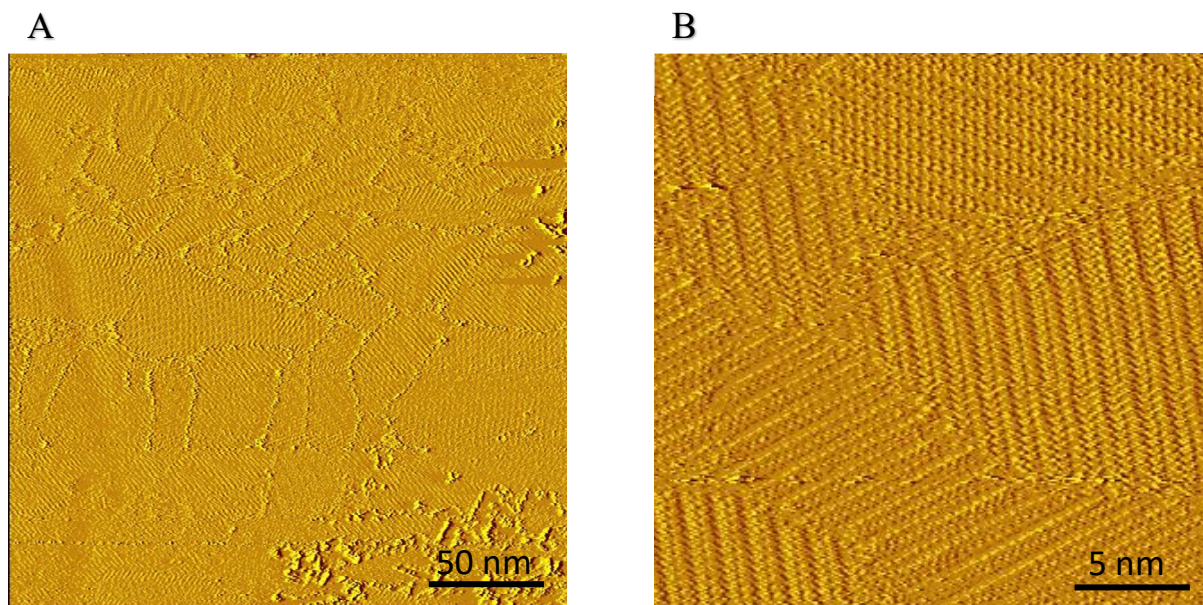
Figure 15: STM measurements of the QAC-Adenine-H2O sample. Only adenine itself formed monolayers on the graphite surface. There were not found any QAC domains. **(A)** shows a scan with 222 nm x 222 nm and **(B)** a scan after zooming in to 22 nm x 22 nm.

Further analysis of the results showed that AMP also leads to a significant higher coverage of the substrate´s surface with QAC SAMs in comparison with the other NMPs (CMP, GMP and UMP) (Fig. 16, Tab. 1). In addition, also GMP, though not leading to a significant increase of SAMs in comparison to H_2O control sample, shows a significant higher coverage of QAC SAMs in comparison with the samples containing CMP and UMP. Ranked this means that AMP leads to the highest coverage, GMP to medium coverage and CMP and UMP show low coverage.
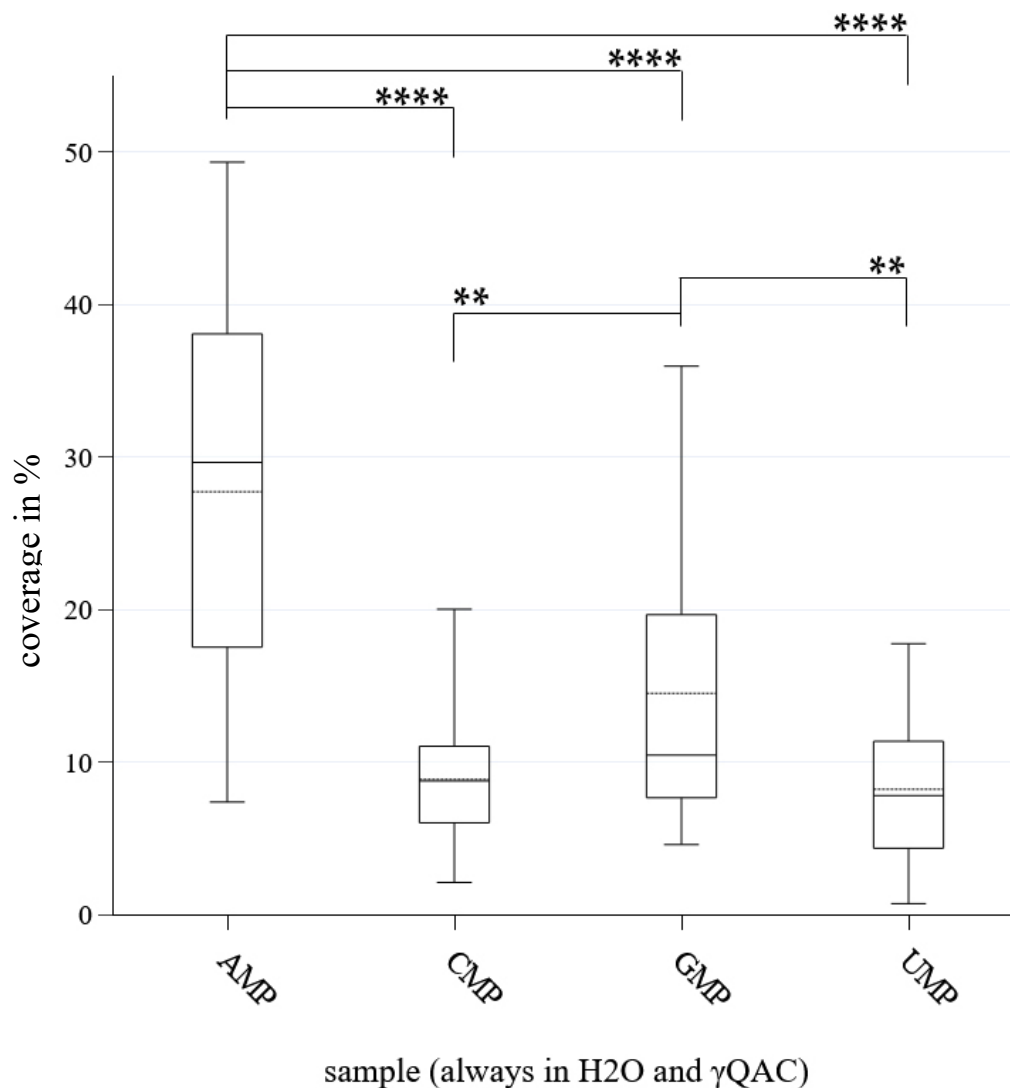
Figure 16: Boxplots and statistical analysis of differences in the coverage rate within the group of nucleotide-monophosphates. Boxplots follow the same usual system of plotting the data as indicated above. Statistical analysis: Samples were analysed using t-test with Welch's correction p-values: *: $p < 0.05$; **: $p < 0.01$; ***: $p < 0.001$; ****: $p < 0.0001$.

Table 1: Coverage in % and significance values of the regarding comparisons (QAC)

QAC	Coverage in %	AMP	CMP	GMP	UMP
AMP	27.7 +/- 2.3	/			
CMP	8.9 +/- 0.7	2.742 E^{-09}	/		
GMP	14.5 +/- 1.7	2.025 E^{-05}	0.004	/	
UMP	8.2 +/- 0.9	1.214 E^{-09}	0.578	0.002	/

To examine if the enhancing effect of AMP on SAM formation by OSWD in water also is true for other organic pigments, γQAC was exchanged with the pigment phthalocyanine (Phth) and the coverage was measured exemplarily for three sample: Phth in water, Phth in water with AMP and Phth in water with GMP (Fig. 17).
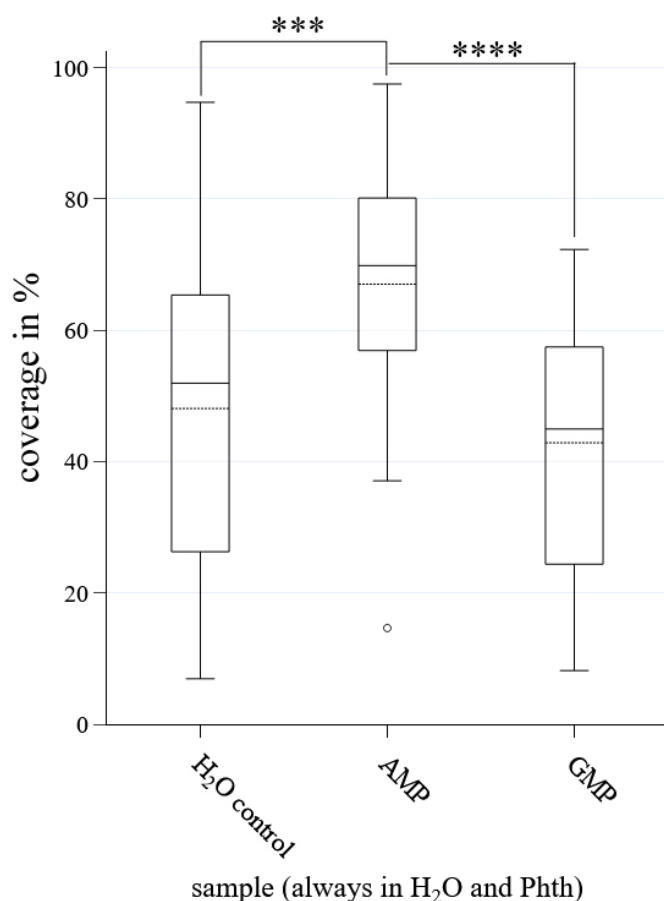
Figure 17: Boxplots and statistical analysis of differences in the coverage rate using phthalocyanine instead of QAC. Boxplots follow the same usual system of plotting the data as indicated above. Statistical analysis: Samples were analysed using t-test with Welch´s correction p-values: *: $p < 0.05$; **: $p < 0.01$; ***: $p < 0.001$; ****: $p < 0.0001$.

Table 2: Coverage in % and significance values of the regarding comparisons (Phth)

Phth	Coverage in %	H_2O only	AMP	GMP
H_2O only	46.2 +/- 4.4	/		
AMP	69.5 +/- 3.2	0.0011	/	
GMP	42.9 +/- 3.6	0.3633	5.405 E^{-06}	/

The H$_2$O control sample, only containing Phth and water generated an average coverage of (46.2 +/- 4.4) %.

Indeed, the sample containing AMP showed again a significant increase of SAM of Phthalocyanine, generated by OSWD in water. AMP enhances the SAM formation by 1.5-fold to (69.5 +/- 3.2) % of SAM covered area, with a p-value of 0.001. In contrast the sample containing GMP again did not show any increase of SAM formation in comparison with the sample without any nucleotide, but an average coverage of (42.9 +/- 3.6) %. However, the AMP containing sample also shows a significant higher coverage than the GMP containing sample (42.9 +/- 3.6) %), with a p-value lower 0.0001.

Based on these results it was subsequently examined, which characteristics make AMP unique in comparison to the other NMPs and if there are similar characteristics for arginine, too.

4.1.2. Comparison of the characteristics of RNA nucleotides

To analyse, which characteristics make AMP unique in comparison to the other molecules used in this study, and what therefore might be the reason for the shown OSWD enhancement effect, six different attributes were analyzed:

- The pH value, as earlier studies showed, that higher pH leads to higher coverage by OSWD[13].
- The zeta potential, as earlier studies showed suspensions with more negative zeta potential lead to higher coverage[13].
- The molecular electrostatic potential, to analyse the distribution of regions with different reactivities and possible different interactions of the NMPs with the QAC molecules.
- Hydrogen bonds, to see, where and how NMPs might interact with the QAC molecules and water molecules.
- stacking abilities, to analyse further intermolecular incidents.

4.1.2.1. pH value

As it was shown before[13], in many cases a higher pH of the sample also leads to a higher coverage, the pH values of a representative sample set were measured, as described, and set into to correlation with the coverage, as analysed above.
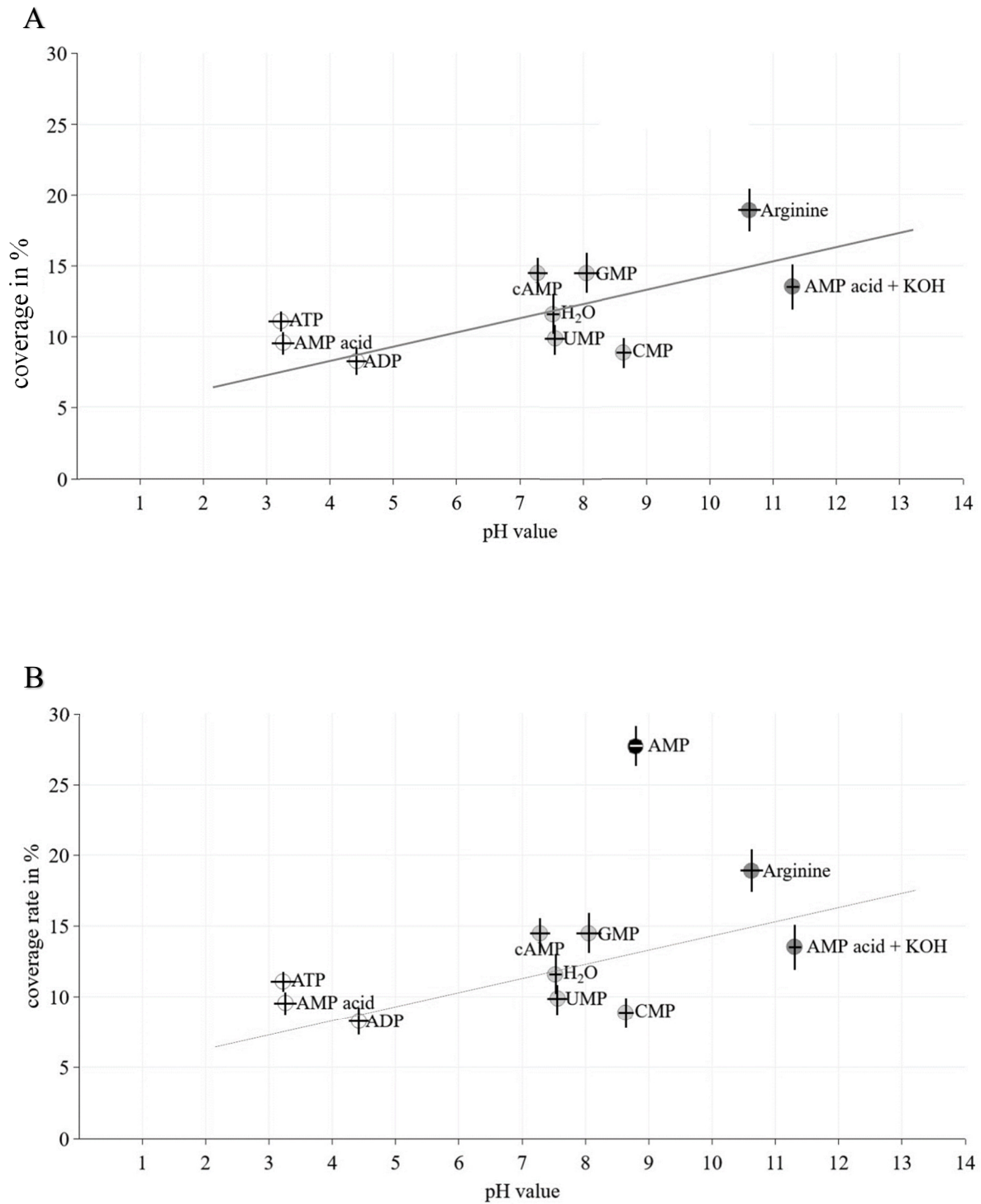
Fig. 18: see next page.

Figure 18: Comparison of pH values of the samples correlated with the regarding coverage rate in %. White dots: low pH and low coverage; light grey dots: medium pH and medium coverage; dark grey spots: high pH and medium or high coverage; dark spot: AMP, medium pH but high coverage. Crosses within the data points indicate the SEM: horizontal lines the SEM of the pH measurements and vertical lines the SEM of the coverage. **A:** sample set without AMP with the diagonal line indicating the correlation trend line within this subgroup. **B:** sample set with AMP, which breaks the correlation.

Visually, as shown in Fig. 18, the results split in three groups and one data point, that does not group with any other subset. There is one group with low pH and low coverage (samples containing ATP, AMP acid and ADP), one group with medium pH and medium coverage (samples containing cAMP, GMP, H_2O, UMP and CMP) and one group with high pH and medium or high coverage (samples containing Arginine and AMP acid with KOH). The results of this subsample set match with the results of previous studies by Eberle et al.[13], who showed that lower pH leads to lower coverage and higher pH leads to higher coverage. Excluding therefore the AMP sample as an outlier from the dataset, the Pearson correlation coefficient of these samples is 0.61 with a p-value of 0.048, and therefore can be defined as a moderately high correlation. The sample containing AMP, however, forms the outlier of the sample set, with medium pH but very high coverage. Including the sample containing AMP in the calculation of the correlation coefficient drops its value to 0.47 with a p-value of 0.14. Though a correlation coefficient of 0.47 is defined as a moderate correlation, the high p-value leads to the rejection of the null hypothesis (correlation between pH and coverage) in the case that AMP is added to the sample set.

These findings led to the assumption, that influencing the OSWD in water with biomolecules indeed also is dependent on the pH, but it seems that further factors do influence the system strongly, especially when it comes to the enhancement using AMP. Therefore, the zeta potential of a group of selected samples was examined.

4.1.2.2. Zeta potential

As Eberle et al. found an indirect proportional connection between the z33 value of the zetapotential (the value where 33 % of the distribution is more negative and 66 % more positive) and the coverage of OSWD[13], the zeta potential of the samples were measured. Four aqueous QAC samples were selected: with AMP, CMP. GMP and the control sample with H_2O, as AMP showed significant high coverage, GMP medium and CMP low coverage.
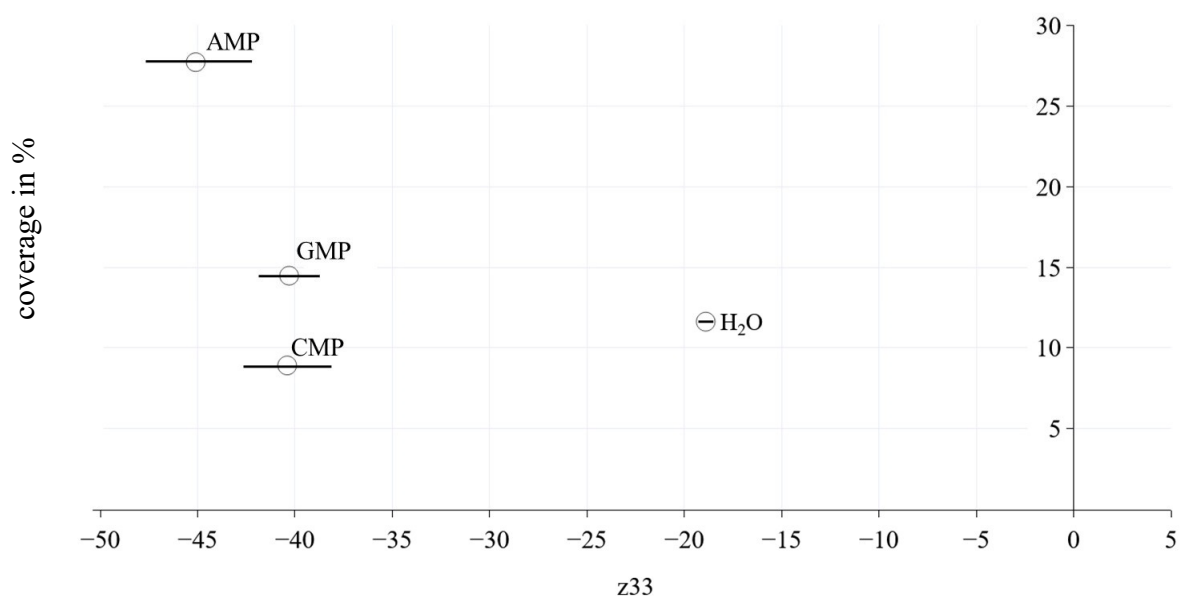
Figure 19: Comparison of z33 values of the samples correlated with the regarding coverage rate in %. The horizontal black lines indicate the SEMs of the z33 measurements. SEMs of the coverage are not shown, due to clarity issues. SEMs of coverage can be seen in previous graphics (Figure 19).

Looking at these results, visualised in Fig. 19, it was found that the AMP sample shows both the lowest z33 value (-45.1 +/- 3.3) and the highest coverage, but the other three samples do not fit in this schema. GMP and CMP show almost the same z33 value (-40.3 +/- 1.5 and -40.4 +/- 2.6) but do differ significantly in their enhancement effect on OSWD in water, with GMP leading to a medium coverage of the substrate´s surface area with QAC SAMs and CMP to a low coverage. Including the H_2O control sample with a z33 value of -18.9 +/- 0.4, only a correlation coefficient of -0.41 was found, which can be seen as slightly moderate correlation.

However, the p-value of the correlation was calculated to be 0.59 and therefore a significant correlation is not given. These results led to the assumption, that further factors influence the OSWD systems that contain biomolecules.

4.1.2.3. Molecular electrostatic potential

Since z33 measurement only resulted in a slightly moderate correlation, further analysis about the differences of the NMPs were conducted. One interesting point seemed to be the possible interactions sides of the NMPs with the γQAC crystal.

To get an overview of these possible interaction sides of the NMPs and the QAC molecules the molecular electrostatic potential (MEP) of AMP, CMP and GMP were analysed as described above. To express the MEP mapping in numbers and to analyse possible correlation between the distribution of the MEP and the coverage, a MEP torque was calculated as described above.
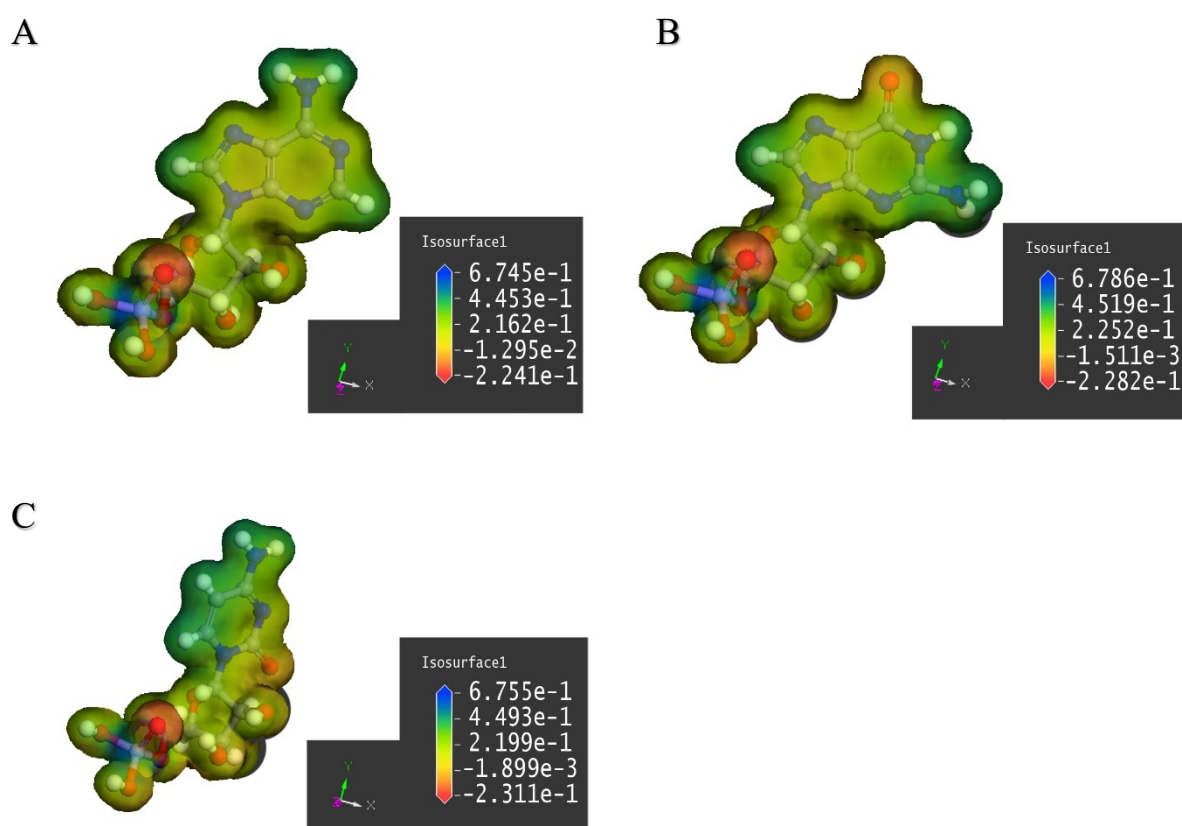
Figure 20: Chemical structure as ball-stick-models with the regarding MEPs depicted as a cloud with colour code of **(A)** AMP, **(B)** GMP and **(C)** CMP.

Logically the ribose-phosphate part of all three molecules do not differ from each other, as it can also be seen in Fig. 20. But comparing the MEPs of the base part of the three NMPs (AMP, CMP and GMP), one can state that only AMP does not show any negative potential area, whereby CMP and GMP do have a slightly negative potential area, which is around the oxygen atom, as one could already suspect. All three molecules, however, show four areas of slightly positive potential areas, which are around the hydrogens, as common. Interestingly the two hydrogens of the amide group of the adenine group of AMP is located more far away from the C1' of the ribose than the amide groups of cytosine (CMP) and guanine (GMP), which might be an important factor when it comes to an interaction with the QAC molecule. Since the ribose-phosphate group also expands in the z-direction the amide group of adenine is less likely to undergo steric hindrance, when it comes to an interaction of the AMP molecule and the γQAC crystal, e.g., between the amide group of AMP and the oxygen of QAC. Furthermore, since negatively charged regions are missing in the adenine group of AMP, the AMP might undergo less repulsive energies, when approaching to a γQAC crystal.

If a possible interaction between the QAC molecules and the NMP is generated via the amino groups of QAC, GMP shows to be a suitable candidate to show the strongest interaction, as the oxygen of the guanine group is located more far away from the more three-dimensional ribose-phosphate part and therefore might undergo less steric hindrance.
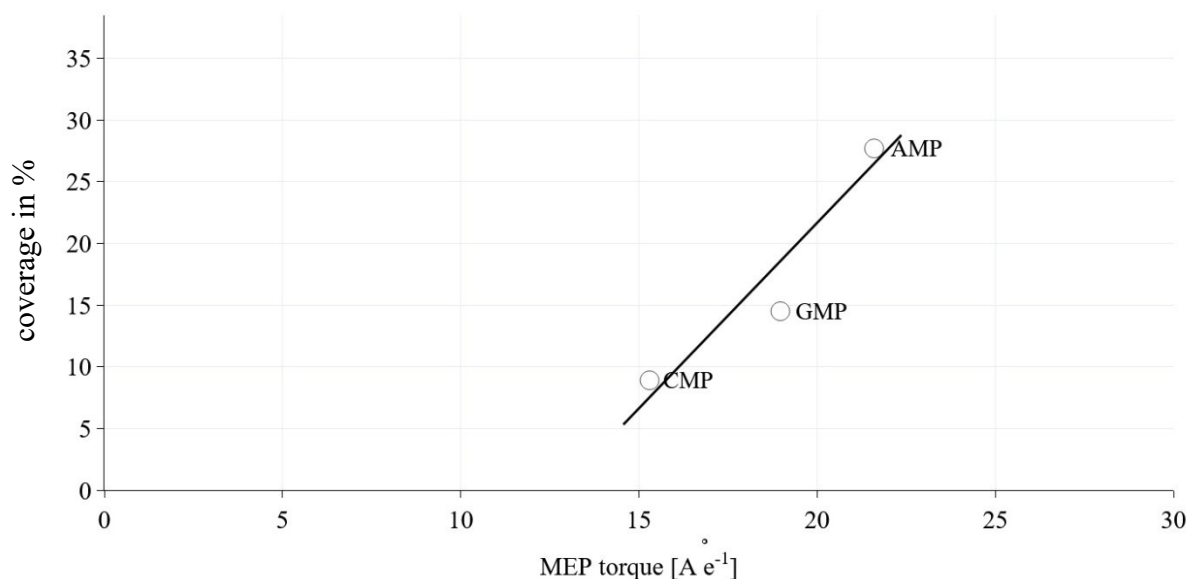
Figure 21: Chemical structure as ball-stick-models with the regarding MEPs. The black line indicates the correlation trendline. SEMs of coverage can be seen in previous graphics.

To test whether there is a relationship between coverage and MEP leverage a Pearson correlation analysis was performed. The Pearson correlation coefficient r was calculated to be 0.95. This means, that there is a very high, positive correlation between the coverage and MEP leverage in this sample set (Fig. 21). However, the calculated p-value of the statistical Pearson correlation analysis is 0.21 and therefore the correlation cannot be taken as significant. For a more reliable statement about the significance of the Pearson correlation the sample set would be needed to be enlarged.

These findings let suppose that the interaction between the biomolecule and the γQAC crystal might be one critical point to explain the extraordinary enhancement effect of AMP on the OSWD in water. But not only interactions between the biomolecule and the γQAC crystal, but also the interaction between the biomolecules themselves are of interest to hypothesise why AMP enhances the OSWD in such a strong way, but other (bio-)molecules do not. Therefore, in a next step interaction between the nucleotides themselves were analysed.

4.1.2.4. Stacking

Further literature search about the different characteristics of the nucleotides brought the study to an interesting point: nucleotides can undergo stacking, that means that the base part of the nucleotide can align over each other by pi-pi-stacking[53–56]. How much and how fast the stacking happens when the nucleotides are brought in solution, can be calculated as equilibrium constants, what has been done by various research groups before[53–56]. As these equilibrium constants describe the stacking ability of the substance, they will further be called stacking constants in this thesis. Interestingly, the different nucleotides do have different stacking constants, both in homogenous mixtures of each nucleotide per se as well as in heterogenous mixtures of different nucleotides.

Table 3: Comparison of stacking constants of selected nucleotides

Sample	Coverage in %	K_{eq} Sigel et al.	K_{eq} Neurohr et al.	K_{eq} Norberg et al. (4.5 Å)*	K_{eq} Norberg et al. (5 Å)*
AMP	27.7 +/- 2.3	15	1.92	0.11	0.97
CMP	8.9 +/- 0.7	1.4	No data	0.01	0.04
GMP	14.5 +/- 1.7	8	1.29	0.02	0.29
AMP + CMP	18.2 +/- 1.9	No data	No data	0.11	0.39
Correlation		0.98	Sample set too small	0.84	0.99
p-value of correlation		0.135	for stat. analysis	0.159	0.009

* Norberg et al. defined two different stacking constants, depending on the distance (4.5 Å and 5.0 Å) of two molecules.

After performing a correlation analysis, it was found that the coverage of substrate covered with SAM of QAC by OSWD in water is highly correlated with the stacking constants. And this is true not only for one data set of constants but for all constants from different research groups. AMP, which enhances the OSWD in the strongest way, leading to the highest coverage also showed up to have the highest stacking constants in comparison with CMP (low coverage, low stacking constant) and GMP (medium coverage and medium stacking constant). Also, the outcome of the sample containing a mixture of AMP and CMP follows the same correlation: medium high coverage and medium high stacking constant (Fig. 22). Though the sample set was very small, in one case the statistical correlation analysis even showed a significant p-value of 0.009.

That means, that the stronger the tendency to undergo stacking the higher the enhancement effect of this nucleotide on the OSWD in water.
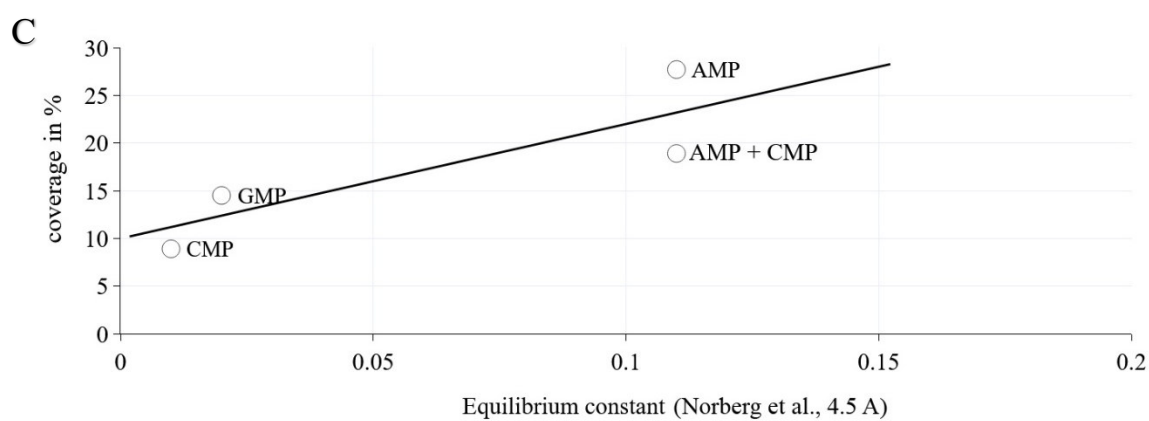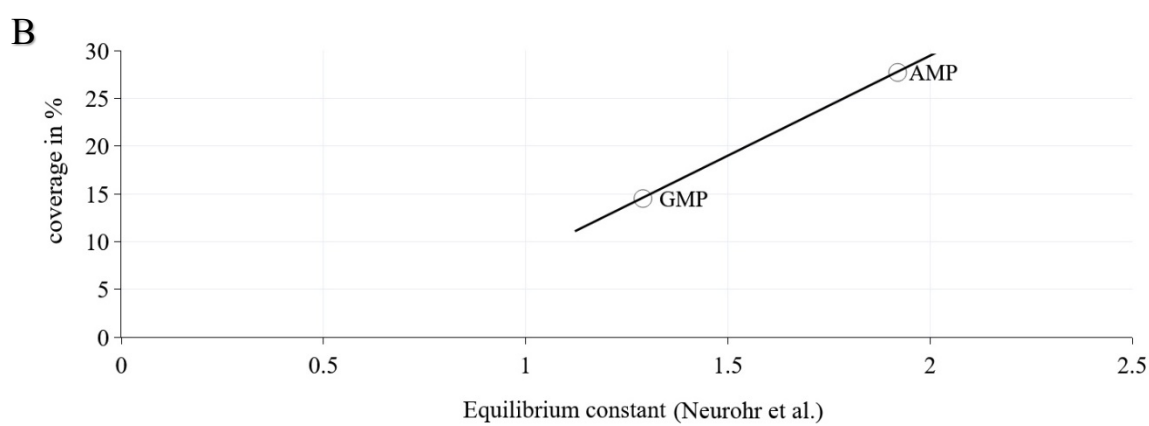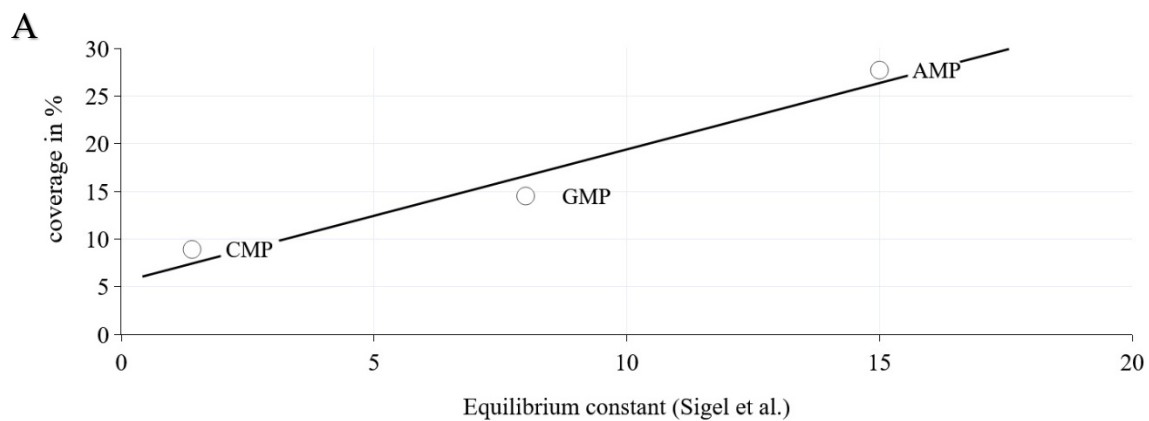
D
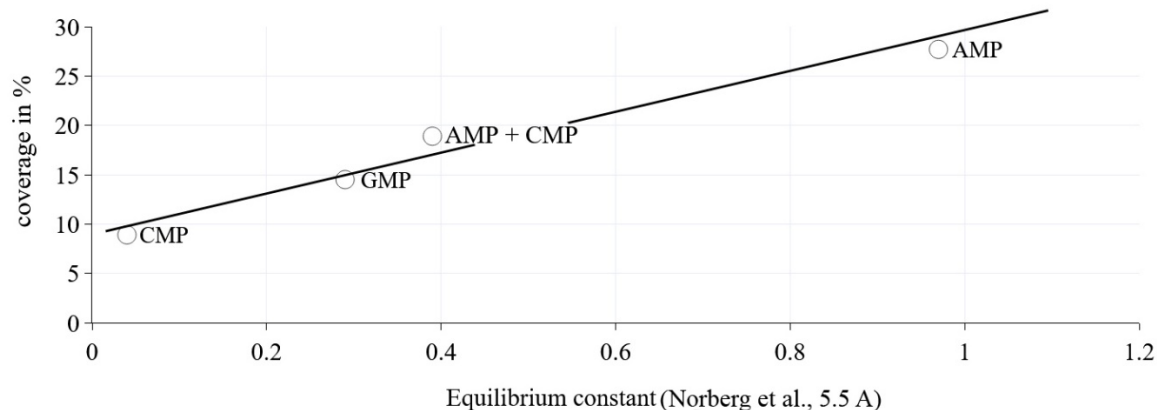
Figure 22: Graphical representation of possible correlations between measured coverage rates and stacking constants published before by (A) Sigel et al. (B) Neurohr et al. (C) Norberg et al. at 4.5 Å* and at (D) 5.5 Å* distance. (* Norberg et al. defined two different stacking constants, depending on the distance (4.5 Å and 5.0 Å) of two molecules.)

Furthermore, Tribolet and Sigel found that AMP is the only NMP that can undergo indefinite stacking, which is another indication, that stacking ability is an important factor to explain the outstanding enhancement effect of AMP on OSWD in water[54].

Moreover, also arginine is known to have a high ability for stacking with aromatic groups[57]. And indeed, arginine does also show a significant higher coverage of graphite surface with the QAC molecules when added to OSWD-sample (Fig. 14).

These findings lead to the assumption that the stacking ability of a biomolecule is a central factor for its enhancement effect on the OSWD.

4.1.3. Summary I

To sum up the findings from chapter 4.1.1. and 4.1.2., the central finding is the extraordinary enhancement effect of AMP on SAM formation of QAC domains by OSWD in water. Even in a mixture with CMP and the other NMPs, some areas of high coverage could be found, likely caused by clusters of AMP in the mixtures. Neither the other NMPs nor the sample containing

derivates of AMP showed an increase of the coverage. Only adding the amino acid arginine, the aqueous γQAC sample led to a slight increase of covered surface area.

Analysing different characteristics of the (bio-)molecules used for the screening, a moderately high correlation between pH and the coverage though was found, but the outstanding increasing of the coverage in the AMP sample could not be explained, as the AMP did not show an extraordinarily high pH value. The enhancing of coverage by adding arginine could be explained by the high pH of the sample.

The same is true for the zeta value analysis: a correlation though was found, but only one of a slightly moderate way. Therefore, also the zeta potential differences within in the different samples do not explain the outstanding enhancement effect of AMP on the OSWD in water.

But indeed, a very strong correlation was found, comparing the MEPs using a MEP torque of three NMPs (AMP, CMP and GMP). That leads to the assumption, that the interaction of the (bio-)molecule with the γQAC, the water and the surface do have a strong influence on the enhancement abilities of AMP.

This assumption is supported by the findings, that AMP in comparison to CMP can interact over several hydrogen bonds with QAC at the same moment and that the AMP molecules can interact via hydrogen bonds in a denser package with the γQAC than CMP can.

With the base-part interacting with the γQAC crystal and the ribose-phosphate-part interacting with the water molecules, the NMPs might function as a kind of mediator between the γQAC and the water, reducing the surface free energy of the γQAC and pulling out some single QAC molecules from the crystal, which then can form SAMs on the substrates surface. As AMP also has the highest stacking ability, even more AMPs, triggered by the formation of the stack, will interact with the γQAC crystal, in comparison to the other NMPs.

These findings are further supported by the strong correlation between the stacking constants found by several other groups before and the coverage of the corresponding OSWD sample. Indeed, does AMP show to have each the highest affinity for stacking and further is the only NMP that can form indefinite stacks.

In the end it is noteworthy that one keeps in mind, that there is not only one factor, which can explain the outstanding enhancement effect of AMP on the OSWD system, but an interplay of many different chemical and physical characteristics.

Either way, the results from chapter 4.1.1. do show, that AMP is a suitable candidate to enhance the OSWD in water, also when other pigments are used. This is a relevant result especially when it comes to the necessity to increase the monolayer formation of semiconductors on substrates, for example to increase the power of possible doping of graphene.

4.2. Doping graphene by OSWD in water at room temperature

The knowledge how to enhance the OSWD in water is a crucial factor when it comes to the application of the OSWD method, for example within the semiconductor technologies, more precise when speaking about the doping of graphene.

In contrast to the commonly known way of doping graphene by substitution of single carbon atoms from its lattice by other atoms or by eliminating them, here it will be demonstrated a surface-transfer doping of graphene by thin film coating. Therefore, OSWD in water and at room temperature was used as a deposition method, to generate SAM of a semiconductive pigment, virtually insoluble in water, on the graphene surface. All experiments can be performed under ambient conditions and in a way, that low experimental effort is needed. These unique characteristics of this method make it an environmentally friendly and low-cost alternative to currently used doping methods.

Furthermore, the here shown technique to induce the OSWD on graphene, enables the application of Raman spectroscopy on the samples, to analyse possible doping effects on the graphene. The development of a method, whose product can be analysed by Raman spectroscopy, is a benefit, as Raman spectroscopy is a fast and precise method to analyse samples under ambient conditions, with few, known, confounding variables.

4.2.1.   Structure Determination
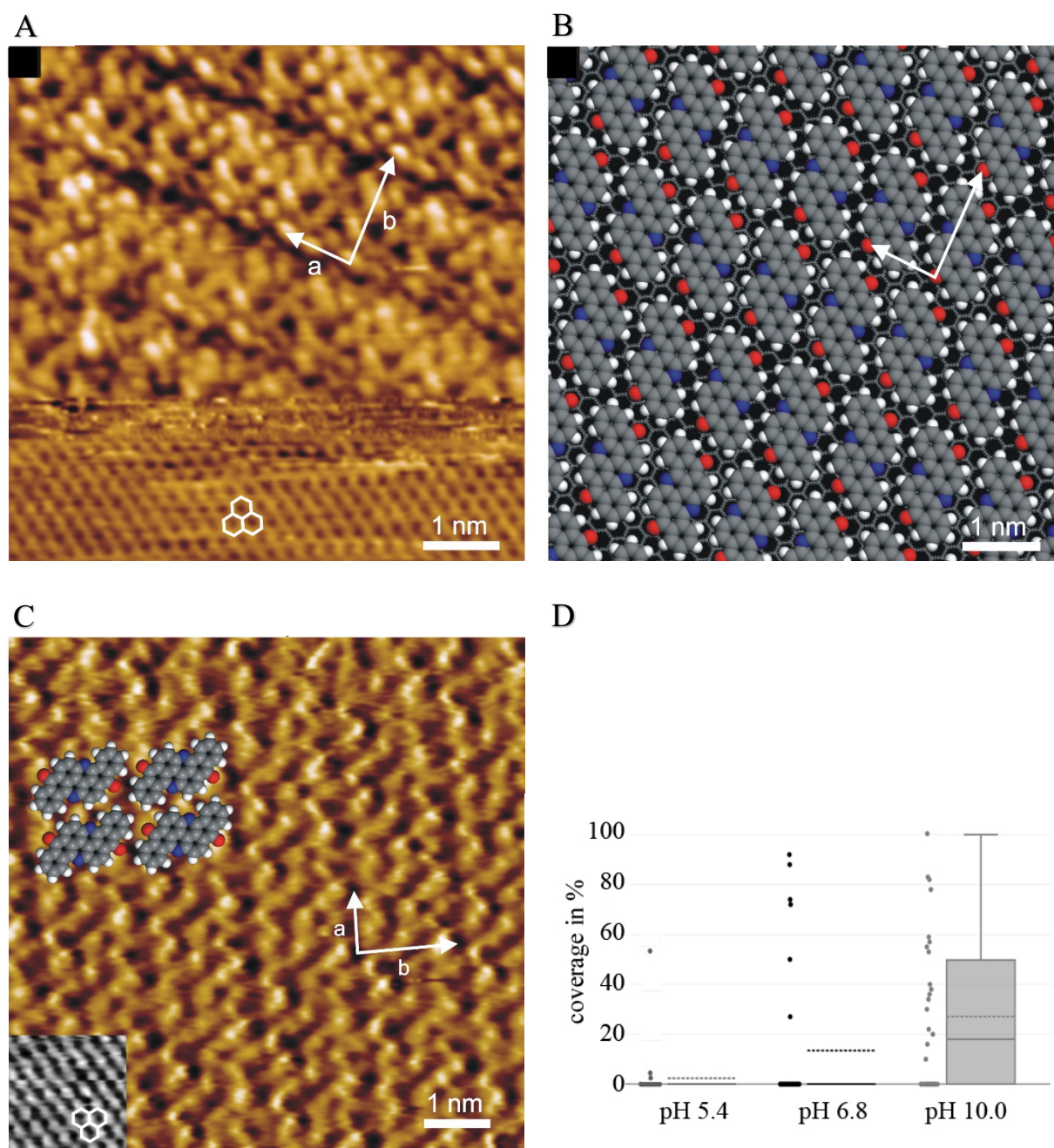
Figure 23: Structure determination of flavanthrone on graphene. **(A)** STM-Image of a flavanthrone adsorbate layer on graphene whereby the upper part shows the adsorbate layer, and the lower part shows the underneath lying graphene surface. The depicted lattice vectors 'a' and 'b' indicate the unit cell of the flavanthrone adsorbate. Furthermore, the honeycomb structure of graphene is shown on top of the graphene surface. **(B)** Force field simulated arrangement of flavanthrone molecules on a graphene surface. The unit cell vectors 'a' and 'b' are depicted in white. **(C)** STM picture of a flavanthrone domain on graphene, without dodecane coating. The measurement was carried out in air, without additional coating of the domain with dodecane to ensure that dodecane does not influence the formed structure. Unit cell vectors a

and b are depicted as well as four flavanthrone molecules simulated with Material Studios package (Accelrys). The corresponding graphene image is shown in the lower left corner. **(D)** Coverage rate of graphene by flavanthrone domains, using suspensions with pH 5.4, pH 6.8 and pH 10.0. Single measurements are depicted as dots besides of a boxplot. The solid line within the box indicates the median, the dotted line the mean. Each 30 images with an image size of 100 nm x 100 nm each one were analysed.

As shown in Fig. 23A-C flavanthrone domains show a characteristic structure, which can also be described as single-row-link-chain-structure, though with wider building blocks then dmQAC described previously[6] . The lattice parameters were measured to be $|a| = 0.94$ nm $\pm$ 0,04 nm; $|b| = 1,52$ nm $\pm$ 0,04 nm; $\alpha = 87° \pm 1°$. These measurements match with the results of the according force field calculations: $|a| = 0,95$ nm, $|b| = 1,51$ nm, $\alpha = 88°$.

The domains are orientated in different directions and depending on the pH of the suspensions they cover the substrate surface per medium between (2.3 +/- 1.9) % and (27.1 +/- 5.7) % (Fig. 23D). The uncomplete coverage of the substrate verifies, that the SAMs are deposited by OSWD.

Taking together this imaging results, we can show here that it is indeed possible to manufacture SAMs by simply applying and taking off again pigment-water-mixtures to the substrates surface, without using any costly approaches or devices.

4.2.2. Force Field Calculations
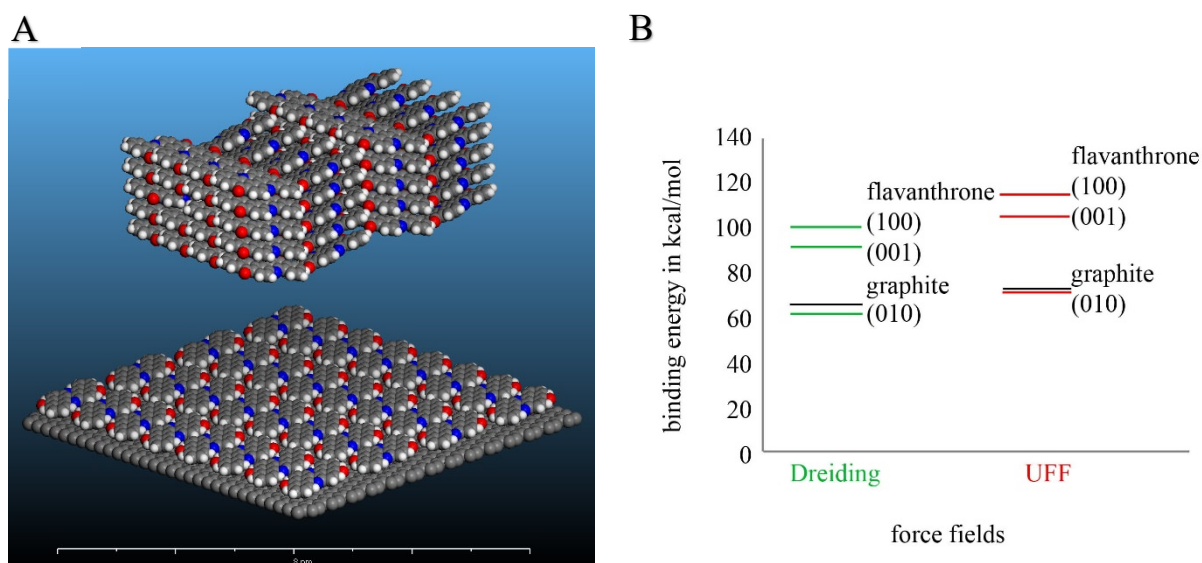
Figure 24: Force Field Calculations. (A) Simulation of a 3D-Crystal of flavanthrone above a graphene surface with a flavanthrone monolayer on top. (B) Diagram of binding energies. Depicted are the calculated binding energies of a flavanthrone molecule within 3 different crystal faces of a flavanthrone crystal ((100), (010), (001)) and of a single flavanthrone molecule adsorbed on graphene layer. Binding energies were calculated with two different force fields: Dreiding and Universal Force Field (UFF).

To proof physico-chemical plausibility of the monolayer formation of flavanthrone induced by OSWD, force field calculations were performed, in collaboration with Thomas Markert, Ulm University. As shown in Fig. 24 the calculated intermolecular binding energy of a flavanthrone molecule within the (010) crystal face of a flavanthrone crystal is lower than the intermolecular binding energy of a flavanthrone molecule adsorbed on and (0001) graphite surface, for both, Dreiding and UFF calculations. These results demonstrate that flavanthrone can indeed adsorb and form monolayers on graphite surfaces by OSWD and is therefore a further candidate for investigating possible doping effects on graphene, after applying SAM by OSWD.

4.2.3. Raman Spectroscopy

As discussed in the sections before, it is possible to generate SAMs on graphene simply by applying an aqueous pigment suspension to the graphene surface and taking it off again. By rinsing the sample additionally with water, left over crystals are mostly flushed away.

This new way of generating the OSWD induced monolayer on graphene is especially important when it comes to spectroscopy methods to analyse possible doping effects on the sample. Therefore, usually the measured surfaces may not show any crystals or agglomerates of the SAM forming substance, like pigment crystals in this case.

Raman spectroscopy is commonly used to analyse the efficiency of doping approaches. Since previous studies showed that Raman spectroscopy match with results of other techniques for bandgap analysis, like 4-probe measuring or tunnelling spectroscopy[58], Raman spectroscopy was chosen, as it is the most suitable approach to perform measurements under ambient conditions (room temperature and without vacuum) with few expenditures of time and in a non-destructive way. Furthermore, interference signals, e.g., results of mechanical strain of the graphene are well understood and the analysis of the peak shift is easy and clear.

The Raman spectrum of graphene can be characterised inter alia by the wavenumber of the D-peak (approximately 1350 cm^{-1}), the G-peak (approx. 1580 cm^{-1}) and the 2D-peak (approx. 2680 cm^{-1}) as well as the ratio of their intensities[59–61]. In pure graphene the D band is known to be an indicator of structural disorder and its intensity will increase by increasing quantity of structural defects[60,61]. Chemical doped graphene however shows significant shifts of the G- and the 2D-peak and a decrease of the intensity ratio of the 2D to G peak (I_{2D}/I_G), while a downshift of the G-peak and an upshift of the 2D-peak indicates n-type doping, upshift of both peaks refers to p-type doping[59,62].

Fig. 24 shows the result of Raman measurements of pure graphene on SiO_2 and graphene covered with flavanthrone. For further verification of the functionality of the here shown approach also a sample of graphene covered with dmQAC was measured Fig. 25 and the findings were compared to former Raman spectroscopy of graphene covered with dmQAC samples, prepared by using thermally triggered OSWD[7].
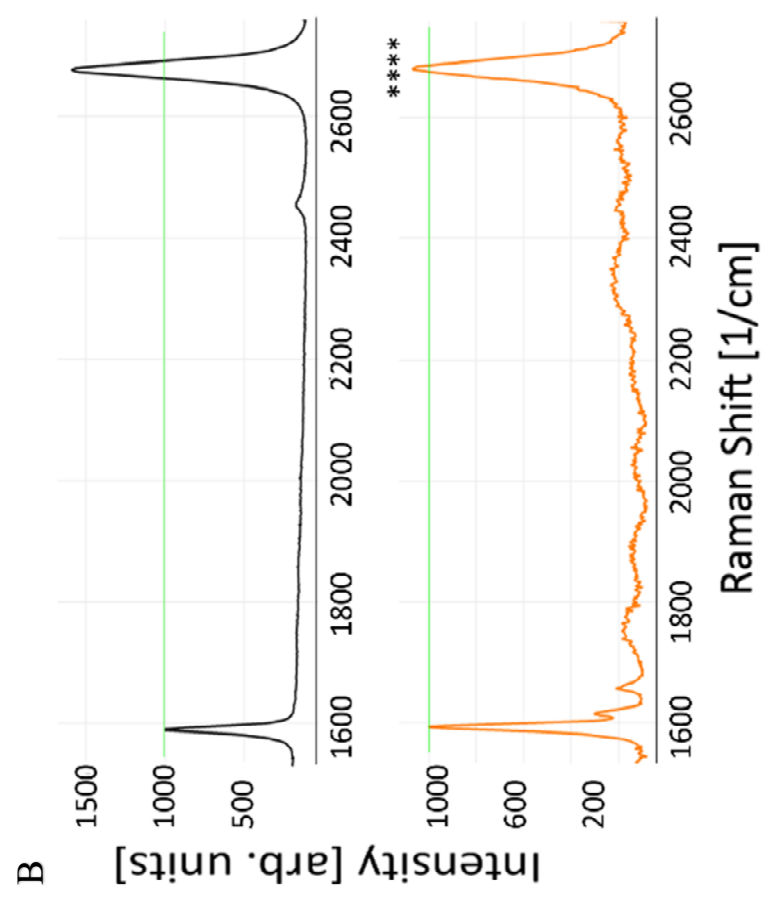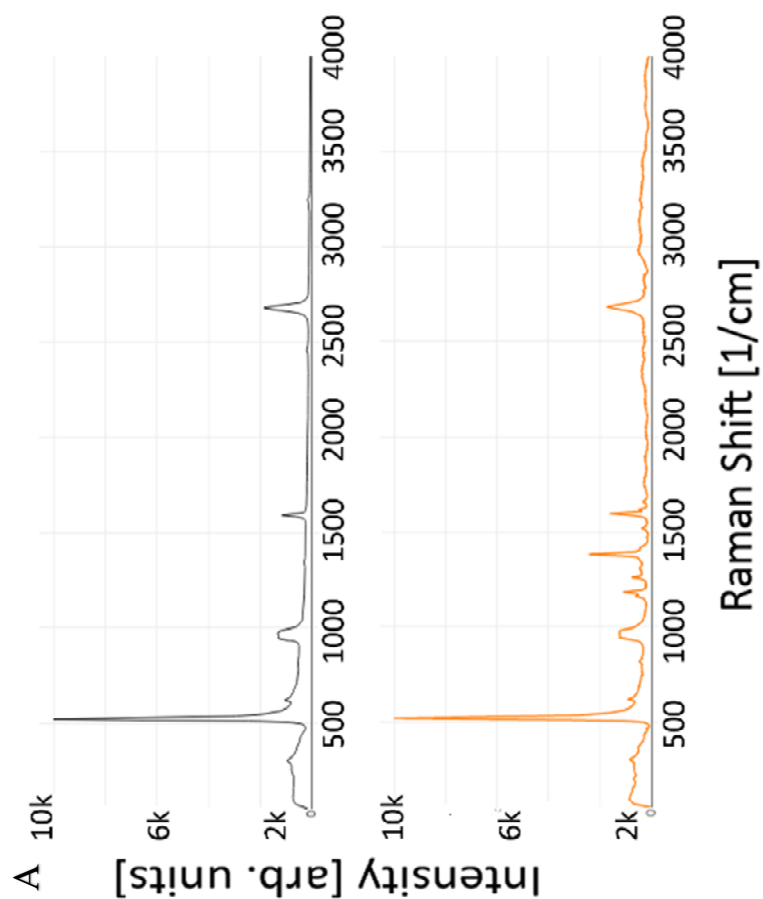
Fig. 25: will be continued on next page.
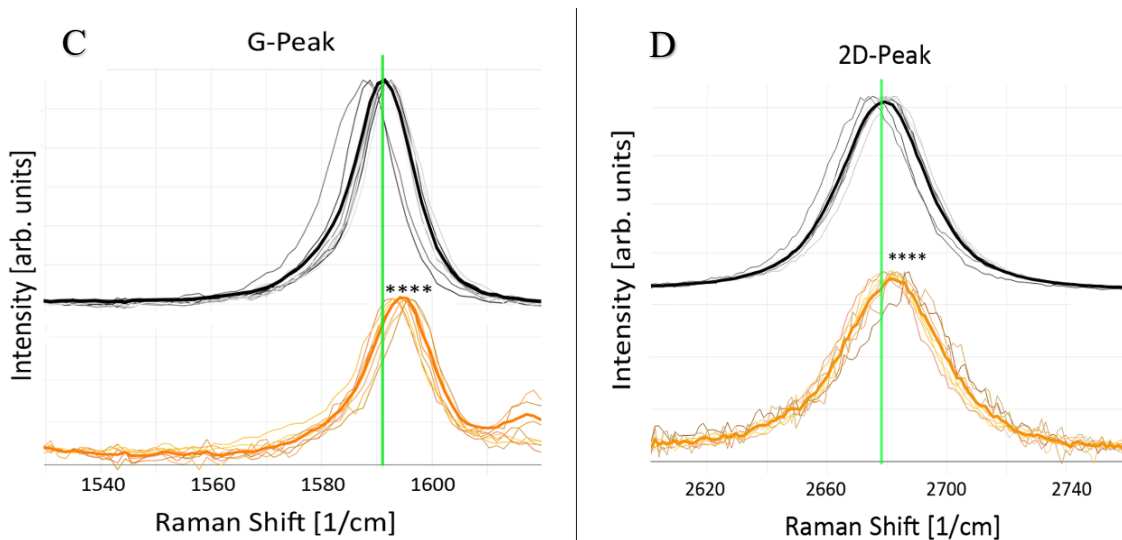
Figure 25: Raman-Spectra to verify doping of graphene by drop casting suspensions of flavanthrone. **(A - D)** The upper graphs (black) show the Raman spectrum for uncovered graphene on SiO_2/Si, the lower graphs (orange) depict the Raman spectrum for graphene covered with flavanthrone. **(A)** Overview of the complete Raman spectrum as averaged graphs over 10 measurements each. **(B)** Zoom-in to the G- and 2D-peak area of Raman spectrum. Depicted are averaged graphs of 10 measurements each one. The horizontal line helps to identify relative intensity differences between the G- and the 2D-peak. **(C, D)** Further zoom-in to **(C)** G-peak area and **(D)** 2D-peak area. All 10 measurements are depicted together with the respective average line. Furthermore, a vertical line helps to identify up-shift of the respective peak for flavanthrone covered graphene. Statistical analysis was performed with t-testing and Welch's correction, with n=10; ****: $p < 0.0001$.
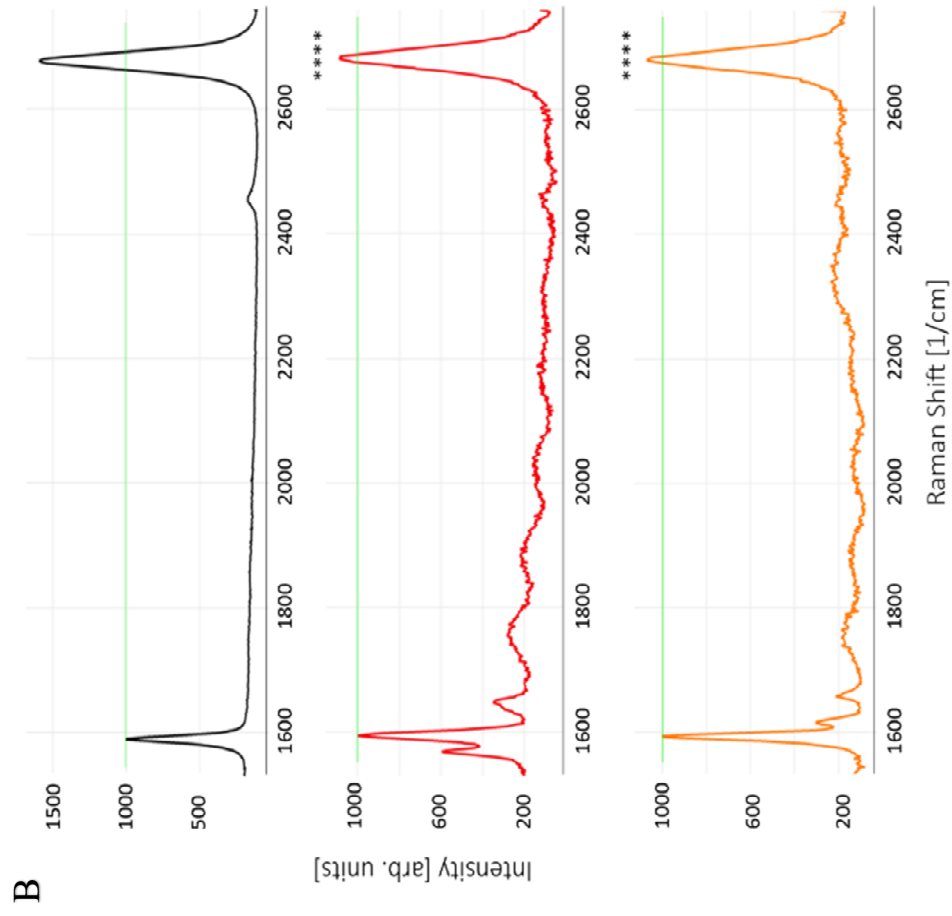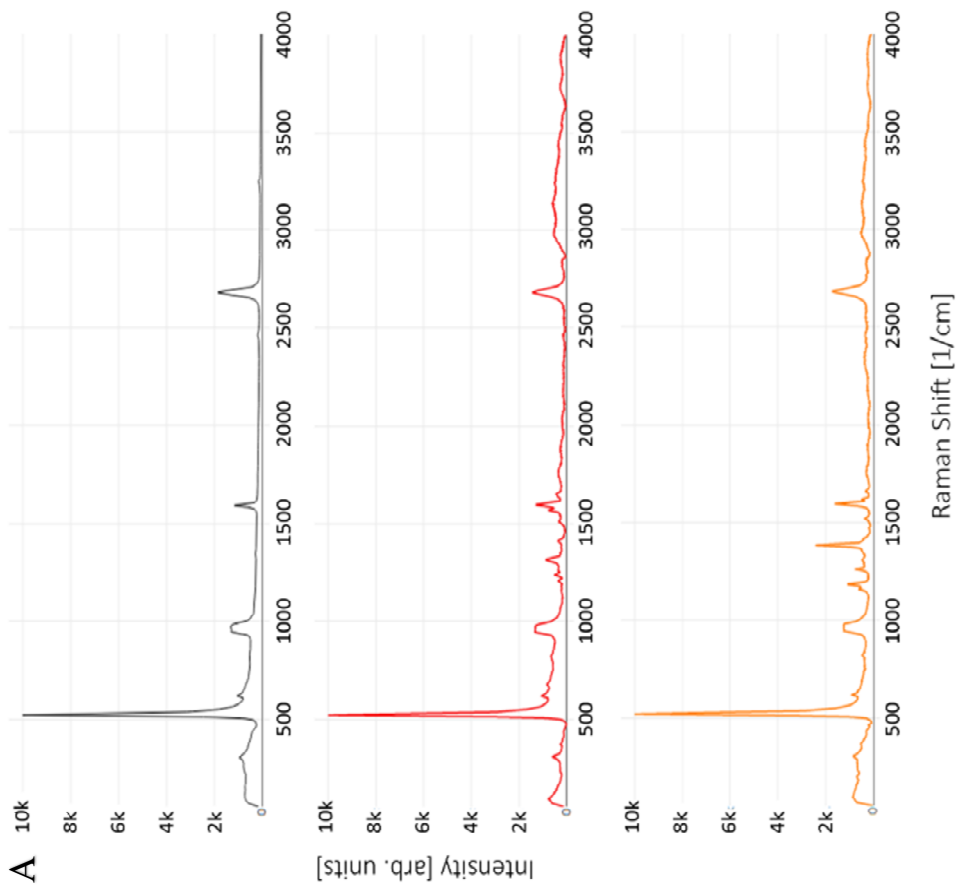
Fig. 26: will be continued on next page.
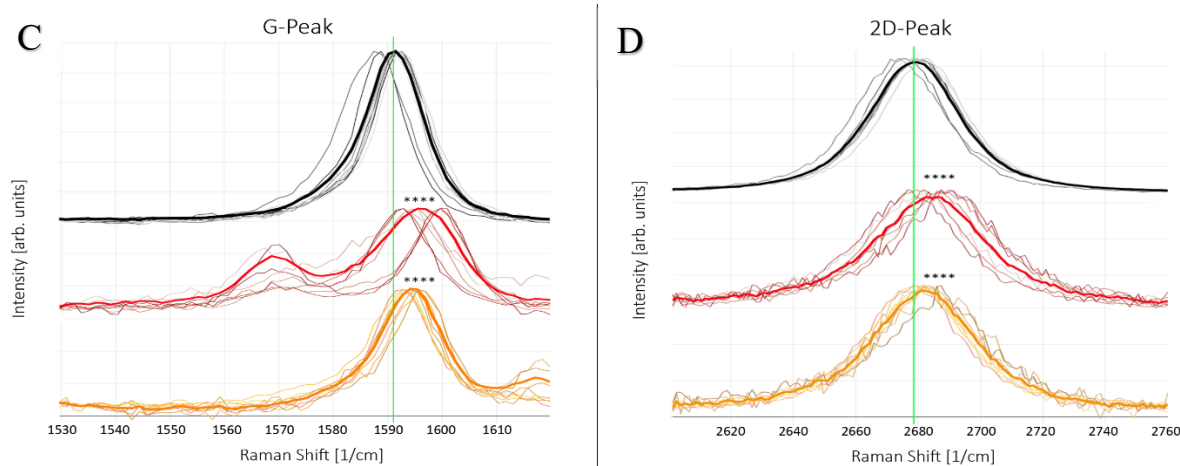
Figure 26: Comparison of Raman-Spectroscopy of empty graphene, graphene covered with dmQAC, and graphene covered with flavanthrone. **(A - D)** The upper graphs (black) show the Raman spectrum for uncovered graphene on SiO_2/Si, the middle graphs (red) show the Raman spectrum for graphene covered with dmQAC and the lower graphs (orange) depict the Raman spectrum for graphene covered with flavanthrone. Both the dmQAC sample and the flavanthrone sample were prepared by drop casting pigment-water suspensions. **(A)** Overview of the complete Raman spectrum as averaged graphs over 10 measurements each. **(B)** Zoom-in to the G- and 2D-peak area of the Raman spectrum. Depicted are averaged graphs of 10 measurements each one. The horizontal line helps to identify relative intensity differences between the G- and the 2D-peak. **(C, D)** Zoom-in to **(C)** G-peak area and **(D)** 2D-peak area. All 10 measurements are depicted together with the respective average line. Furthermore, a vertical line helps to identify up-shift of the G-peak for the dmQAC and flavanthrone covered graphene. Statistical analysis was performed with t-testing and Welch's correction, with n=10; ****: p < 0.0001.

For each sample 10 measurements were averaged and the difference in Raman shift was analysed by t-test and Welch's correction.

The G-peak was found to be located at 1590.66 cm^{-1} for graphene, at 1595.7 cm^{-1} for the dmQAC covered sample and at 1594.36 cm^{-1} for the flavanthrone covered sample (Fig. 26A-C). Both covered samples show a significant up-shift of the G-peak in comparison to the pure graphene sample with a p-value of 0.00037 for the dmQAC sample and 8.06 x 10^{-5} for the flavanthrone sample. Furthermore, the 2D-peak was found to be situated at 2678.28 cm^{-1} for graphene, at 2683.84 cm^{-1} for the dmQAC covered sample and at 2682.83 cm^{-1} for the flavanthrone covered sample (Fig. 26A-B, D). Additionally, both covered samples show a significant up-shift of the 2D-peak in comparison to the pure graphene sample with a p-value

of 0.0042 for the dmQAC sample and 0.0029 for the flavanthrone sample. Moreover, the intensity ratio of the 2D- to G-peak (I_{2D}/I_G) was measured to be 1.56 for the graphene sample, 1.05 for the dmQAC samples and 1.17 for the flavanthrone sample (Fig. 26B). Both samples showed significant decrease of the ratio with a p-value of 2.08×10^{-5} for dmQAC and 0.0042 for flavanthrone respectively. Furthermore, changes in the D-peak were not detected, i.e., that mechanical strain or structural disorder inside the graphene as a driving force for the upshift of the 2D- and G-peak can be excluded.

Putting these findings together, it can be shown that flavanthrone functions as a p-type dopant, which corresponds to its molecular properties. The two imine groups that provide the PHA core with strong electron withdrawing properties function as electron acceptor, producing electron holes inside the graphene, when stacking on it.

Furthermore, we proof by comparing the dmQAC sample from our new approach with the dmQAC sample produced by thermally triggered OSWD[7] that the new method leads to the same doping effect as it found in a previous study.

Moreover, the undetectable D-peak indicates the new pipetting method to be innoxious for the graphene itself, meaning that no damage of the graphene surface was detected.

4.2.4. Tunnelling spectroscopy

To validate the doping effect with an independent method and analyse the set band gap, the samples were additionally analysed by Tunnelling Spectroscopy (TS), as described in the methods section (Fig. 27).
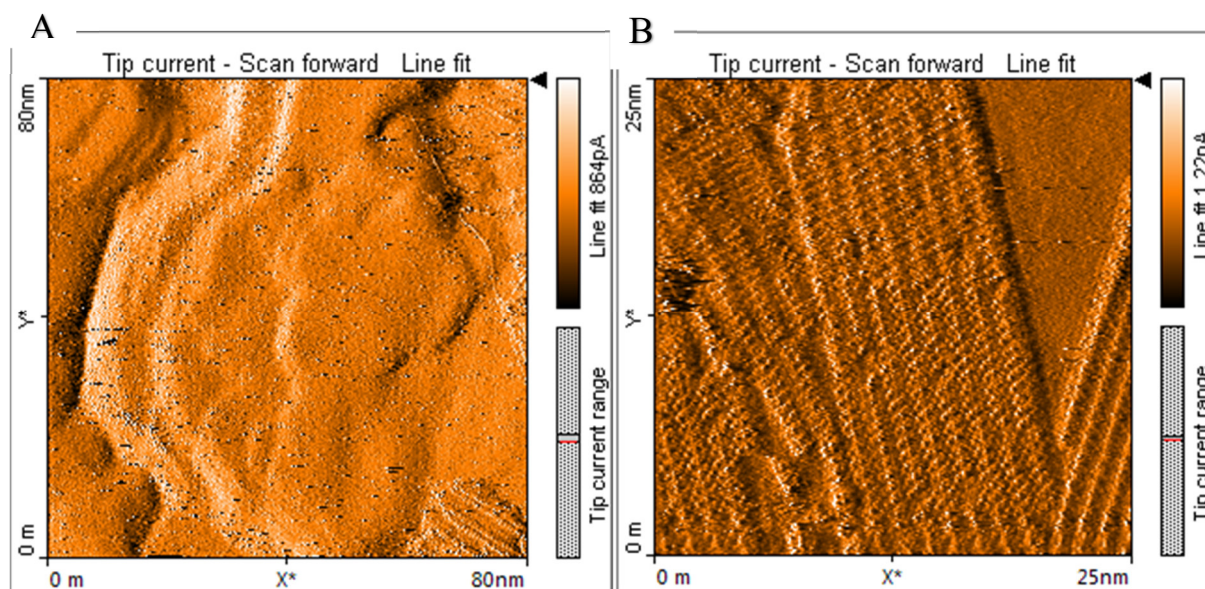
Figure 27: STM images right before STS of **(A)** flavanthrone on graphene, with the monolayer domain on the right lower corner and **(B)** QAC on graphene with the monolayer domain on the left side and the right lower corner.
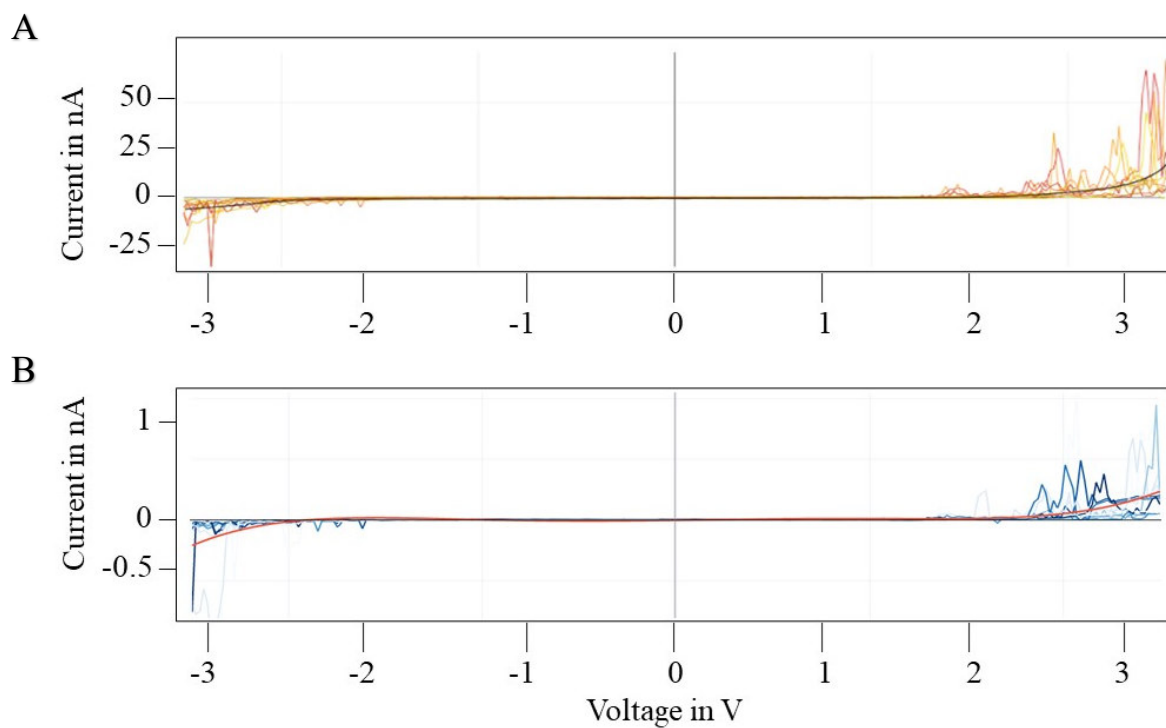
Figure 28: Tip current – tip voltage curves with a range from -3.0 V to +3.0 V for TS measurements right on top of the monolayer domain. Replicates and trendline were performed as described in the methods section. **(A)** Flavanthrone on graphene; **(B)** QAC on graphene.
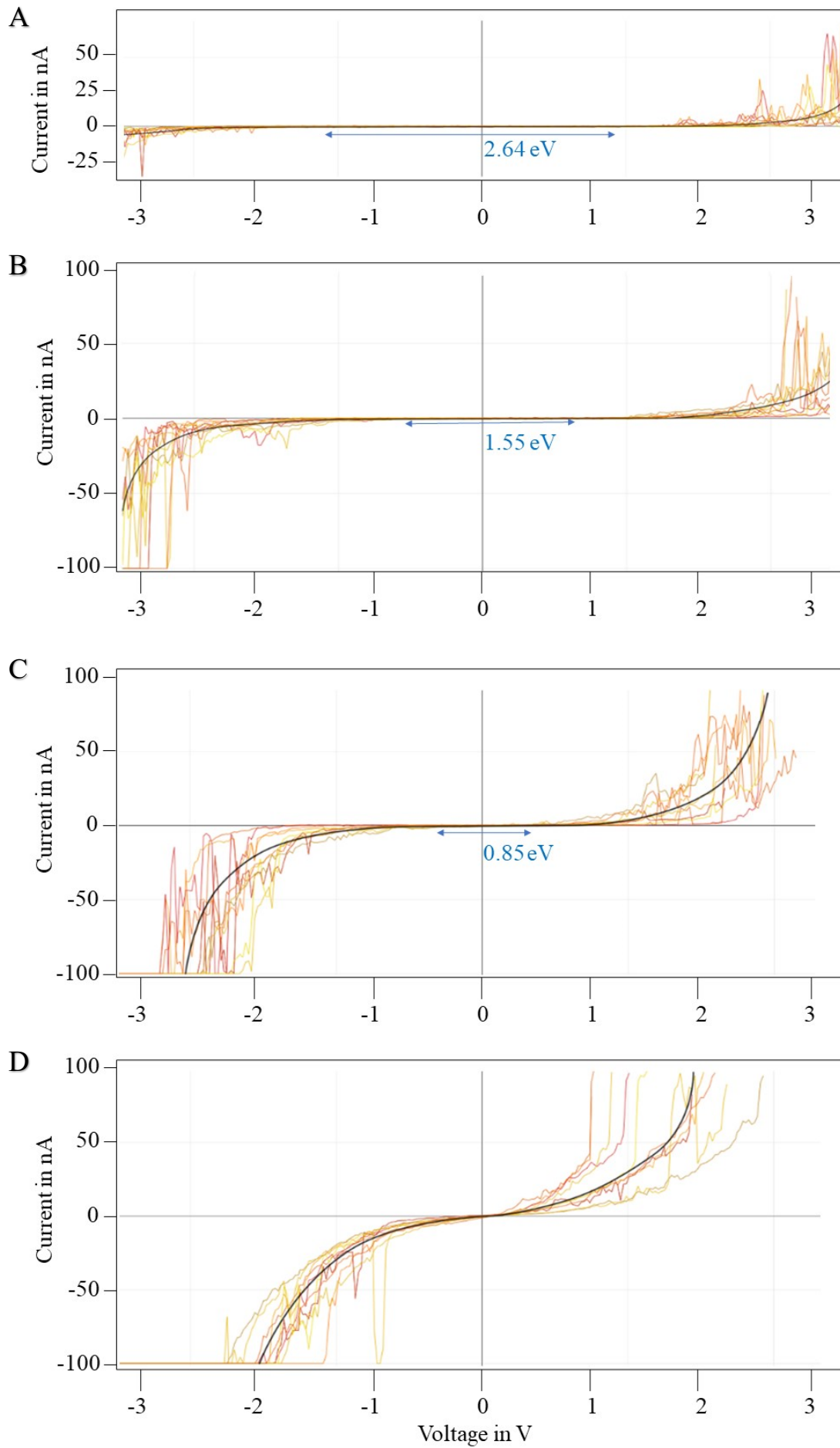
Fig. 29: see next page.

Figure 29: Tip current – tip voltage curves with a range from -3.0 V to +3.0 V for TS measurements at different distances to the flavathrone domain. Replicates and trendline were performed as described in the methods section. **(A)** Measurements on top of the flavanthrone domain. **(B)** Measurements in a distance of 1 nm of the domain. **(C)** Measurements in a distance of 15 nm of the domain. **(D)** Measurements in a distance of 30 nm of the domain.

The bandgap of flavanthrone was measured to be 2.64 eV ± 0.39 eV and the bandgap of QAC to be 2.44 eV ± 0.18 eV (Fig. 28). These values match with the results of cyclic voltammetry measurements of previous studies, where Glowacki et al. [63] found the bandgap of QAC to be 2.5 eV and Leonat et al.[64] the bandgap of flavanthrone to be 2.7 eV. Like shown before, also the bandgap of the flavanthrone sample decreases linearly with increasing distance of the measuring point to the domain (Fig. 29) until no more band gap can be detected in a distance of more than 15 nm to the domain.
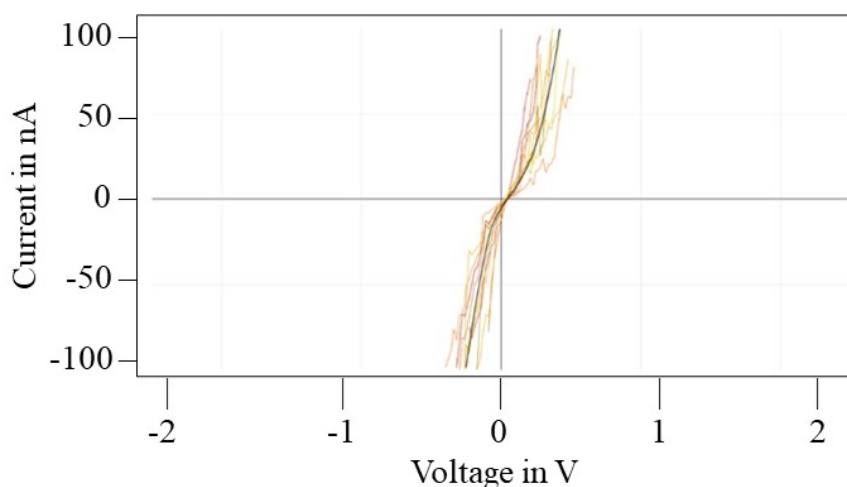
Figure 30: Tip current – tip voltage curves with a range from –2.0 V to +2.0 V for TS measurements on graphene only, covered with dodecane. Replicates and trendline were performed as described in the methods section.

TS measurements of graphene covered only with dodecane were performed to exclude any doping effects or artefacts genereated by dodecane. As known for graphene[65], the results of these measurements did not show any bandgap formation or other artefacts (Fig. 30) and any doping effect or artefact generated by dodencane can be excluded.

4.2.5.   Dirac Peak shift

As a third independent analysis method, the Dirac peak shift between an uncovered graphene and a sample with drop casted dmQAC was analysed using source-drain resistance measuring. dmQAC was chosen in this approach, since it generates quantitatively more and better distributed monolayers on graphene, than flavanthrone. For p-doped graphene an upshift of the Dirac peak, generated by source-drain measurements is expected[66]. To generate a reliable data set, regarding the position of the Dirac peak within the uncovered graphene sample, 15 measurements of the source-drain resistance have been performed on three different single layer graphene flakes. The middle position of the Dirac peak was found to be at 83.4 V $\pm$ 13.8 V, due to the SiO_2 substrate (Fig. 31 A). Source-drain resistance measurements of dmQAC covered graphene constantly showed an upshift of the Dirac peak to more than 160 V. As described in the methods section, the concrete position of the Dirac peak could be located only in two measurements and was found to be at 168,8 $\pm$ 3,9V. Statistical analysis of the shift lead to a significant up shift (Fig. 31 B) with a p-value of 4.2 x 10^{-7} (t-test with Welch's correction).

This shift corroborates the results of the Raman and the Tunneling Spectroscopy: by covering the graphene with dmQAC-SAMs the graphene gets doped. The up-shifting validates the previous findings that dmQAC acts as a p-dopant[7]: When the gate voltage required to reach the charge neutrality point is higher than the applied gate voltage, then the Fermi level is located in the valence band and holes are the majority charge carriers, which indicates the presence of a p-dopant[67]. The up shift by 160 V can be taken as enormous, as up shifts usually occur in a range lower than 50 V[68,69].
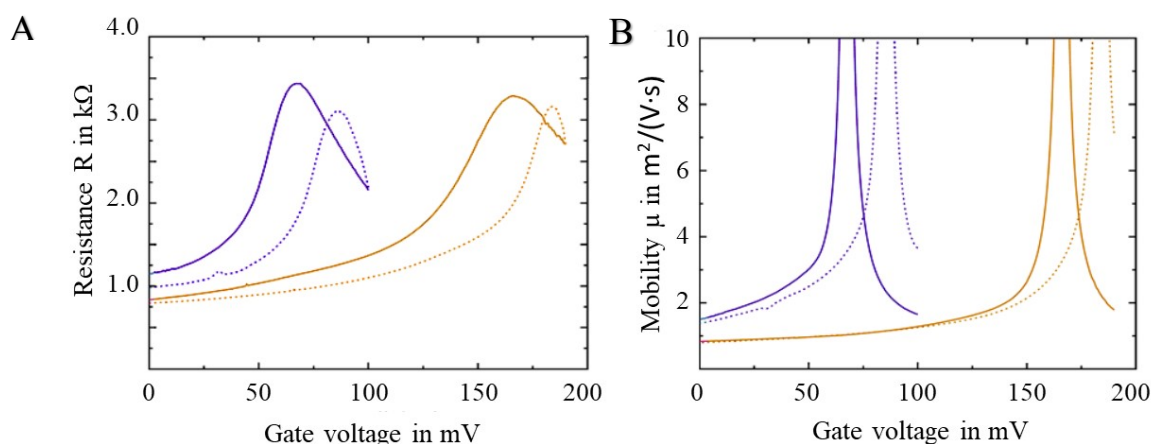
Figure 31: Electrical charge transport measurements. Measurements were performed on exfoliated graphene flakes on Si/SiO2 before (purple) and after (yellow) deposition of dmQAC. Dotted lines show the hysteresis of each measurement. A clear upshift of both **(A)** the resistance peak and **(B)** the electron mobility peak, which indicates the voltage, were the highest electron mobility is given, can be seen, indicating a p-doping of the graphene by the organic semiconductor.

4.2.6.   Summary II

To sum up the results, it was shown here with three different techniques (Raman spectroscopy, tunnelling spectroscopy, and Dirac peak measurements) that chemical doping of graphene is possible by thin film coating using OSWD in water as a deposition method and drop casting as an application technique.

The feasibility of the method for two different PHA, dmQAC and flavanthrone was shown. Furthermore, the results showed that the bandgap of flavanthrone is about 2.64 eV, what coincides with previous findings[70]. By Raman spectroscopy it was further shown, that flavanthrone acts as a p-type dopant.

OSWD in water, for this reason, represents an easy, cheap, and fast way of doping graphene. There are no toxic or expensive chemicals needed, nor heat, high vacuum, or high professional skills to apply the drop cast technique.

4.3. Condensation of RNA in aqueous particle suspensions

The previously shown results, the strong enhancement effect of AMP on the OSWD in water and the possible application of the OSWD as a deposition method for semiconductor science, by doping graphene using thin film coating, inspired to connect the OSWD system with other scientific fields (prebiotic chemistry and research on the origin of life), to examine if vice versa the environments present in the OSWD process can also influence the chemical behaviour of the NMPs. As shown before[5,13], the explanatory model for OSWD involves nanofluid effects that occur during the OSWD process and the resulting SAM formation. Interestingly this kind of effects can also be found within the active centres of enzymes, like polymerases, where – as a result – the activity of water, i.e., the water as the main component of cytoplasm of the cell, is reduced and the condensation of nucleotides to form RNA and DNA is enabled. However, it is assumed that the first polynucleotides, like RNA and DNA, did arise without the assistance of enzymes and without a biological cell, but in water[71].

Thus, within the so far mainly discussed pathways for the possible origin of polynucleotides in water, like wetting-drying cycles, lighting strikes, or extraordinary and rare molecule species, or species that do not play a functional role in modern biochemistry, these scenarios show general weaknesses when appraising their prebiotic plausibility[14,18].

"[…] the water problem within a stable environment full of water and does not rely on physical conditions and chemical substances proposed in these concepts. This aspect is of particular relevance regarding evolutionary conservatism — the principle that evolution builds on existing pathways[…][72]. In this context, the principle indicates that the same physicochemical effects were involved in the abiotic origin of biopolymers, as is now being tapped by living systems via complex enzymes."[14]

Based on the findings shown above, the hypothesis was formed that the OSWD might also influence the chemical behaviour of the NMPs vice versa; to be precise, if the nanoconfinements, that appear during the OSWD between the substrate and the pigment crystal could catalyse the formation by condensation reactions of NMPs to oligo- or even polynucleotides, like short pieces of RNA.

Precipitations of the supernatant of aqueous suspensions of substrate powder, PHA crystals and NMP(s) were performed as described in the method section. To analyse, if oligo- and/or polynucleotides have been formed, fluorometry and RT-qPCR were performed. Furthermore,

to gather a better understanding for the ongoing processes, computational analysis was performed by Thomas Markert, Institute of Theoretical Chemistry, Ulm University.

4.3.1. RNA analysis
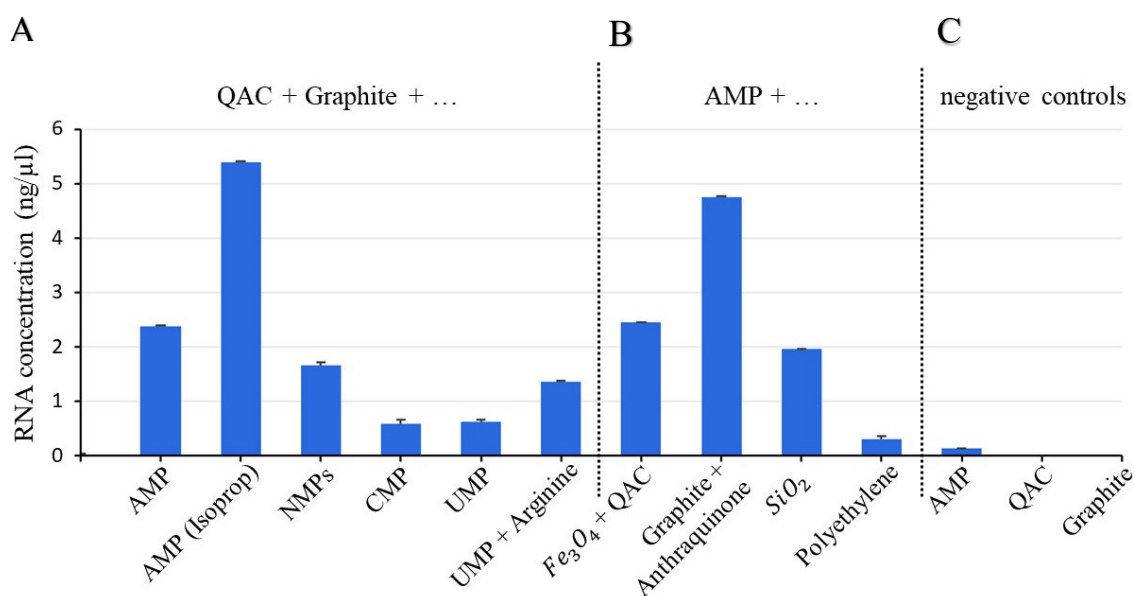
Figure 32: "Fluorometric results of RNA concentration measurements in aqueous particle suspensions. Displayed are the mean values of three measurement replicates and standard deviations. If not differently indicated, nucleotide suspensions had a final concentration of 50 mM and RNA isolation was performed from aqueous suspensions of particles containing dissolved biomolecules using EthOH and NaCl for precipitation. **(A)** Detected RNA concentrations in samples based on QAC + graphite suspensions: AMP: 2.38 ng per µl; AMP (isoprop.): precipitation was performed using isopropanol and NaOAc; detected concentration: 5.4 ng per µl; mixture of NMPs (AMP, UMP, GMP, CMP, 12.5 mM each): 1.66 ng per µl; CMP: 0.59 ng per µl; UMP: 0.62 ng per µl; mixture of UMP and arginine: 1.36 ng per µl. **(B)** Detected poly(A) RNA concentrations in suspensions based on: Fe3O4/QAC: 2.45 ng per µl; graphite/anthraquinone: 4.76 ng per µl; SiO2 : 1.96 ng per µl; polyethylene: 0.3 ng per µl. **(C)** Results of the negative controls: aqueous samples containing AMP but without suspended particles: 0.14 ng per µl; pure aqueous samples only containing QAC or graphite: both underneath the detection level."[14]

"[…][Fig. 32] shows the results of fluorometric RNA concentration measurements of the […] samples [prepared as described above]. Both ethanol precipitation and isopropanol precipitation were applied. The results of both precipitation methods reveal that poly(A) RNA strands have formed in significant amount with respect to the negative."[14]
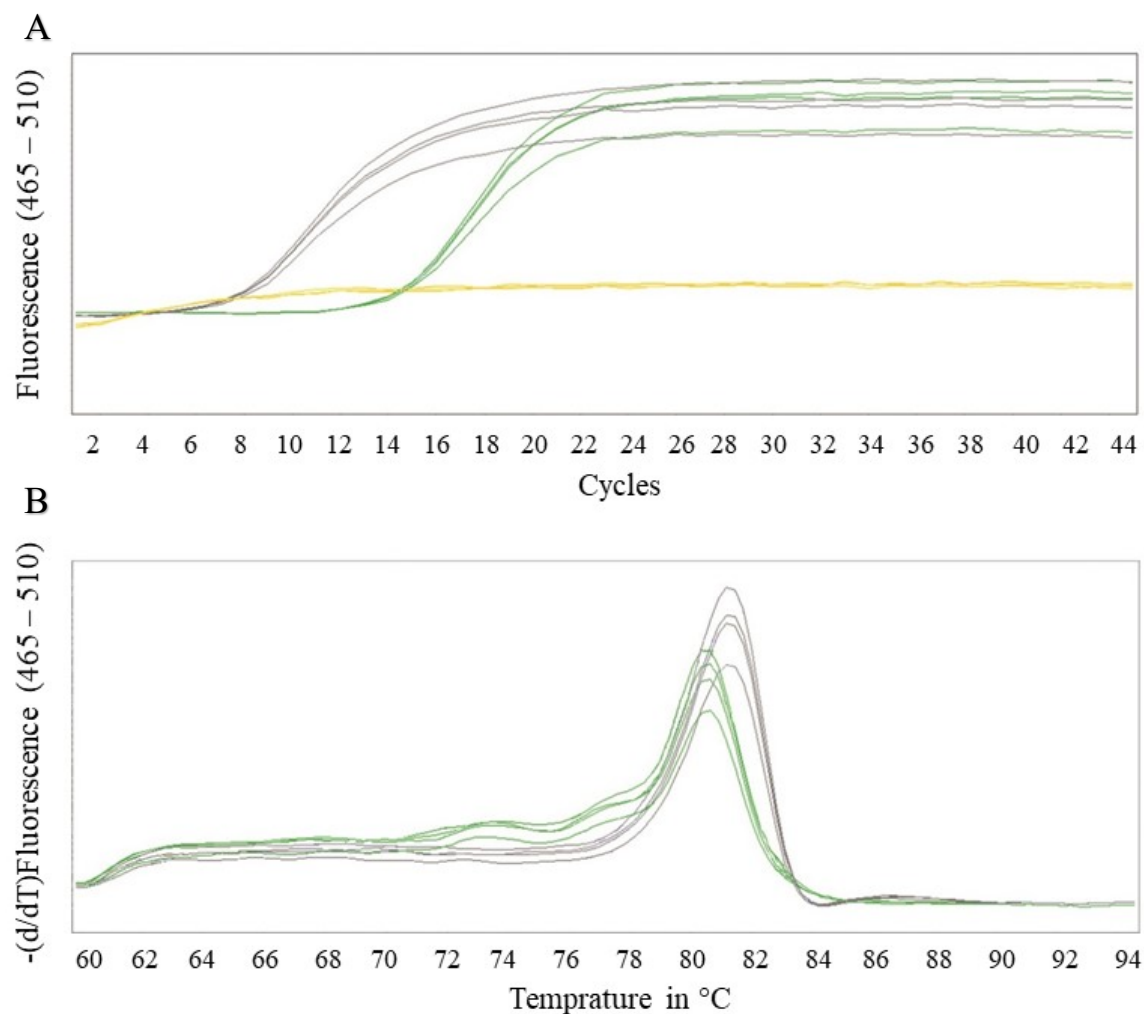
Figure 33: Results of quantitative polymerase chain reaction. Grey: sample (AMP + QAC + Graphite (resuspended gel-pellet from precipitation of an aqueous AMP-QAC-Graphite suspension, prepared as described in the method section)); green: control sample (miRNA of 23nt length); yellow: negative control. **(A)** Fluorescent curve, **(B)** Melting curve.

"To cross-check the fluorometric quantification with a totally independent but also highly specific method, we performed quantitative polymerase chain reaction after reverse transcription (RT-qPCR). The results ([…][Fig. 33A]) show that the fluorescence signal of the sample [(grey)] exceeds the background fluorescence after 7.57 cycles. This indicates a high yield (103-fold) of input RNA in comparison to the respective signal of the positive control miRNA ([green,]14.25 cycles). To obtain indications on the length of formed RNA, we performed a comparative melting curve analysis after the last cycle of the qPCR. This analysis includes the sample RNA [(grey)] and a positive control miRNA [(green)] with a length of 23 nt. The comparison reveals that the medium melting point of the sample is at higher temperature than the positive control ([…][Fig. 33B]). These results suggest that the sample contains created oligonucleotides with lengths of equally or longer than 23 nt."[14]

4.3.2. Capillary gel electrophoresis of RNA
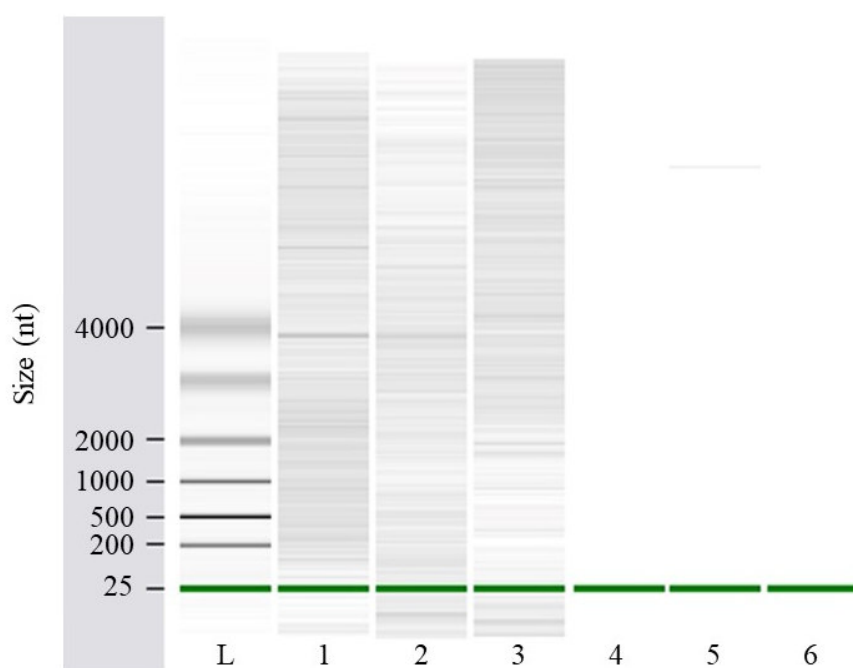
Figure 34: "Lane L shows the RNA bands of the molecular weight marker (ladder). Lanes 1–3 represent the triplicate of a typical incubated, precipitated sample made of suspended QAC and graphite particles and dissolved AMP. This sample was analysed with fluorometry prior to gel electrophoresis and showed an RNA concentration of 2.0 ng per µl. Lanes 4–6 represent triplicates of a negative control sample with no detectable RNA concentration according to fluorometric results. The prominent, isolated sharp signal in lane 5 is interpreted as an artifact, arising from the instrument's sensitivity to even low vibrations of the laboratory bench."[14]

"As an additional approach to cross-check the presence of RNA and to acquire more information on the length distribution of any formed RNA strands in our samples, we applied capillary gel electrophoresis by using the Agilent RNA 6000 Nano Kit. We chose this technique due to its high specificity for RNA and—like the other RNA detection techniques we selected for our study — due to its tolerance against residual crystal particles suspended in our samples. For the analysis, we chose a sample that contained QAC and graphite particles suspended in an aqueous solution of AMP and applied EtOH/NaCl for precipitation. The results show a broad distribution of RNA bands in the triplicates of the sample (Fig. 34, lanes 1–3). These clear and numerous bands further support our previous findings that RNA is present in our samples and also give a strong indication not only for the existence of short RNAs lengths below 25 nt but also for the presence of a large fraction of formed RNA strands with lengths of up to 4000 nt and more.

Contamination with any natural RNA can be excluded due to the lack of the prominent rRNA double bands of the smaller and the larger ribosome subunits. To identify possible background noises in gel electrophoresis that might be caused by residual nanoparticles in the samples after precipitation, a negative control with a typical particle concentration was used that represented a sample with no detectable RNA signal from fluorometry. The results (Fig. 34, lanes 4–6) suggest that such possible background noise from residual particles is below the detection limit of the used electrophoresis system. The outcome also indicates that the results of fluorometry and electrophoresis concerning the presence or absence of RNA are consistent."[14]

4.3.3.   Stacking and dielectric constant

"To identify substantial factors that lead to the observed abiotic polymerisation we first analysed the possible role of π-stacking of nucleoside monophosphates (NMPs) as stacking has been suggested to be an important factor for RNA polymerisation in terms of bringing the monomers in close contact[…][73]. To perform this analysis, we extended the fluorometric analysis of ethanol precipitated AMP-based samples to CMP and UMP-based samples and compared the relation of the different RNA concentration results with the relation of respective published stacking equilibrium constants and stacking free energies of NMPs. The comparison reveals that the detected relative concentration of poly(A) RNA is about four times higher than poly(C) RNA and poly(U) RNA ([…][Fig. 32A]) and that this order (poly(A) RNA >> poly(C) RNA ~ poly(U) RNA) correlates to the order of the respective stacking equilibrium constants

and stacking abilities as derived from stacking free energy profiles of NMPs[…][56]. This correlation suggests that in particle suspensions, stacking and polymerisation of nucleotides is linked. Therefore, enhancing the stacking ability of a nucleotide should result in a higher RNA concentration. To test this, we selected UMP due to its low self-stacking ability and its comparatively low poly(U) RNA formation and added the amino acid arginine to the sample. Arginine is known for its high stacking ability with aromatic groups[…][57]. Fluorometric analysis of such UMP/arginine-based samples revealed that arginine increased the formation of poly(U) RNA by more than 100% ([…][Fig. 32A]). This observation supports the necessity of π-stacking for the polymerisation in aqueous suspensions and points to a possibly prebiotic relevant kind of interplay between amino acids and nucleic acids.

However, base stacking cannot be the key factor for RNA formation in the described samples. This becomes evident when taking the water paradox into account and when considering the result of a negative control based on an AMP solution without suspended particles ([…][Fig. 32C]): although AMP has the highest self-stacking constant among all NMPs[…][56] and is the only NMP with the ability to self-associate in indefinite stacks[…][54], the negative control shows that in comparison to the poly(A) RNA concentrations reported above, only minute amounts can be found when the sample contains no added particles. This result suggests that there is a key factor in promoting both stacking and polymerisation that is closely linked to the particle suspension nature of the samples.

It is known that reducing the dielectric constant of water favours stacking[…][54], and reducing the activity of water (e.g. by adding alternative solvents, inducing wet/dry cycles or intercalation) promotes polymerisation[…][74–76]. As nanofluid phenomena emerging in temporal nanoconfined water can reduce both properties simultaneously[…][77,78] and watery suspensions of particles give rise to such phenomena[…][79], we infer that the occurrence of nanofluid phenomena in our samples is the key factor for the observed nucleotide polymerisation. This implies that the enhancement of nanofluid phenomena should correlate with an increase of polymerisation reactions."[14]

4.3.4. OSWD as a probe

"Nanoconfining environments change the behaviour of water especially in terms of its hydrogen bond network dynamics[…][77] which, in turn, affects the thermodynamic property of water activity[…][78]. The anomalous behaviour of nanoconfined water results from a highly complex interplay of various nanofluid phenomena and forces that are related to, for example, the surface energy and size of the confining boundaries, shear, molecular structure, electrical double layer and fluctuations of general order parameter[…][79,80]. To cope with this high complexity when assessing a possible synergy between nanofluid phenomena and polymerisation we chose an experimental approach that allows us to focus on a single, quantifiable effect. This approach uses the effect of Organic Solid/Solid Wetting Deposition (OSWD) as a probe. OSWD is the final result of a network of various nanofluid phenomena on confined water between suspended organic crystals, including double-layer forces, Casimir-like fluctuation-induced forces and dewetting-induced hydrophobic collapse[…][13]. It manifests as the adsorption and self-assembly of insoluble polyaromatic heterocycles at solid/solid interfaces and thus is quantifiable via surface coverage determination.

We quantified the efficiency of OSWD as a function of different biomolecules dissolved in watery suspensions of particles of the organic semiconductor QAC. For the quantification, we measured the surface coverage of graphite crystals with QAC monolayers via scanning tunnelling microscopy […][see chapter 4.1.]. The results ([…][Fig. 14]) reveal that adding AMP to the particle suspension enhances the coverage with very high statistical significance ($p < 0.0001$) in relation to QAC suspensions based on pure water (w/o, […][Fig. 14]), though the pH was not increased to the same extent (pH of aqueous suspension of QAC: 7.5; pH with AMP added: 8.8). A significant increase in coverage ($p < 0.01$) also occurs when using arginine as the added biomolecule (pH 10.6). By contrast, coverages found in samples based on CMP or UMP are statistically nearly identical and significantly lower with respect to the AMP- and arginine-based samples. Using a mixture of different NMPs leads to no significant increase of coverage but results in some very high single coverage measurements regarding the CMP and UMP samples ([…][Fig. 14 and Fig. 16]), possibly caused by clusters of the AMP fraction of the mixture. The comparison of these OSWD induced coverages with RNA quantities ([…][Fig. 32A]) indicates that relative differences in the extent of nanofluid phenomena between the samples correlate with relative differences in detected RNA concentrations. This supports the hypothesis of a synergy between nanoconfinement effects and nucleotide polymerisation in aqueous particle suspensions. We thus propose that the emergence of nanofluid effects on

confined water is the key factor in the promotion of both stacking and polymerisation of nucleotides within aqueous suspensions of particles."[14]

4.3.5.   Magnetite, silica and anthraquinone

"Thus far, we used QAC/graphite particle systems to ensure comparability of the results from different experimental approaches. To test whether the formation of RNA in such an environment is generalisable, we measured samples prepared by the same protocol but containing particles based on other compounds. As inorganic substitutes, we chose magnetite and silica as geologically widespread compounds and selected the organic compound anthraquinone due to its abundance in carbonaceous meteorites[…][81]. Fluorometric measurements of partly or fully substituted samples show poly(A) RNA concentrations that are similar to or substantially higher than the comparable output of the QAC/graphite model system ([…][Fig. 32B]). This indicates that the abiotic formation of RNA within nanofluid environments of aqueous suspensions is of general nature. Our results also imply that the output of RNA can be increased to higher concentrations by identifying appropriate particle suspension systems. The influence of the particle species on the RNA concentration, as indicated by […][Fig. 32B] (including results from inert polyethylene particles as a comparison), is consistent with the fact that the anomalous behaviour of nanoconfined water is partly determined by the characteristics of the confining surfaces[…][77]."[14]

4.3.6.   Computational analysis

"For nanofluid effects to become dominant, the confining surfaces must approach, at a conservative estimate, within the range of 10 nm and below[…][77]. To evaluate whether stacking of nucleotides within such nanoconfinements is possible in a sufficiently stable and ordered way to prime polymerisation, we performed dynamic molecular mechanics calculations. For performing these calculations, we modelled a stack of 12 AMPs as an example system referring to the observation that polymerised AMPs of more than 10 nt length were abundant in our samples. We arranged this stack in parallel between two nanoscale separated crystals of a QAC/graphite system and added water to the confinement. […][Fig. 35] shows the condition of the stack at the end of a dynamic simulation modelled with a confinement gap size

of about 4 nm. This condition implies that the nucleotide stack remained arranged in such confinement when surrounded by water […]. Comparative calculations suggest that such stacks are deformed, but stable even when the density of water—which can be lower in nanoconfined conditions[…][77] – is decreased to ~60% […]. It requires a reduction of the gap size to about 3 nm and below to finally destabilise a stack due to increased interactions with confining surfaces […]. In sum, these simulations indicate that it is feasible to assume that nucleotides can associate in stable stacks within nanoconfinement gap sizes well below 10 nm for priming polymerisation."[14]
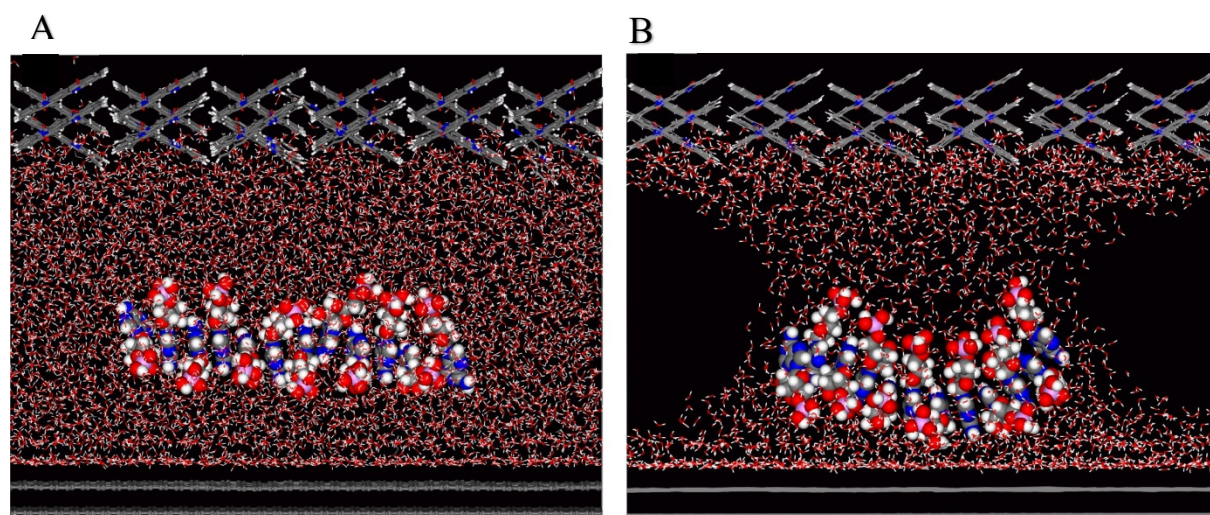
Figure 35: "Dynamic force field calculation of a nucleotide stack in nanoconfined water. The system is modelled within a supercell containing two graphene layers (bottom), two layers of a QAC crystal (top) and a stack of 12 AMP molecules placed between the confining surfaces. Vertical dimension of the gap: 43 Å. […][**(A)**] Condition of the stack after a simulated time span of 50 ps. The confinement is filled with water molecules. […][**(B)**] Condition of the stack after a simulated time span of 60 ps and a water density of ~60%."[14]

4.3.7.   Thermodynamic considerations

"Nucleotide polymerisation into RNA is a water-releasing condensation reaction that faces a thermodynamic barrier as the change in the Gibbs free energy of such a reaction is positive. Consequently, nucleotide polymerisation in water is a thermodynamically uphill reaction that

is extremely inefficient to occur spontaneously under ambient conditions. However, if the entropic part (ΔS) of the Gibbs free energy change ($\Delta G = \Delta H - T\,\Delta S$) becomes very positive, the reaction can become exergonic ($\Delta G < 0$) and thus favourable. As the entropic part is positive when the activity of water is low[…][75] the thermodynamic barrier can be overcome by reducing water activity[…][82]. Against this background, we propose that our observed abiotic formation of RNA within aqueous particle suspensions can be explained by the rise of anomalous properties of water when getting temporarily confined between suspended particles: nanoscale confinements change, among others, the vapour pressure[…][83] and hydrogen-bond network dynamic[…][77] of water. This can reduce water activity[…][78,83] as a function of gap size and the characteristics of the confining surfaces. We suggest that in comparison with other ways to circumvent the thermodynamic barrier of such condensation reactions, the exergonic impact of nanofluid phenomena in aqueous particle suspensions on RNA polymerisation and stabilisation is of high relevance for prebiotic plausibility, as it does not require nonphysiological conditions such as temperatures well above 100 °C, alternative solvents, or wet/dry cycles."[14]

4.3.8.   Summary III

"Our results indicate that abiotic temporal nanoconfinements of water within aqueous particle suspensions serve as nanoscopic, flexible reaction vessels for prebiotic, nonenzymatic RNA formation. The findings can solve the water paradox in such a way that nanofluid effects in aqueous particle suspensions open up an abiotic route to biopolymerisation and polymer stabilisation under chemical and thermodynamic conditions that are also prevalent within the crowded intracellular environment of living cells. The fact that polymerase enzymes also form temporal nanoconfined water clusters inside their active site[…][84,85] implies that the same physicochemical effects are tapped for nucleotide condensation in water both by biochemical pathways and our reported abiotic route. These aspects indicate that our model is consistent with evolutionary conservatism stretching back to the era of prebiotic chemical evolution and the origin of cellular life[…][86]. The consistency is further supported by the fact that water is not trapped by nanoconfinements within the polymerase core but can exchange with the surrounding intracellular fluid[…][85] — a situation that also exists in abiotic nanoconfinements of water emerging temporarily between approaching crystal particles in aqueous suspensions. Our experimental finding that under these conditions an amino acid catalyses the abiotic

polymerisation of nucleotides supports first indications of the role of minerals for the origin of cooperation between amino acids and nucleotides[…][87] evolving to the interdependent synthesis of proteins and nucleic acids in living cells[…][88].

Abiotic RNA polymerisation under nanofluid conditions in aqueous particle suspensions does not depend on specific mineralogical and geological environments: now as then, in the prebiotic world, watery suspensions of micro- and nanoparticles are virtually ubiquitous[…][89]. They exist, for example, in the form of sediments with pore water[…][90], hydrothermal vent fluids containing precipitated inorganic[…][91,92] and polyaromatic[…][91,93] particles, atmospheric aerosols with organic and inorganic particle burden[…][94,95], or crowded. dispersed aggregates inside water-filled cracks in the crust of the earth[…][96,97] and possibly of icy moons such as Enceladus[…][98]."[14]

5. Conclusion and Outlook

This thesis was dealing with several aspects of the organic solid/solid wetting deposition (OSWD), a novel method to form monolayers of insoluble organic semiconductor molecules on crystal surfaces, like graphite or graphene, without the need for demanding experimental approaches. In difference to previous studies, this thesis concentrated in the possibilities and its advantages to perform OSWD in water. Hereby, three main aspects were analysed:

- a screening of (bio-)molecules regarding their possible influence on OSWD in water,

- the OSWD in water was applicated for doping of graphene and

- its concept was transferred to the field of origin of life research.

The three main findings of this thesis are:

The OSWD can be influenced by addition of (bio-)molecules to the sample. Whereby the addition of AMP resulted in a strong enhancement of the efficiency of the OSWD. Also, the addition of arginine resulted in a moderate enhancement. These new findings make the OSWD method an even more attractive method when it comes to the need of an environment friendly deposition method, e.g., in the semiconductor industry.

The OSWD in water can be used as a method to generate a doping of graphene, by drop casting it on the graphene´s surface. With this new developed method, neither toxic, expensive chemicals, nor experimentally demanding approaches are needed.

Temporal formed nanoconfinements, that occur during the OSWD process (prebiotic reaction vessel), can explain the enzyme-free condensation of nucleotides to RNA in water and therefore give a plausible and new explanation to how the first RNA molecules might have formed on planet earth.

5.1. Influencing and using the OSWD

The question on how OSWD at room temperature can be improved in terms of the amount of resulting substrate surface area covered with the deposited SAMs was addressed in chapter 4.1.. Here it was shown, that and how the OSWD efficiency can be manipulated by adding different

(bio-)molecules to the aqueous pigment suspensions before applying them to the carrier materials surface (here: graphite or graphene). These findings are especially relevant when it comes to a possible application of the OSWD, e.g., in semiconductor technologies, where SAMs need to cover a high percentage of the substrates (graphene) surface to generate a sufficiently strong doping effect. The results of the performed screening revealed that it is indeed possible to enhance the amount of substrate surface area, covered with SAM domains, by using distinct biomolecules, like AMP and arginine, as it was found in the here presented screening. Hereby, the best enhancement of OSWD was shown by adding AMP to the sample, as this sample resulted in more than two times higher coverage than the sample without any additive. Interestingly, the nucleotide AMP, which is also a building block of RNA (and DNA with a deoxyribose instead of ribose), also plays many crucial roles inside the cell, in difference to the other nucleotides. It can be found in many metabolic and cell signalling pathways as a basic building block of molecules and all natural mRNAs are marked with a poly-A tail. Furthermore, also the addition of the amino acid arginine resulted in an enhancement of the coverage rate. In the case of arginine this effect can partially be explained with the increased pH of the arginine containing sample in comparison to the control sample. For AMP, however, no connection between the pH and the coverage rate was found. Interestingly, both AMP and arginine show a high tendency for stacking, which might be a crucial influence factor regarding the impact of a distinct molecule on enhancing the SAM formation. This finding is also consistent with the results of the residual (bio-)molecules used in the study: no sample that did not contain either AMP or arginine showed a significant change of the amount of covered surface area and none of those (bio-)molecules used in the presented screening is known to have a high stacking affinity, besides of AMP and arginine. Summing up, only those (bio-)molecules used in this study that do undergo high stacking also increased the percentage of SAM covered substrate surface area – here AMP and arginine.

Though in this study a broad field of different biomolecules was analysed as possible enhancer candidates, plenty more biomolecules were still not included and might be examined in further studies. A promising group of (bio-)molecules might be amino acids as well as those that do show high stacking affinity as also the amino acid arginine showed an enhancement effect on the OSWD, when it was added to the suspension.

The findings of this screening are especially important for the development of environmentally friendly an low-cost applications of molecular deposition methods. like for example needed for doping methods in nanoelectronics, as mainly biomolecules were used and no toxic or rare chemicals. Using biomolecules to enhance the OSWD in aqueous environments, does make this

deposition method an environment friendly and low-cost method. Furthermore, the execution of the method is easy and does not require specific skills or expansive and complex instruments. Therefore, by being able to influence the OSWD in water makes it a suitable deposition method, particularly interesting for the semiconductor industry.

5.2. Doping of graphene

In a second part (chapter 4.2.) it was investigated, if the OSWD in water can also be used to dope graphene by surface transfer doping. That means, the substrate graphene becomes doped by charge separation induced by adding a layer of dopant molecules on top of its surface. Surface transfer doping is of particular relevance as a non-destructive doping method of materials in a nanometre range, which makes it especially interesting for nanoelectronics.

Indeed, it could be shown, that a surface transfer doping can be achieved, by depositing SAM on a graphene surface by applying OSWD in water.

The particularity about the demonstrated method is, that it can be performed under ambient conditions, i.e., at room temperature and without vacuum or under clean room conditions. The materials that were used in this thesis, were selected in a way, that all of them are non-toxic and any person, also outside a researching institution, can purchase and handle them. Furthermore, it was taken care, that the materials are of low cost: e.g., to prepare 1 ml of the used flavanthrone dispersion, about 27.5 mg of flavanthrone are needed. Subsequently from this amount only 1-10 µl are consumed for the preparation of 1 cm^2 of graphene covered with flavanthrone domains. The costs for the used flavanthrone powder, to cover 1 cm^2 of graphene produce 10 µl of the suspension, is about 0.01 €; for QAC and dmQAC it is even less than The same calculation for QAC and dmQAC[7] results in less than 0.005 € / cm^2.

With three independent methods, Raman Spectroscopy, Tunnelling Spectroscopy, and measurement of the Dirac peak shift, it was shown, that the underlying graphene indeed was doped, by surface transfer doping after OSWD of flavanthrone. It was also validated that flavanthrone acts as a p-dopant[47,48].

The results offer a new method, easy, low cost, and environment friendly, to produce graphene doped with heteroaromatic semiconductors. Combined with the results from chapter 4.1. even the possibility of an up- (or down) scale of the number of formed domains on the graphene

surface is given. Though it was shown here that AMP also enhances the degree of coverage of the OSWD when using other pigments, it would be necessary to control if this is also true for flavanthrone (if this shall be the pigment of choice for the surface transfer doping). Furthermore, it would be needed to be investigated, if the used (bio-)molecule (AMP or others) influences the doping effect; even if the molecule itself would not deposit on the graphene surface, but probably being washed away in the washing step, as it is soluble in water.

5.3. RNA formation in water

In a third chapter, 4.3., it was addressed if biomolecules do not only influence the efficiency of the OSWD, but also if the chemical behaviour of the biomolecules themselves is impacted during OSWD. Indeed, it was shown that this vice versa interplay occurs. To be precise, nanoconfinements occurring between two surfaces, which are comparable to those occurring during the OSWD process, do probably act like active centres of enzymes, like RNA- and DNA-polymerase. Adequate experimental settings and literature search led to the assumption, that the water activity is reduced within and at the close surrounding of the nanoconfinements, what is analogous in the active centres of enzymes.

These findings enable to create an explanatory model with chemo evolutionary consensus to overcome the water paradox, appearing in many origin of life theories addressing the topic, how the first RNA molecules might have formed on planet earth, in water, without enzymes. It needs to be empathised that in comparison to other origin of RNA / origin of life theories, the here presented hypothesis works without the need of wetting/drying cycles, lightning strikes, or any rare molecules, that probably did not even exist on earth in the moment that the first RNA was formed.

In further studies however, more replicates of the different samples compared in this study should be examined, to get a more reliable statement on the efficiency of the RNA condensation in water without enzymes.

References

1. Oparin, A. I. *The origin of life.* 2nd ed. (Dover Publications, Mineola, New York, 2003).

2. Cooper, G. M. *The cell* (Sinauer Associates, New York, Oxford, 2019).

3. Alberts, B. *Molecular biology of the cell* (Garland Science Taylor and Francis Group, New York, NY, 2015).

4. Tietze, U. & Schenk, C. *Halbleiter-Schaltungstechnik. Mit 189 Tabellen.* 11th ed. (Springer, Berlin, 2001).

5. Trixler, F. *Erzeugung organischer Halbleiternanostrukturen durch Festphasenbenetzung* (2007).

6. Eberle, A., Nosek, A., Büttner, J., Markert, T. & Trixler, F. Growing low-dimensional supramolecular crystals directly from 3D particles. *CrystEngComm* **19,** 1417–1426; 10.1039/C6CE02348G (2017).

7. Eberle, A., Greiner, A., Ivleva, N., Arumugam, B., Niessner, R., Trixler, F. Doping graphene via organic solid-solid wetting deposition. *Carbon* **125,** 84–92; 10.1016/j.carbon.2017.09.043 (2017).

8. Oh, J. S., Kim, K. N. & Yeom, G. Y. Graphene doping methods and device applications. *Journal of nanoscience and nanotechnology* **14,** 1120–1133; 10.1166/jnn.2014.9118 (2014).

9. Hannah Mahoney. The Origins of Life. *Sciential,* 2–7; 10.15173/sciential.v1i4.2241 (2020).

10. Smith, E. *The origin and nature of life on Earth* (Cambridge University Press, Cambridge, 2016).

11. Prosdocimi, F., José, M. V. & Farias, S. T. de. The Theory of Chemical Symbiosis: A Margulian View for the Emergence of Biological Systems (Origin of Life). *Acta Biotheor* **69,** 67–78; 10.1007/s10441-020-09388-7 (2020).

12. Trixler, F., Markert, T., Lackinger, M., Jamitzky, F. & Heckl, W. M. Supramolecular self-assembly initiated by solid-solid wetting. *Chemistry*

(Weinheim an der Bergstrasse, Germany) **13,** 7785–7790; 10.1002/chem.200700529 (2007).

13. Eberle, A., Markert, T. & Trixler, F. Revealing the Physicochemical Basis of Organic Solid-Solid Wetting Deposition: Casimir-like Forces, Hydrophobic Collapse, and the Role of the Zeta Potential. *Journal of the American Chemical Society* **140,** 1327–1336; 10.1021/jacs.7b10282 (2018).

14. Herrera, A. G. de, Markert, T. & Trixler, F. Temporal nanofluid environments induce prebiotic condensation in water. *Communications chemistry* **6,** 69; 10.1038/s42004-023-00872-y (2023).

15. Herbst, W. *Industrielle Organische Pigmente* (Wiley-VCH, Hoboken, 2009).

16. Paulus, E. F., Leusen, F. J. J. & Schmidt, M. U. Crystal structures of quinacridones. *CrystEngComm* **9,** 131–143; 10.1039/B613059C (2007).

17. Kruse, F. M., Teichert, J. S. & Trapp, O. Prebiotic Nucleoside Synthesis: The Selectivity of Simplicity. *Chemistry (Weinheim an der Bergstrasse, Germany)* **26,** 14776–14790; 10.1002/chem.202001513 (2020).

18. Yadav, M., Kumar, R. & Krishnamurthy, R. Chemistry of Abiotic Nucleotide Synthesis. *Chemical reviews* **120,** 4766–4805; 10.1021/acs.chemrev.9b00546 (2020).

19. Cafferty, B. J. & Hud, N. V. Abiotic synthesis of RNA in water: a common goal of prebiotic chemistry and bottom-up synthetic biology. *Current opinion in chemical biology* **22,** 146–157; 10.1016/j.cbpa.2014.09.015 (2014).

20. Yamagishi, A. *Astrobiology. From the Origins of Life to the Search for Extraterrestrial Intelligence* (Springer, Singapore, 2019).

21. Jauker, M., Griesser, H. & Richert, C. Spontaneous Formation of RNA Strands, Peptidyl RNA, and Cofactors. *Angewandte Chemie (International Ed. in English)* **54,** 14564–14569; 10.1002/anie.201506593 (2015).

22. Eberle, A. R. *Growing low-dimensional supramolecular crystals via Organic Solid-Solid Wetting Deposition* (Dissertation, München, 2019; DOI: 10.5282/edoc.24600).

23. Stokes, R. J. & Evans, D. F. *Fundamentals of interfacial engineering* (Wiley-VCH, New York, NY, 1997).

24. Jacobasch, H.-J., Simon, F. & Weidenhammer, P. Adsorption of ions onto polymer surfaces and its influence on zeta potential and adhesion phenomena. *Colloid & Polymer Science* **276,** 434–442; 10.1007/s003960050263 (1998).

25. Christenson, H. K. & Claesson, P. M. Direct measurements of the force between hydrophobic surfaces in water. *Advances in Colloid and Interface Science* **91,** 391–436; 10.1016/S0001-8686(00)00036-1 (2001).

26. Leong, Y. K., Scales, P. J., Healy, T. W., Boger, D. V. & Buscall, R. Rheological evidence of adsorbate-mediated short-range steric forces in concentrated dispersions. *Faraday Trans.* **89,** 2473; 10.1039/ft9938902473 (1993).

27. Berne, B. J., Weeks, J. D. & Zhou, R. Dewetting and hydrophobic interaction in physical and biological systems. *Annual review of physical chemistry* **60,** 85–103; 10.1146/annurev.physchem.58.032806.104445 (2009).

28. Hammer, M. U., Anderson, T. H., Chaimovich, A., Shell, M. S. & Israelachvili, J. The search for the hydrophobic force law. *Faraday discussions* **146,** 299-308; discussion 367-93, 395-401; 10.1039/b926184b. (2010).

29. Remsing, R. C. *et al.* Pathways to dewetting in hydrophobic confinement. *Proceedings of the National Academy of Sciences of the United States of America* **112,** 8181–8186; 10.1073/pnas.1503302112 (2015).

30. Tandon, V., Bhagavatula, S. K., Nelson, W. C. & Kirby, B. J. Zeta potential and electroosmotic mobility in microfluidic devices fabricated from hydrophobic polymers: 1. The origins of charge. *Electrophoresis* **29,** 1092–1101; 10.1002/elps.200700734 (2008).

31. Tandon, V. & Kirby, B. J. Zeta potential and electroosmotic mobility in microfluidic devices fabricated from hydrophobic polymers: 2. Slip and interfacial water structure. *Electrophoresis* **29,** 1102–1114; 10.1002/elps.200800735 (2008).

32. Vrbka, L. *et al.* Propensity of soft ions for the air/water interface. *Current Opinion in Colloid & Interface Science* **9,** 67–73; 10.1016/j.cocis.2004.05.028 (2004).

33. Hölzl, C. & Horinek, D. Pressure increases the ice-like order of water at hydrophobic interfaces. *Physical chemistry chemical physics : PCCP* **20,** 21257–21261; 10.1039/c8cp03057j (2018).

34. Clayden, J., Greeves, N. & Warren, S. G. *Organische Chemie.* 2nd ed. (Springer Spektrum, Berlin, Heidelberg, 2013).

35. *EBOOK PACKAGE Physics, Chemistry, Materials Sc, Geosc 2018 :* (De Gruyter, Berlin, Boston,).

36. Dimitrakopoulos, C. D. & Malenfant, P.R.L. Organic Thin Film Transistors for Large Area Electronics. *Adv. Mater.* **14,** 99–117; 10.1002/1521-4095(20020116)14:2<99::AID-ADMA99>3.0.CO;2-9 (2002).

37. Hunger, K. & Schmidt, M. U. *Industrial organic pigments. Production, crystal structures, properties, applications* (Wiley-VCH Verlag GmbH & Co. KGaA, Weinheim, 2018).

38. Samorì, P. & Palermo, V. (eds.). *Flexible carbon-based electronics* (Wiley-VCH, Weinheim, Germany, 2018).

39. Kobayashi, H. *et al.* A novel RGB multicolor light-emitting polymer display. *Synthetic Metals* **111-112,** 125–128; 10.1016/S0379-6779(99)00322-7 (2000).

40. Rogers, J. A. *et al.* Paper-like electronic displays: Large-area rubber-stamped plastic sheets of electronics and microencapsulated electrophoretic inks. *Proceedings of the National Academy of Sciences* **98,** 4835–4840; 10.1073/pnas.091588098 (2001).

41. Campbell, N. A. *Campbell, Biologie.* 11th ed. (Pearson, Hallbergmoos, 2019).

42. Purves, W. K. *Life. The science of biology.* 7th ed. (Sinauer Associates, Sunderland, Mass., 2004).

43. Voet, D. *Lehrbuch der Biochemie* (Wiley-VCH, Weinheim, 2019).

44. Neveu, M., Kim, H.-J. & Benner, S. A. The "strong" RNA world hypothesis: fifty years old. *Astrobiology* **13,** 391–403; 10.1089/ast.2012.0868 (2013).

45. *Organische Chemie* (De Gruyter, Berlin, 1980).

46. PubChem. Quinacridone (Compound); 3.2.5Solubility. Insoluble in water ITC/USEPA; Information Review #315 (Draft) Cinquasia Red p.1 (1982) Hazardous Substances Data Bank (HSDB) Insoluble in organic solvents and dispersion media. Insoluble in water ITC/USEPA; Information Review #315 Cinquasia Red p.1 (1982). Available at Quinacridone.

47. Hiramoto, M., Kawase, S. & Yokoyama, M. Photoinduced Hole Injection Multiplication in p-Type Quinacridone Pigment Films. *Jpn. J. Appl. Phys.* **35,** L349-L351; 10.1143/JJAP.35.L349 (1996).

48. Kotwica, K. *et al.* Soluble Flavanthrone Derivatives: Synthesis, Characterization, and Application to Organic Light-Emitting Diodes. *Chemistry (Weinheim an der Bergstrasse, Germany)* **22,** 7978–7986; 10.1002/chem.201600513 (2016).

49. Garcia-Elias, A. *et al.* Defining quantification methods and optimizing protocols for microarray hybridization of circulating microRNAs. *Sci Rep* **7**; 10.1038/s41598-017-08134-3 (2017).

50. Life Technologies (ed.). *Quibit(R) 3.0 Fluorometer. Catalog Number Q33216* (2014).

51. Flocco, M. M. & Mowbray, S. L. Planar stacking interactions of arginine and aromatic side-chains in proteins. *Journal of molecular biology* **235**; 10.1006/jmbi.1994.1022 (1994).

52. Mehran Kardar & Ramin Golestanian. The `Friction' of Vacuum, and other Fluctuation-Induced Forces. *Review of Modern Physics* **71**; 10.1103/RevModPhys.71.1233 (1997).

53. Sigel, H. Self-association of nucleotides. Effects of protonation and metal ion coordination. *Biological trace element research* **21,** 49–59; 10.1007/BF02917236 (1989).

54. Tribolet, R. & Sigel, H. Self-association of adenosine 5'-monophosphate (5'-AMP) as a function of pH and in comparison with adenosine, 2'-AMP and 3'-AMP. *Biophysical chemistry* **27,** 119–130; 10.1016/0301-4622(87)80052-2 (1987).

55. Neurohr, K. J. & Mantsch, H. H. The self-association of naturally occurring purine nucleoside 5′-monophosphates in aqueous solution. *Can. J. Chem.* **57,** 1986–1994; 10.1139/v79-318 (1979).

56. Norberg, J. & Nilsson, L. Stacking Free Energy Profiles for All 16 Natural Ribodinucleoside Monophosphates in Aqueous Solution. *Journal of the American Chemical Society* **117,** 10832–10840; 10.1021/ja00149a006 (1995).

57. Vernon, R. M. *et al.* Pi-Pi contacts are an overlooked protein feature relevant to phase separation. *eLife* **7**; 10.7554/eLife.31486 (2018).

58. Ferrari, A. C. Raman spectroscopy of graphene and graphite: Disorder, electron–phonon coupling, doping and nonadiabatic effects. *Solid State Communications* **143,** 47–57; 10.1016/j.ssc.2007.03.052 (2007).

59. Dong, X. *et al.* Doping single-layer graphene with aromatic molecules. *Small (Weinheim an der Bergstrasse, Germany)* **5,** 1422–1426; 10.1002/smll.200801711 (2009).

60. Casiraghi, C. Probing disorder and charged impurities in graphene by Raman spectroscopy. *phys. stat. sol. (RRL)* **3,** 175–177; 10.1002/pssr.200903135 (2009).

61. Ferrari, A. C. & Basko, D. M. Raman spectroscopy as a versatile tool for studying the properties of graphene. *Nature nanotechnology* **8,** 235–246; 10.1038/nnano.2013.46 (2013).

62. Liu, H., Liu, Y. & Zhu, D. Chemical doping of graphene. *J. Mater. Chem.* **21,** 3335–3345; 10.1039/C0JM02922J (2011).

63. Głowacki, D., *et al.* Intermolecular hydrogen-bonded organic semiconductors—Quinacridone versus pentacene. *Appl. Phys. Lett.* **101,** 23305; 10.1063/1.4736579 (2012).

64. Leonat, L., Sbârcea, G., Brânzoi, I. V., Cyclic voltammetry for energy levels estimation of organic materials. *U.P.B. Sci. Bull., Series B, Vol. 75* (2013).

65. Li, G., Luican, A. & Andrei, E. Y. Scanning tunneling spectroscopy of graphene on graphite. *Physical review letters* **102,** 176804; 10.1103/PhysRevLett.102.176804 (2009).

66. Casiraghi, C., Doping dependence of the Raman peaks intensity of graphene near the Dirac point. *Physical review. B, Condensed matter* **80**; 10.1103/PhysRevB.80.233407 (2009).

67. Jones, G. Graphene doping and Dirac point position. Available at Retrieved from: https://www.researchgate.net/post/Graphene_doping_and_Dirac_point_positi on/58e78168cbd5c2879e0c8bcc/citation/download.

68. Shimatani, M. *et al.* Giant Dirac point shift of graphene phototransistors by doped silicon substrate current. *AIP Advances* **6,** 35113; 10.1063/1.4944622 (2016).

69. Singh, A. K., Chaudhary, V., Singh, A. K. & Sinha, S. R. P. Investigation of electronic properties of chemical vapor deposition grown single layer graphene via doping of thin transparent conductive films. *RSC advances* **11,** 3096–3103; 10.1039/D0RA10057A (2021).

70. Suzuki et al. *Organic photovoltaic element.* U.S. patent, publishing nb. 5,350,459; (1994)

71. Neubeck, A. *Prebiotic Chemistry and the Origin of Life* (Springer International Publishing AG, Cham, 2021).

72. Lazcano, A. Prebiotic Evolution and Self-Assembly of Nucleic Acids. *ACS Nano* **12,** 9643–9647; 10.1021/acsnano.8b07605 (2018).

73. Yokosawa, T. *et al.* A step into the RNA world: Conditional analysis of hydrogel formation of adenosine 5'-monophosphate induced by cyanuric acid. *Bio Systems* **162,** 53–58; 10.1016/j.biosystems.2017.09.004 (2017).

74. Lang, C., Lago, J. & Pasek, M. A. *Handbook of astrobiology. Phosphorylation on the early earth: the role of phosphorous in biochemistry and its bioavailability.* (CRC PRESS, Boca Raton, Florida, 2019).

75. Georgelin, T., Jaber, M., Bazzi, H. & Lambert, J.-F. Formation of activated biomolecules by condensation on mineral surfaces--a comparison of peptide bond formation and phosphate condensation. *Origins of life and evolution of the biosphere : the journal of the International Society for the Study of the Origin of Life* **43,** 429–443; 10.1007/s11084-013-9345-2 (2013).

76. Kaddour, H. *et al.* Nonenzymatic RNA Oligomerization at the Mineral–Water Interface: An Insight into the Adsorption–Polymerization Relationship. *J. Phys. Chem. C* **122,** 29386–29397; 10.1021/acs.jpcc.8b10288 (2018).

77. Knight, A. W., Kalugin, N. G., Coker, E. & Ilgen, A. G. Water properties under nano-scale confinement. *Sci Rep* **9,** 8246; 10.1038/s41598-019-44651-z (2019).

78. Dass, A. V. *et al.* Potential Role of Inorganic Confined Environments in Prebiotic Phosphorylation. *Life (Basel, Switzerland)* **8**; 10.3390/life8010007 (2018).

79. Eijkel, J. C. T. & van den Berg, A. Nanofluidics: what is it and what can we expect from it? *Microfluid Nanofluid* **1,** 249–267; 10.1007/s10404-004-0012-9 (2005).

80. Podgornik, R. & Dobnikar, J. Casimir and pseudo-Casimir interactions in confined polyelectrolytes. *The Journal of Chemical Physics* **115,** 1951–1959; 10.1063/1.1383052 (2001).

81. Milshteyn, D., Cooper, G. & Deamer, D. Chemiosmotic energy for primitive cellular life: Proton gradients are generated across lipid membranes by redox reactions coupled to meteoritic quinones. *Sci Rep* **9,** 12447; 10.1038/s41598-019-48328-5 (2019).

82. Ross, D. S. & Deamer, D. Dry/Wet Cycling and the Thermodynamics and Kinetics of Prebiotic Polymer Synthesis. *Life (Basel, Switzerland)* **6**; 10.3390/life6030028 (2016).

83. Jonchhe, S. *et al.* Decreased water activity in nanoconfinement contributes to the folding of G-quadruplex and i-motif structures. *Proceedings of the National Academy of Sciences of the United States of America* **115,** 9539–9544; 10.1073/pnas.1805939115 (2018).

84. Tropp, B. E. & Freifelder, D. *Molecular biology. Genes to proteins.* 3rd ed. (Jones and Bartlett Publishers, Sudbury (Mass.), 2008).

85. Qin, Y. *et al.* Direct probing of solvent accessibility and mobility at the binding interface of polymerase (Dpo4)-DNA complex. *The journal of physical chemistry. A* **117,** 13926–13934; 10.1021/jp410051w (2013).

86. Saha, R., Pohorille, A. & Chen, I. A. Molecular crowding and early evolution. *Origins of life and evolution of the biosphere : the journal of the International Society for the Study of the Origin of Life* **44,** 319–324; 10.1007/s11084-014-9392-3 (2014).

87. Namani, T. *et al.* Amino Acid Specific Nonenzymatic Montmorillonite-Promoted RNA Polymerization. *ChemSystemsChem* **3,** 2; 10.1002/syst.202000060 (2021).

88. Kolb, V. M. *Handbook of Astrobiology* (CRC PRESS, Boca Raton, Florida : CRC Press, [2019], 2018).

89. Alekseyev, V. A. Nanoparticles and Nanofluids in Water–Rock Interactions. *Geochem. Int.* **57,** 357–368; 10.1134/S0016702919040037 (2019).

90. *Marine chemistry and geochemistry* (Elservier/Academic Press, Amsterdam, Boston, 2010).

91. Gartman, A. *et al.* The role of nanoparticles in mediating element deposition and transport at hydrothermal vents. *Geochimica et Cosmochimica Acta* **261,** 113–131; 10.1016/j.gca.2019.06.045 (2019).

92. Russell, M. J. The "Water Problem"(sic), the Illusory Pond and Life's Submarine Emergence-A Review. *Life (Basel, Switzerland)* **11**; 10.3390/life11050429 (2021).

93. Konn, C. *et al.* Organic, Gas, and Element Geochemistry of Hydrothermal Fluids of the Newly Discovered Extensive Hydrothermal Area in the Wallis and Futuna Region (SW Pacific). *Geofluids* **2018,** 1–25; 10.1155/2018/7692839 (2018).

94. Buseck, P. R. & Pósfai, M. Airborne minerals and related aerosol particles: effects on climate and the environment. *Proceedings of the National Academy of Sciences* **96,** 3372–3379; 10.1073/pnas.96.7.3372 (1999).

95. Trainer, M. G. Atmospheric Prebiotic Chemistry and Organic Hazes. *COC* **17,** 1710–1723; 10.2174/13852728113179990078 (2013).

96. Grevemeyer, I., Ranero, C. R. & Ivandic, M. Structure of oceanic crust and serpentinization at subduction trenches. *Geosphere* **14,** 395–418; 10.1130/GES01537.1 (2018).

97. do Nascimento Vieira, A., Kleinermanns, K., Martin, W. F. & Preiner, M. The ambivalent role of water at the origins of life. *FEBS Lett* **594,** 2717–2733; 10.1002/1873-3468.13815 (2020).

98. Postberg, F. *et al.* Macromolecular organic compounds from the depths of Enceladus. *Nature* **558,** 564–568; 10.1038/s41586-018-0246-4 (2018).

List of Figures

particles: 0.14 ng per µl; pure aqueous samples only containing QAC or graphite: both underneath the detection level."[14] 84

Figure 33: Results of quantitative polymerase chain reaction. Grey: sample (AMP + QAC + Graphite (resuspended gel-pellet from precipitation of an aqueous AMP-QAC-Graphite suspension, prepared as described in the method section)); green: control sample (miRNA of 23nt length); yellow: negative control. (A) Fluorescent curve, (B) Melting curve.................. 85

Figure 34: "Lane L shows the RNA bands of the molecular weight marker (ladder). Lanes 1–3 represent the triplicate of a typical incubated, precipitated sample made of suspended QAC and graphite particles and dissolved AMP. This sample was analysed with fluorometry prior to gel electrophoresis and showed an RNA concentration of 2.0 ng per µl. Lanes 4–6 represent triplicates of a negative control sample with no detectable RNA concentration according to fluorometric results. The prominent, isolated sharp signal in lane 5 is interpreted as an artifact, arising from the instrument's sensitivity to even low vibrations of the laboratory bench."[14].. 86

Figure 35: "Dynamic force field calculation of a nucleotide stack in nanoconfined water. The system is modelled within a supercell containing two graphene layers (bottom), two layers of a QAC crystal (top) and a stack of 12 AMP molecules placed between the confining surfaces. Vertical dimension of the gap: 43 Å. […][(A)] Condition of the stack after a simulated time span of 50 ps. The confinement is filled with water molecules. […][(B)] Condition of the stack after a simulated time span of 60 ps and a water density of ~60%."[14]..................................... 91

List of Tables

Appendix

Temporal nanofluid environments induce prebiotic condensation in water

Andrea Greiner de Herrera[1,2,3], Thomas Markert [4] & Frank Trixler [1,3,5✉]

Water is a problem in understanding chemical evolution towards life's origins on Earth. Although all known life is being based on water key prebiotic reactions are inhibited by it. The prebiotic plausibility of current strategies to circumvent this paradox is questionable regarding the principle that evolution builds on existing pathways. Here, we report a straightforward way to overcome the water paradox in line with evolutionary conservatism. By utilising a molecular deposition method as a physicochemical probe, we uncovered a synergy between biomolecule assembly and temporal nanofluid conditions that emerge within transient nanoconfinements of water between suspended particles. Results from fluorometry, quantitative PCR, melting curve analysis, gel electrophoresis and computational modelling reveal that such conditions induce nonenzymatic polymerisation of nucleotides and promote basic cooperation between nucleotides and amino acids for RNA formation. Aqueous particle suspensions are a geochemical ubiquitous and thus prebiotic highly plausible setting. Harnessing nanofluid conditions in this setting for prebiotic syntheses is consistent with evolutionary conservatism, as living cells also work with temporal nanoconfined water for biosynthesis. Our findings add key insights required to understand the transition from geochemistry to biochemistry and open up systematic pathways to water-based green chemistry approaches in materials science and nanotechnology.

[1] Department of Earth and Environmental Sciences, Ludwig-Maximilians-Universität München, Theresienstraße 41, 80333 Munich, Germany. [2] Center for Neuropathology and Prion Research (ZNP), Ludwig-Maximilians-Universität München, Feodor-Lynen-Str. 23, 81377 Munich, Germany. [3] School of Education, Technical University of Munich and Deutsches Museum, Museumsinsel 1, 80538 Munich, Germany. [4] Institute of Theoretical Chemistry, Ulm University, Albert-Einstein-Allee 11, 89081 Ulm, Germany. [5] Center for NanoScience (CeNS), Ludwig-Maximilians-Universität München, Schellingtr. 4, 80799 Munich, Germany. ✉email: trixler@lrz.uni-muenchen.de

Prebiotic chemistry is facing a serious problem in regard to the role of water in the emergence of life on Earth: although water is essential for all life as we know it, key biochemical reactions such as the polymerisation of nucleotides into ribonucleic acid (RNA) are impeded in watery solutions[1]. In aiming to overcome this so-called "water problem" in prebiotic chemistry[2], several hypotheses have been proposed[3–6]. Among them are concepts of adding condensing agents such as cyanamide, using alternative solvents such as formamide, setting high temperatures of about 160 °C, or designing prebiotic scenarios based on wet/dry cycles. However, when appraising the plausibility of such concepts and scenarios, general weaknesses appear[4]. A key aspect is that all known life manages the water problem within a stable environment full of water and does not rely on physical conditions and chemical substances proposed in these concepts. This aspect is of particular relevance regarding evolutionary conservatism—the principle that evolution builds on existing pathways[7]. In this context, the principle indicates that the same physicochemical effects were involved in the abiotic origin of biopolymers, as is now being tapped by living systems via complex enzymes.

Living cells contain an intracellular aqueous fluid that is crowded with large, complex biomolecules. In this environment, virtually all water exists as interfacial water[8]. When viewing this dense mixture from the perspective of materials science, it is describable as an aqueous suspension of highly concentrated nanoparticles. In the vicinity of such particles, various nanofluid phenomena emerge in interfacial and nanoconfined water[9, 10]. Consequently, such water differs significantly compared to bulk water in terms of properties such as flow behaviour, reactivity, H-bonding network dynamics, density, dielectric constant, or the quantum state of protons[11–14]. From a geochemical point of view, aqueous suspensions of mineral particles of micro- and nanoscopic size can be regarded as a comparable environment that generates nanofluid effects.

Inspired by this similarity, we designed experiments to test the potential of nanofluid environments within aqueous suspensions of particles for inducing key biochemical reactions in a possibly prebiotic context. As various prebiotic synthesis pathways of nucleosides[15] and nucleotides[4] have been proposed and because the abiotic condensation of nucleotides into RNA within water is a common goal of prebiotic chemistry[16, 17], we chose the polymerisation of nucleotides into RNA as an example reaction. The focus was set on the formation of a pure adenosine-based RNA (poly(A) RNA) since adenosine monophosphate (AMP) is the most common nucleotide in living cells[18]. Furthermore, poly(A) RNAs are common RNAs in cells in the form of poly(A)-tails of messenger RNAs during the process of protein biosynthesis. Thus, we first prepared samples that contained dissolved AMP. To create a nanofluid environment for AMP solutions, we selected quinacridone (QAC) as an example of polyaromatic heterocycle particles and graphite as an inorganic suspended particle species, as both compounds have been well characterised in terms of inducing nanofluid phenomena in aqueous suspensions[19].

According to our results on fluorometric RNA quantification, reverse transcription quantitative polymerase chain reaction (RT-qPCR), melting curve analysis, and capillary gel electrophoresis, abiotic polymerisation of nucleotides into RNA can occur within aqueous dispersions of polyaromatic hydrocarbons and inorganic minerals in the absence of enzymes or additives. We present the synthesis of various amounts of RNA depending on variations of the experimental parameters and propose an explanatory model based on nonclassical effects on water when temporally confined by suspended particles. The model describes how such temporal, fluctuating nanoconfinements can solve the water paradox by altering crucial physicochemical properties of water and how evolutionary conservatism can link these dynamic natural nanofluid reaction vessels to enzymatic biopolymerisation in biological cells.

Results and discussion

Fluorometric poly(A) RNA quantification. Figure 1a shows the results of fluorometric RNA concentration measurements of such samples. Both ethanol precipitation and isopropanol precipitation
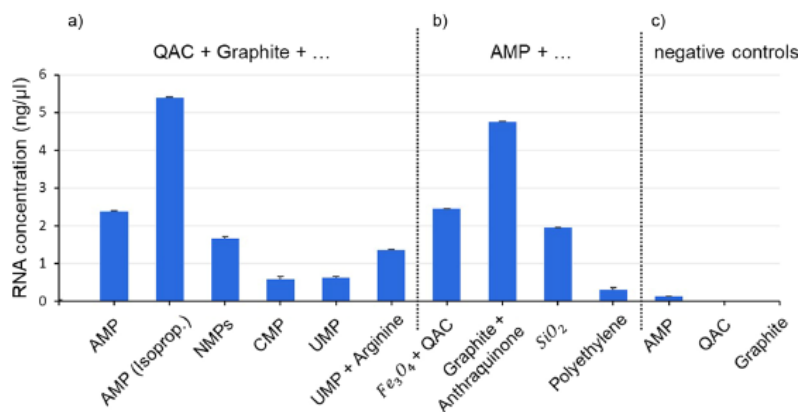

Fig. 1 Fluorometric results of RNA concentration measurements in aqueous particle suspensions. Displayed are the mean values of three measurement replicates and standard deviations. If not differently indicated, nucleotide suspensions had a final concentration of 50 mM and RNA isolation was performed from aqueous suspensions of particles containing dissolved biomolecules using EtOH and NaCl for precipitation. **a** Detected RNA concentrations in samples based on QAC + graphite suspensions: AMP: 2.38 ng per µl; AMP (isoprop.): precipitation was performed using isopropanol and NaOAc; detected concentration: 5.4 ng per µl; mixture of NMPs (AMP, UMP, GMP, CMP, 12.5 mM each): 1.66 ng per µl; CMP: 0.59 ng per µl; UMP: 0.62 ng per µl; mixture of UMP and arginine: 1.36 ng per µl. **b** Detected poly(A) RNA concentrations in suspensions based on: Fe3O4/QAC: 2.45 ng per µl; graphite/anthraquinone: 4.76 ng per µl; SiO₂: 1.96 ng per µl; polyethylene: 0.3 ng per µl. **c** Results of the negative controls: aqueous samples containing AMP but without suspended particles: 0.14 ng per µl; pure aqueous samples only containing QAC or graphite: both underneath the detection level.

were applied. The results of both precipitation methods reveal that poly(A) RNA strands have formed in significant amounts regarding the negative controls (Fig. 1c). After having incubated a sample for over 4 weeks at room temperature, the presence of poly(A) RNA was still detected in a concentration (2.53 ng per µl) similar to a comparable suspension sample to which the standard incubation protocol was applied (2.38 ng per µl, Fig. 1a). Negative controls had been performed with all substrate and organic pigment powders used in this study. None of those powders led to a detectable RNA concentration. Furthermore, the RNA concentration of aqueous solutions of mononucleotides was measured, resulting in no detectable RNA signal in the Qubit® Fluorometer. Therefore, RNA contamination of the educts can be excluded. Furthermore, a negative sample using only AMP was analysed to find out if poly-A-RNA is also formed by incubation or precipitation when no substrate or organic pigment is present. The concentration of this sample is lower than the level of RNA amount, reproducibly quantified by the manufacturer of the Qubit® Assay, and can therefore be taken as lower than the reliable detection level, though it seems that very small amounts of poly-A-RNA are also formed without adding substrates or organic pigments.

Quantitative RT-qPCR. To cross-check the fluorometric quantification with a totally independent but also highly specific method, we performed quantitative polymerase chain reaction after reverse transcription (RT-qPCR). The results (Fig. 2a) show that the signal of the sample exceeds the background fluorescence after 7.57 cycles. This indicates a high yield (103-fold) of input RNA in comparison to the respective signal of the positive control miRNA (14.25 cycles). To obtain indications on the length of the formed RNA, we performed a comparative melting curve analysis after the last cycle of the qPCR. This analysis included the sample RNA and a positive control miRNA with a length of 23 nt. The comparison reveals that the medium melting point of the sample
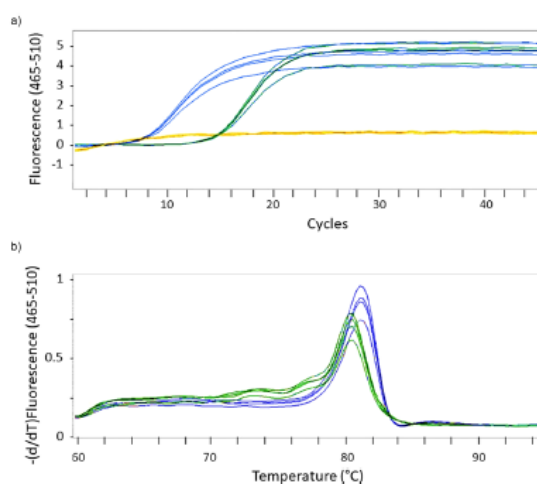
is at a higher temperature than the positive control (Fig. 2b). These results suggest that the sample contains created oligonucleotides with lengths equal to or longer than 23 nt.

Capillary gel electrophoresis of RNA. As an additional approach to cross-check the presence of RNA and to acquire more information on the length distribution of any formed RNA strands in our samples, we applied capillary gel electrophoresis by using the Agilent RNA 6000 Nano Kit. We chose this technique due to its high specificity for RNA and—like the other RNA detection techniques we selected for our study—due to its tolerance against residual crystal particles suspended in our samples. For the analysis, we chose a sample that contained QAC and graphite particles suspended in an aqueous solution of AMP and applied EtOH/NaCl for precipitation. The results show a broad distribution of RNA bands in the triplicates of the sample (Fig. 3, lanes 1–3). These clear and numerous bands further support our previous findings that RNA is present in our samples and also give a strong indication not only for the existence of short RNAs lengths below 25 nt but also for the presence of a large fraction of formed RNA strands with lengths of up to 4000 nt and more.

Contamination with any natural RNA can be excluded due to the lack of the prominent rRNA double bands of the smaller and the larger ribosome subunits. To identify possible background noises in gel electrophoresis that might be caused by residual nanoparticles in the samples after precipitation, a negative control with a typical particle concentration was used that represented a sample with no detectable RNA signal from fluorometry. The results (Fig. 3, lanes 4–6) suggest that such possible background noise from residual particles is below the detection limit of the used electrophoresis system. The outcome also indicates that the results of fluorometry and electrophoresis concerning the presence or absence of RNA are consistent.

Identifying factors that determine abiotically induced polymerisation. To identify substantial factors that lead to the observed abiotic polymerisation, we first analysed the possible role of π-stacking of nucleoside monophosphates (NMPs), as
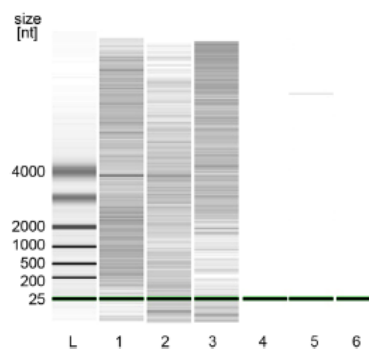

Fig. 2 Quantitative PCR after reverse transcription (RT-qPCR) applied to an aqueous particle suspension with dissolved AMP. Yellow: negative control; green: positive control (synthetic miRNA hsa-miR-134-3p (5´-phosphorylated)); blue: sample (precipitation from sample "QAC + Graphite + AMP", Fig. 1a). **a** Fluorescent signals of qPCR. The signals exceed the background fluorescence (yellow) after 7.57 cycles (sample) and 14.25 cycles (positive control). **b** Melting curves. Medium melting point: positive control (green): 80.53 °C, sample (blue): 81.31 °C.

Fig. 3 Results of RNA gel electrophoresis. Lane L shows the RNA bands of the molecular weight marker (ladder). Lanes 1–3 represent the triplicate of a typical incubated, precipitated sample made of suspended QAC and graphite particles and dissolved AMP. This sample was analysed with fluorometry prior to gel electrophoresis and showed an RNA concentration of 2.0 ng per µl. Lanes 4–6 represent triplicates of a negative control sample with no detectable RNA concentration according to fluorometric results. The prominent, isolated sharp signal in lane 5 is interpreted as an artifact, arising from the instrument's sensitivity to even low vibrations of the laboratory bench.
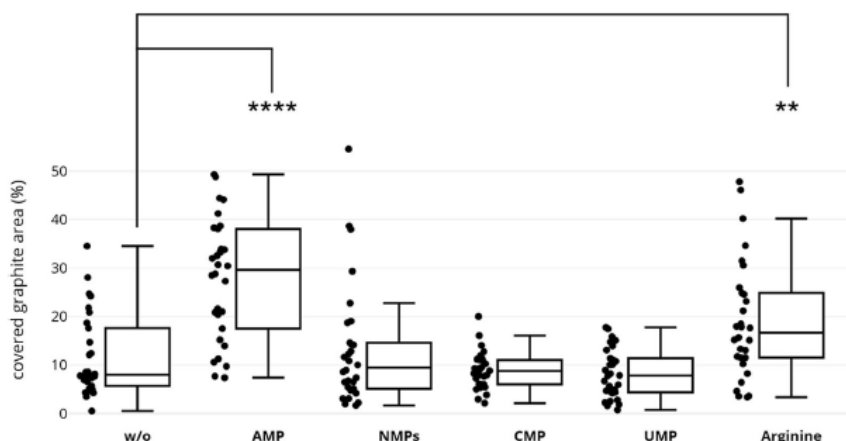
Fig. 4 OSWD efficiency as a function of biomolecular species added to aqueous particle suspensions. The box plots and distributions of values are based on results obtained by STM. The statistical analysis of the results reveals the coverage of graphite surfaces with organic semiconductor QAC monolayer. The adsorbate forms after graphite has been brought into contact with a watery suspension of QAC particles that either contains dissolved biomolecules (AMP, NMPs, CMP, UMP, arginine) or no biomolecules (w/o). Testing: t-test with Welch's correction; $n = 30$ independent scans; $**p < 0.01$; $****p < 0.0001$.

stacking has been suggested to be an important factor for RNA polymerisation in terms of bringing the monomers in close contact[20]. To perform this analysis, we extended the fluorometric analysis of ethanol precipitated AMP-based samples to CMP- and UMP-based samples and compared the relationship of the different RNA concentration results with the relationship of respective published stacking equilibrium constants and stacking free energies of NMPs. The comparison reveals that the detected relative concentration of poly(A) RNA is about four times higher than that of poly(C) RNA and poly(U) RNA (Fig. 1a) and that this order (poly(A) RNA >> poly(C) RNA ~ poly(U) RNA) correlates to the order of the respective stacking equilibrium constants and stacking abilities derived from the stacking free energy profiles of NMPs[21]. This correlation suggests that in particle suspensions, stacking and polymerisation of nucleotides are linked. Therefore, enhancing the stacking ability of a nucleotide should result in a higher RNA concentration. To test this hypothesis, we selected UMP due to its low self-stacking ability and its comparatively low poly(U) RNA formation and added the amino acid arginine to the sample. Arginine is known for its high stacking ability with aromatic groups[22]. Fluorometric analysis of UMP/arginine-based samples revealed that arginine increased the formation of poly(U) RNA by more than 100% (Fig. 1a). This observation supports the necessity of π-stacking for polymerisation in aqueous suspensions and points to a possibly prebiotic relevant kind of interplay between amino acids and nucleic acids.

However, base stacking cannot be the key factor for RNA formation in the described samples. This becomes evident when taking the water paradox into account and when considering the result of a negative control based on an AMP solution without suspended particles (Fig. 1c): although AMP has the highest self-stacking constant among all NMPs[21] and is the only NMP with the ability to self-associate in indefinite stacks[23], the negative control shows that in comparison to the poly(A) RNA concentrations reported above, only minute amounts can be found when the sample contains no added particles. This result suggests that there is a key factor in promoting both stacking and polymerisation that is closely linked to the particle suspension nature of the samples.

It is known that reducing the dielectric constant of water favours stacking[23], and reducing the activity of water (e.g. by adding alternative solvents, inducing wet/dry cycles, or intercalation) promotes polymerisation[3, 24, 25]. As nanofluid phenomena emerging in temporal nanoconfined water can reduce both properties simultaneously[13, 26] and watery suspensions of particles give rise to such phenomena[9], we infer that the occurrence of nanofluid phenomena in our samples is the key factor for the observed nucleotide polymerisation. This implies that the enhancement of nanofluid effects should correlate with an increase in polymerisation reactions.

Comparing the extent of nanofluid effects to polymerisation efficiency. Nanoconfining environments change the behaviour of water, especially in terms of its hydrogen bond network dynamics[13], which, in turn, affects the thermodynamic property of water activity[26]. The anomalous behaviour of nanoconfined water results from a highly complex interplay of various nanofluid phenomena and forces that are related to, for example, the surface energy and size of the confining boundaries, shear, molecular structure, electrical double layer, and fluctuations of general order parameter[9, 27]. To cope with this high complexity when assessing a possible synergy between nanofluid phenomena and polymerisation, we chose an experimental approach that allows us to focus on a single, quantifiable effect. This approach uses the effect of organic solid/solid wetting deposition (OSWD) as a probe. OSWD is the final result of a network of various nanofluid phenomena on confined water between suspended organic crystals, including double-layer forces, Casimir-like fluctuation-induced forces, and dewetting-induced hydrophobic collapse[19]. It manifests as the adsorption and self-assembly of insoluble polyaromatic heterocycles at solid/solid interfaces and thus is quantifiable via surface coverage determination.

We quantified the efficiency of OSWD as a function of different biomolecules dissolved in watery suspensions of particles of the organic semiconductor QAC. For quantification, we measured the surface coverage of graphite with QAC monolayers via scanning tunnelling microscopy (see Supplementary Figs. 1 and 2). The results (Fig. 4) reveal that adding AMP to
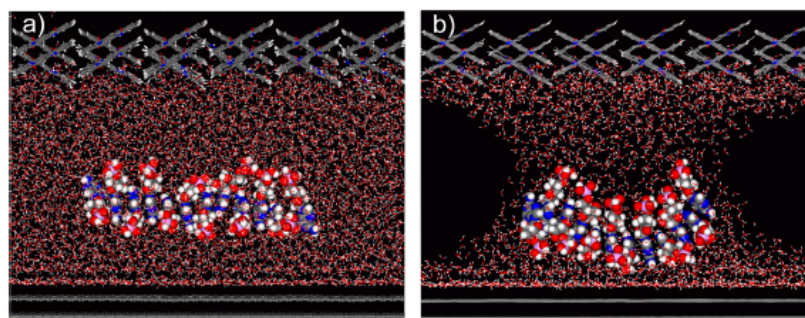
Fig. 5 Dynamic force field calculation of a nucleotide stack in nanoconfined water. The system is modelled within a supercell containing two graphene layers (bottom), two layers of a QAC crystal (top) and a stack of 12 AMP molecules placed between the confining surfaces. Vertical dimension of the gap: 43 Å. **a** Condition of the stack after a simulated time span of 50 ps. The confinement is filled with water molecules. **b** Condition of the stack after a simulated time span of 60 ps and a water density of ~60%.

the particle suspension enhances the coverage with very high statistical significance ($p < 0.0001$) in relation to QAC suspensions based on pure water (w/o, Fig. 4), though the pH was not increased to the same extent (pH of aqueous suspension of QAC: 7.5; pH with AMP added: 8.8). A significant increase in coverage ($p < 0.01$) also occurred when using arginine as the added biomolecule (pH 10.6). By contrast, coverages found in samples based on CMP or UMP are statistically nearly identical and significantly lower with respect to the AMP- and arginine-based samples. Using a mixture of different NMPs leads to no significant increase in coverage but results in some very high single coverage measurements regarding the CMP and UMP samples (NMPs, dot plot, Fig. 4), possibly caused by clusters of the AMP fraction of the mixture. The comparison of these OSWD induced coverages with RNA quantities (Fig. 1a) indicates that relative differences in the extent of nanofluid phenomena between the samples correlate with relative differences in detected RNA quantities. This supports the hypothesis of synergy between nanoconfinement effects and nucleotide polymerisation in aqueous particle suspensions. We thus propose that the emergence of nanofluid effects on confined water is the key factor in the promotion of both stacking and polymerisation of nucleotides within aqueous suspensions of particles.

Assessing the generalisability of suspension-induced polymerisation. Thus far, we used QAC/graphite particle systems to ensure comparability of the results from different experimental approaches. To test whether the formation of RNA in such an environment is generalisable, we measured samples prepared by the same protocol but containing particles based on other compounds. As inorganic substitutes, we chose magnetite and silica as geologically widespread compounds and selected the organic compound anthraquinone due to its abundance in carbonaceous meteorites[28]. Fluorometric measurements of partly or fully substituted samples show poly(A) RNA concentrations that are similar to or substantially higher than the comparable output of the QAC/graphite model system (Fig. 1b). This indicates that the abiotic formation of RNA within nanofluid environments of aqueous suspensions is of general nature. Our results also imply that the output of RNA can be increased to higher concentrations by identifying appropriate particle suspension systems. The influence of the particle species on the RNA concentration, as indicated by Fig. 1b (including results from inert polyethylene particles as a comparison), is consistent with the fact that the anomalous behaviour of nanoconfined water is partly determined by the characteristics of the confining surfaces[12].

Dynamic molecular mechanics calculations. For nanofluid effects to become dominant, the confining surfaces must approach, at a conservative estimate, within the range of 10 nm and below[13]. To evaluate whether stacking of nucleotides within such nanoconfinements is possible in a sufficiently stable and ordered way to prime polymerisation, we performed dynamic molecular mechanics calculations. For performing these calculations, we modelled a stack of 12 AMPs as an example system referring to the observation that polymerised AMPs of more than 10 nt length were abundant in our samples. We arranged this stack in parallel between two nanoscale separated crystals of a QAC/graphite system and added water to the confinement. Figure 5a shows the condition of the stack at the end of a dynamic simulation modelled with a confinement gap size of about 4 nm. This condition implies that the nucleotide stack remained arranged in such confinement when surrounded by water (see also Supplementary Movie 1). Comparative calculations suggest that such stacks are deformed, but stable even when the density of water—which can be lower in nanoconfined conditions[13]—is decreased to ~60% (Fig. 5b and Supplementary Movie 2). It requires a reduction of the gap size to about 3 nm and below to finally destabilise a stack due to increased interactions with confining surfaces (Supplementary Fig. 3). In sum, these simulations indicate that it is feasible to assume that nucleotides can associate in stable stacks within nanoconfinement gap sizes well below 10 nm for priming polymerisation.

Thermodynamic considerations. Nucleotide polymerisation into RNA is a water-releasing condensation reaction that faces a thermodynamic barrier as the change in the Gibbs free energy of such a reaction is positive. Consequently, nucleotide polymerisation in water is a thermodynamically uphill reaction that is extremely inefficient to occur spontaneously under ambient conditions. However, if the entropic part (ΔS) of the Gibbs free energy change ($\Delta G = \Delta H - T\,\Delta S$) becomes very positive, the reaction can become exergonic ($\Delta G < 0$) and thus favourable. As the entropic part is positive when the activity of water is low[24], the thermodynamic barrier can be overcome by reducing water activity[29]. Against this background, we propose that our observed abiotic formation of RNA within aqueous particle suspensions can be explained by the rise of anomalous properties of water when getting temporarily confined between suspended particles: nanoscale confinements change, among others, the vapour pressure[30] and hydrogen-bond network dynamics[13] of water. This can reduce water activity[26, 30] as a function of gap size and the characteristics of the confining surfaces. We suggest that in

118

comparison with other ways to circumvent the thermodynamic barrier of such condensation reactions, the exergonic impact of nanofluid phenomena in aqueous particle suspensions on RNA polymerisation and stabilisation is of high relevance for prebiotic plausibility, as it does not require nonphysiological conditions such as temperatures well above 100 °C, alternative solvents, or wet/dry cycles.

Conclusion

Our results indicate that abiotic temporal nanoconfinements of water within aqueous particle suspensions serve as nanoscopic, flexible reaction vessels for prebiotic, nonenzymatic RNA formation. The findings can solve the water paradox in such a way that nanofluid effects in aqueous particle suspensions open up an abiotic route to biopolymerisation and polymer stabilisation under chemical and thermodynamic conditions that are also prevalent within the crowded intracellular environment of living cells. The fact that polymerase enzymes also form temporal nanoconfined water clusters inside their active site[31, 32] implies that the same physicochemical effects are tapped for nucleotide condensation in water both by biochemical pathways and our reported abiotic route. These aspects indicate that our model is consistent with evolutionary conservatism stretching back to the era of prebiotic chemical evolution and the origin of cellular life[33]. The consistency is further supported by the fact that water is not trapped by nanoconfinements within the polymerase core but can exchange with the surrounding intracellular fluid[32]—a situation that also exists in abiotic nanoconfinements of water emerging temporarily between approaching crystal particles in aqueous suspensions. Our experimental finding that under these conditions an amino acid catalyses the abiotic polymerisation of nucleotides supports first indications of the role of minerals for the origin of cooperation between amino acids and nucleotides[34] evolved to the interdependent synthesis of proteins and nucleic acids in living cells[35]. Abiotic RNA polymerisation under nanofluid conditions in aqueous particle suspensions does not depend on specific mineralogical and geological environments: now as then, in the prebiotic world, watery suspensions of micro- and nanoparticles are virtually ubiquitous[36]. They exist, for example, in the form of sediments with pore water[37], hydrothermal vent fluids containing precipitated inorganic[38, 39] and polyaromatic[40] particles, atmospheric aerosols with organic and inorganic particle burden[41, 42], or crowded, dispersed aggregates inside water-filled cracks in the crust of the earth[43, 44], and possibly of icy moons such as Enceladus[45].

Beyond the discussed importance of our findings for prebiotic chemistry and theories on the transition from geochemistry to biochemistry in the course of life's emergence, the results are also highly relevant for the development of sustainable chemistry approaches in applied sciences: the detected substantial efficiency increase of OSWD induced monolayer formation of widely used industrial organic semiconductors such as QAC (Fig. 4) or phthalocyanine[46, 47] (see Supplementary Fig. 4) via biomolecules with a prominent stacking capability such as AMP and arginine provides a systematic path to catalyse the deposition of water-insoluble organic semiconductors on 2D materials via nanofluid water. This insight is substantial for the development of green chemistry approaches to chemical surface engineering, band-gap engineering, and low-dimensional crystal engineering in materials science and nanotechnology.

Methods

Compounds. Adenosine-5′-monophosphate (AMP, Sigma, disodium salt, CAS-Nr. 61-19-8); Uridine-5′-monophosphate (UMP, Alfa Aesar, disodium salt, CAS-Nr. 58-97-9); Cytidine-5′-monophosphate (CMP, Alfa Aesar, disodium salt, CAS-Nr. 6757-06-8); Guanosine-5′-monophosphate (GMP, Alfa Aesar, disodium salt, CAS-

Nr. 85-32-5); L-Arginine (Alfa Aesar, CAS-Nr. 74-79-3); graphite (HOPG, purchased from NT-MDT, item no. GRBS/1.0); Quinacridone (average primary particle size: 70 nm, Clariant GmbH, CAS-Nr. 1047-16-1); Anthraquinone (purity 97%, Fluka, CAS-Nr. 84-65-1); Phthalocyanine (β-form, purity 98%, Sigma-Aldrich, CAS-Nr. 574-93-6); carbon nanopowder (<50 nm (TEM), purity ≥ 99%, Sigma-Aldrich, CAS-Nr. 7440-44-0); carbon (mesoporous, 0.25 cm³/g pore volume, Sigma-Aldrich, CAS-Nr. 1333-86-4); Iron (II, III) oxide (magnetite, 50–100 nm particle size, purity 97%, Sigma-Aldrich, CAS-Nr. 1317-61-9); Silicon dioxide (-325mesh, purity 99.5%, Sigma-Aldrich, CAS-Nr. 60676-86-0); Polyethylene (<400 micron, Alfa Aesar, CAS-Nr. 9002-88-4).

Suspension preparation. Three millilitre of aqueous suspension was made of each 0.1 g/ml inorganic substrate (e.g., graphite powder) and/or organic pigment with a total nucleoside monophosphate concentration of 50 mM. Samples were incubated overnight at 60 °C while mixed horizontally at 300 rpm, to avoid sedimentation of substrates and pigment. After incubation, samples were centrifuged at 8000 × g for 1 min at room temperature (RT). The supernatant was transferred to a new collection tube.

Precipitation. If not differently indicated, precipitation was carried out with 0.2 M NaCl and 3.5 volumes of EtOH. One sample was precipitated with 0.3 M NaOAc (pH 5.2) and 0.7 volumes of isopropanol to test the efficacy of a different precipitation method. After the addition of the appropriate amount of salt solution and alcohol, samples were mixed by inverting the tubes 5 times, and precipitation reactions were incubated 24 h at −20 °C. Afterwards the samples were subsequently centrifuged at 14,000 × g, for 1 h without cooling (room temperature between 20 and 25 °C). The supernatant was discarded, leaving ~20 µl of it inside the reaction tube, in addition to any formed gel pellet. Formed gel pellets were dried at 37 °C for 20 min and resuspended in an appropriate amount of nuclease-free water, as little as possible needed to dissolve the gel pellet. Depending on the volume of the gel pellet, more or less volume of water was added. Final RNA concentrations were then normalised to a uniform volume of 200 µl, using the total RNA amount measured and the final volume.

Fluorometric RNA quantification. Concentrations of microRNA suspensions were measured using a Qubit® 3 Fluorometer (Invitrogen™)[47] and the Qubit® microRNA Assay Kit (Invitrogen™) due to its high specificity and reliability: "The assay is highly selective for small RNA over rRNA or large mRNA (>1000 nt) (…), and tolerant of common contaminants such as salts, free nucleotides, solvents, detergents, or protein (…)."[48] This declaration was controlled by measuring a 50 mM aqueous AMP solution with the Qubit® 3 Fluorometer and was validated. Concentrations were calculated by the chosen microRNA or RNA program of the Qubit® 3 Fluorometer. Standard curves and samples were prepared following the manuals[49]. Concentrations were calculated and normalised regarding the respective volume of each sample.

Quantitative RT-qPCR analysis. For RT-qPCR, selected samples were reverse transcribed using the TaqMan™ Advanced miRNA cDNA Synthesis Kit (Thermo Fisher) following the manual. As a positive control, the synthetic miRNA hsa-miR-134-3p (5′-phosphorylated) (eurofins) with an oligonucleotide length of 23 nt was used. As a negative control nuclease-free water was used. For qPCR, the Master Mix reaction was composed of 10 µl QuantiTect SYBR® Green (Qiagen), 2 µl amplification primer mix from the TaqMan™ Advanced miRNA cDNA Synthesis Kit (Thermo Fisher), and 8 µl of diluted sample. qPCR, including a melting curve of the formed amplicons after the last cycle, was run on a LightCycler® 480 Instrument II with the following settings: 15 min 95 °C, 40x: 15 s 94 °C—30 s 60 °C—30 s 72 °C—Single Data Acquisition, 72 °C 2 min, Melting curve.

Capillary gel electrophoresis. For RNA gel electrophoresis the Agilent RNA 6000 Nano Kit was used and the gel setting was prepared following the manual. Samples were run on a 2100 Bioanalyzer Instrument with the 2100 Expert Software (Agilent). Samples were applied in triplicates. As a negative control a particle suspension based sample was used that resulted in a "too low" signal in the Qubit® concentration measurement, to identify possible background noises that might have been generated by residual nanoparticles leftover in the samples after precipitation, like those of inorganic substrates or organic pigments.

Scanning tunnelling microscopy. For scanning tunnelling microscopy (STM) investigations aqueous suspensions were prepared of each 2% w/w quinacridone pigment and a nucleotide monophosphate or amino acid final total concentration of 25 mM, if required. Suspensions were drop cast onto graphite substrates to induce OSWD and dried overnight. The samples were subsequently covered with dodecane to achieve a defined, stable environment between the STM tip and substrate. Each sample was prepared twice. From each replicate, 15 images of 200 nm × 200 nm size were generated from three different spots. Images were acquired with a self-built STM combined with an SPM 100 control system supplied by RHK Technology. The scan settings were: bias = 1 V, tunnel current = 300 pA, and line time = 50 ms. Further, the voltage pulses used to improve the scan quality

were applied within the range of 4.3 V to 10 V. All STM measurements were performed under ambient conditions.

Surface coverage determination. To determine coverage, meaning how much area of graphite is covered by supramolecular adsorbate structures (see Supplementary Fig. 1), black/white histograms were created. For this purpose, depicted adsorbate structures were masked out in the STM image (white) while setting the background (graphite without adsorbate structures) to black (see Supplementary Fig. 2). Black/white histogram values were calculated using "histogram" within the "analyse" menu of the software ImageJ. The mean values given in the histogram data box were then converted to percentages of the graphite area covered with adsorbate structures, whereby a histogram value of 0 means 0% of the graphite surface is covered with adsorbate and a histogram value of 255 means 100% of the graphite surface is covered. Note that AMP itself does not form monolayer on graphite due to its 3D-structure. For statistical analysis of the coverage results, a t-test with Welch's corrections was used since the samples show unequal distribution variance. The calculations were performed using Excel, giving the results of a two sided unequal variance t-test.

Computer simulations. All molecular mechanics calculations were performed with the Materials Studio package (Accelrys). The force field used was Dreiding[50], where partial charges of atoms within the molecule are calculated with the Gasteiger method[51]. Geometry optimisation calculations were calculated where convergence tolerance regarding energy was 1.0e−4 kcal/mol, force was 0.005 kcal/mol/Å and displacement was 5.0e−5 Å. The Smart algorithm was used which is a concatenation of steepest descent, Newton-Raphson and quasi-Newton methods, to obtain better behaviour for the different stages of downstream minimisation. Dynamic calculations were performed for an NVE ensemble with a temperature of 298 K, random values assigned for the initial velocities of the atoms and a time step of 0.1 fs for the integration algorithm.

A chain of 12 AMP molecules was constructed starting with building an AMP dimer. The dimer itself was built by duplicating an AMP and performing an 180° rotation related to the axis lying in the plane of the adenine molecule and passing through the centres of the hexagon and pentagon. Afterwards, the rotated AMP was translated normal to the plane of the adenine by a distance of 3.5 Å. This dimer was stacked 6 times in a row such that all planes of the adenine molecules were parallel each by a distance of 3.5 Å. This artificially constructed model was finally optimised related to geometry.

The entire system is modelled within a supercell containing two graphene layers, on top at some distance a chain of AMP molecules and finally two layers of a QAC crystal above the AMP chain. The entire system was filled with water molecules at different concentrations. The initial position of the AMP chain related to the graphene layers and the QAC crystal layers is stated below for the different calculations performed. The vertical dimension of the supercell has been chosen to be safe so that an interaction of the graphene layers and the QAC crystal layers can be neglected (gap is 43 Å). The rectangular in-plane dimensions of the supercell have been determined to minimise the distortion of the periodic structure of the QAC crystal layers. The deviation of the unit cell vectors of the QAC layers is almost zero in one direction (0.1%) but quite large in the other direction (5.6%). However, because the outer layer of the QAC crystal is always kept fixed, the adjacent free movable QAC layer was observed to be stable throughout all simulations. This observation was the reason why this significant deviation was accepted for all calculations. The graphene layers are not distorted with regard to the optimal unit cell dimensions. The dimensions of the supercell are: plane x, y: 80.956 Å, 56.58 Å, and z: 103.4 Å.

Data availability

Supplementary Information contains: STM images and simulation results on the QAC adsorbate structure; additional dynamic force field calculation results on AMP in nanoconfined water; phthalocyanine related STM results and box plots on AMP catalysed OSWD. Videos of a simulated AMP stack within a confinement filled with water (Supplementary Movie 1, mp4) and with water of a reduced density to ~60% (Supplementary Movie 2, mp4). The datasets generated during and/or analysed during the current study are available from the corresponding author on reasonable request.

References

1. Benner, S. A. Paradoxes in the origin of life. *Orig. Life Evol. Biosph.* **44**, 339–343 (2014).
2. Benner, S. A., Kim, H. J. & Carrigan, M. A. Asphalt, water, and the prebiotic synthesis of ribose, ribonucleosides, and RNA. *Acc. Chem. Res.* **45**, 2025–2034 (2012).
3. Lang, C., Lago, J. & Pasek, M. A. Phosphorylation on the early earth: the role of phosphorous in biochemistry and its bioavailability. In *Handbook of Astrobiology* (ed. Kolb, V. M.) 361–369 (CRC Press, 2019).
4. Yadav, M., Kumar, R. & Krishnamurthy, R. Chemistry of abiotic nucleotide synthesis. *Chem. Rev.* **120**, 4766–4805 (2020).
5. Marshall, M. The water paradox and the origins of life. *Nature* **588**, 210–213 (2020).
6. Gibard, C. et al. Geochemical sources and availability of amidophosphates on the early Earth. *Angew. Chem. Int. Ed.* **131**, 8235–8239 (2019).
7. Burton, Z. F. *Evolution Since Coding: Cradles, Halos, Barrels, and Wings* (Academic Press, 2018).
8. Brovchenko, I. & Oleinikova, A. *Interfacial and Confined Water* (Elsevier, 2008).
9. Eijkel, J. C. & Van den Berg, A. Nanofluidics: what is it and what can we expect from it. *Microfluid. Nanofluid.* **1**, 249–267 (2005).
10. Bocquet, L. & Charlaix, E. Nanofluidics, from bulk to interfaces. *Chem. Soc. Rev.* **39**, 1073–1095 (2010).
11. Wu, K. et al. Wettability effect on nanoconfined water flow. *Proc. Natl Acad. Sci. USA* **114**, 3358–3363 (2017).
12. Hart-Cooper, W. M. et al. Protein-like proton exchange in a synthetic host cavity. *Proc. Natl Acad. Sci.* **112**, 15303–15307 (2015).
13. Knight, A. W., Kalugin, N. G., Coker, E. & Ilgen, A. G. Water properties under nano-scale confinement. *Sci. Rep.* **9**, 8246 (2019).
14. Reiter, G. F. et al. Evidence for an anomalous quantum state of protons in nanoconfined water. *Phys. Rev. B* **85**, 045403 (2012).
15. Kruse, F. M., Teichert, J. S. & Trapp, O. Prebiotic nucleoside synthesis: the selectivity of simplicity. *Chem. Eur. J.* **26**, 14776–14790 (2020).
16. Cafferty, B. J. & Hud, N. V. Abiotic synthesis of RNA in water: a common goal of prebiotic chemistry and bottom-up synthetic biology. *Curr. Opin. Chem. Biol.* **22**, 146–157 (2014).
17. Furukawa, Y. RNA synthesis before the origin of life. In *Astrobiology: From the Origins of Life to the Search for Extraterrestrial Intelligence* (eds Yamagishi, A., Kakegawa, T. & Usui, T.) 63–74 (Springer, 2019).
18. Jauker, M., Griesser, H. & Richert, C. Spontaneous formation of RNA strands, peptidyl RNA, and cofactors. *Angew. Chem. Int. Ed.* **54**, 14564–14569 (2015).
19. Eberle, A., Markert, T. & Trixler, F. Revealing the physicochemical basis of organic solid–solid wetting deposition: casimir-like forces, hydrophobic collapse, and the role of the zeta potential. *J. Am. Chem. Soc.* **140**, 1327–1336 (2018).
20. Yokosawa, T. et al. A step into the RNA world: conditional analysis of hydrogel formation of adenosine 5'-monophosphate induced by cyanuric acid. *Biosystems* **162**, 53–58 (2017).
21. Norberg, J. & Nilsson, L. Stacking free energy profiles for all 16 natural ribodinucleoside monophosphates in aqueous solution. *J. Am. Chem. Soc.* **117**, 10832–10840 (1995).
22. Vernon, R. M. et al. Pi-Pi contacts are an overlooked protein feature relevant to phase separation. *elife* **7**, e31486 (2018).
23. Tribolet, R. & Sigel, H. Self-association of adenosine 5'-monophosphate (5'-AMP) as a function of pH and in comparison with adenosine, 2'-AMP and 3'-AMP. *Biophys. Chem.* **27**, 119–130 (1987).
24. Georgelin, T., Jaber, M., Bazzi, H. & Lambert, J. F. Formation of activated biomolecules by condensation on mineral surfaces—a comparison of peptide bond formation and phosphate condensation. *Orig. Life Evol. Biosph.* **43**, 429–443 (2013).
25. Kaddour, H. et al. Nonenzymatic RNA oligomerization at the mineral–water interface: an insight into the adsorption–polymerization relationship. *J. Phys. Chem. C.* **122**, 29386–29397 (2018).
26. Dass, A. V. et al. Potential role of inorganic confined environments in prebiotic phosphorylation. *Life* **8**, 7 (2018).
27. Podgornik, R. & Dobnikar, J. Casimir and pseudo-Casimir interactions in confined polyelectrolytes. *J. Chem. Phys.* **115**, 1951–1959 (2001).
28. Milshteyn, D., Cooper, G. & Deamer, D. Chemiosmotic energy for primitive cellular life: proton gradients are generated across lipid membranes by redox reactions coupled to meteoritic quinones. *Sci. Rep.* **9**, 12447 (2019).
29. Ross, D. S. & Deamer, D. Dry/wet cycling and the thermodynamics and kinetics of prebiotic polymer synthesis. *Life* **6**, 28 (2016).
30. Jonchhe, S. et al. Decreased water activity in nanoconfinement contributes to the folding of G-quadruplex and i-motif structures. *Proc. Natl Acad. Sci. USA* **115**, 9539–9544 (2018).
31. Tropp, B. E. *Molecular Biology: Genes to Proteins* (Jones and Bartlett, 2008).
32. Qin, Y. et al. Direct probing of solvent accessibility and mobility at the binding interface of polymerase (Dpo4)-DNA complex. *J. Phys. Chem. A* **117**, 13926–13934 (2013).
33. Saha, R., Pohorille, A. & Chen, I. A. Molecular crowding and early evolution. *Orig. Life Evol. Biosph.* **44**, 319–324 (2014).
34. Namani, T. et al. Amino acid specific nonenzymatic montmorillonite-promoted RNA polymerization. *ChemSystemsChem* **3**, e2000060 (2021).
35. Fry, I. The origin of life as an evolutionary process: representative case studies. in *Handbook of Astrobiology* (ed. Kolb, V. M.) 437 (CRC Press, 2019).

36. Alekseyev, V. A. Nanoparticles and nanofluids in water–rock interactions. *Geochem. Int.* **57**, 357–368 (2019).

37. Hammond, D. Pore water chemistry. In *Marine Chemistry & Geochemistry: A Derivative of Encyclopedia of Ocean Sciences* (eds Steele, J. H., Thorpe, S. A. & Turekian, K. K.) 2263–2271 (Academic Press, 2001).

38. Gartman, A. et al. The role of nanoparticles in mediating element deposition and transport at hydrothermal vents. *Geochim. Cosmochim. Acta* **261**, 113–131 (2019).

39. Russell, M. J. The "Water Problem"(sic), the illusory pond and life's submarine emergence—a review. *Life* **11**, 429 (2021).

40. Konn, C. et al. Organic, gas, and element geochemistry of hydrothermal fluids of the newly discovered extensive hydrothermal area in the Wallis and Futuna region (SW Pacific). *Geofluids* **2018**, 692839 (2018).

41. Buseck, P. R. & Pósfai, M. Airborne minerals and related aerosol particles: effects on climate and the environment. *Proc. Natl Acad. Sci. USA* **96**, 3372–3379 (1999).

42. Trainer, M. G. Atmospheric prebiotic chemistry and organic hazes. *Curr. Org. Chem.* **17**, 1710–1723 (2013).

43. Grevemeyer, I., Ranero, C. R. & Ivandic, M. Structure of oceanic crust and serpentinization at subduction trenches. *Geosphere* **14**, 395–418 (2018).

44. do Nascimento Vieira, A., Kleinermanns, K., Martin, W. F. & Preiner, M. The ambivalent role of water at the origins of life. *FEBS Lett.* **594**, 2717–2733 (2020).

45. Postberg, F. et al. Macromolecular organic compounds from the depths of Enceladus. *Nature* **558**, 564–568 (2018).

46. Zhang, Y., Cai, X., Bian, Y. & Jiang, J. Organic semiconductors of phthalocyanine compounds for field effect transistors (FETs). In *Functional Phthalocyanine Molecular Materials. Structure and Bonding* (ed. Jiang, J.) 275–321 (Springer, 2010).

47. Determine microRNA concentration in solution: fluorescence-based small RNA quantitation for both conventional and high-throughput assays. *BioProbes® 70*, 32–36 (ThermoFisher Scientific, 2014).

48. Garcia-Elias, A. et al. Defining quantification methods and optimizing protocols for microarray hybridization of circulating microRNAs. *Sci. Rep.* **7**, 1–14 (2017).

49. Thermo Fisher Scientific Inc., "Qubit® 3.0 Fluorometer". Publication MAN0010866 http://tools.thermofisher.com/content/sfs/manuals/qubit_3_fluorometer_man.pdf (2014).

50. Mayo, S. L., Olafson, B. D. & Goddard, W. A. DREIDING: a generic force field for molecular simulations. *J. Phys. Chem.* **94**, 8897–8909 (1990).

51. Gasteiger, J. & Marsili, M. Iterative partial equalization of orbital electronegativity—a rapid access to atomic charges. *Tetrahedron* **36**, 3219–3228 (1980).

Author contributions

The manuscript was written through contributions of all authors. All authors have given approval to the final version of the manuscript. A.G.H. designed and performed experiments and data analysis, T.M. designed and performed computer simulations, F.T. conceived the project and directed the research.

Competing interests

The authors declare no competing interests.

Additional information

Supplementary information The online version contains supplementary material available at https://doi.org/10.1038/s42004-023-00872-y.

Correspondence and requests for materials should be addressed to Frank Trixler.

Peer review information *Communications Chemistry* thanks the anonymous reviewers for their contribution to the peer review of this work. Peer reviewer reports are available.

Reprints and permission information is available at http://www.nature.com/reprints

Publisher's note Springer Nature remains neutral with regard to jurisdictional claims in published maps and institutional affiliations.

Acknowledgement

List of Publications

Journal Publications

Temporal nanofluid environments induce prebiotic condensation in water; **Herrera, A.G. de;** Markert T.; Trixler F.; *nature - communications chemistry 6,* 69 (2023); DOI: 10.1038/s42004-023-00872-y

Doping graphene under ambient conditions using organic solid/solid wetting deposition in water - A Low-cost and environment friendly method (working title); **Herrera, A.G. de**; Markert T; Hille L; Weitz R. T. ; Trixler F.; in preparation

Abiotic synthesis of complex RNA within silica based nanogeochemical model systems (working title); **Herrera, A.G. de**; Yalu Zheng R.; Trigo-Rodriguez, J.; Brandmiller F.; Josef F.; Trixler F.; in preparation

Doping graphene via organic solid-solid wetting deposition; Eberle, A.; **Greiner, A.**; Ivleva, N. P.; Arumugam, B.; Niessner, R.; Trixler, F. *Carbon* 2017**,** *125*, 84–92, DOI:10.1016/j.carbon.2017.09.043.

Talks and Conferences

Prebiotic Reaction Vessels - RNA Formation in nanoconfined water; **Andrea Greiner** and Frank Trixler; 3-6 Sept. 2019; Orleans, France

Projektvorstellung: Das gläserne Forscherlabor im Deutschen Museum; **Andrea Greiner**; Forum Wissenschaftskommunikation; 7-9 Nov. 2018; Bonn, Germany

Adenosine Monophosphate Catalyzes Molecular Self-Assembly: Temporal Nanoconfined Water as a biochemical reaction vessel; **Andrea Greiner**; Early Earth and ExoEarths: origin and evolution of life; 3-7 April 2017; Warsaw, Poland

Research and Science Communication Strategies of the Open Research Lab; **Andrea Greiner**; Surface Acoustic Waves Train; Oct. 2016; Potsdam, Germany

Poster Presented at Conferences

Organic solid-solid wetting: a green chemistry approach to surface engineering of low-dimensional materials; **Andrea Greiner de Herrera** and Frank Trixler; 22nd International Conference on the Science and Applications of Nanotubes and Low-Dimensional Materials; 19-24 June 2022; Suwon, Republic of Korea (online)

Raster-Tunnel-Mikroskopie – selbst ausprobieren und mit der eigenen Messung Atome sichtbar machen; **Andrea Greiner**; NIM NanoDay; 10 Sept. 2017; Munich, Germany

Adenosine Monophosphate in Temporal Nanoconfined Water Catalyzes Molecular Self-Assembly; **Andrea Greiner** and Frank Trixler, Young Ideas in Nanoscience, 2nd May 2017; Munich, Germany

Nucleotide Catalysis of Molecular Self-Assembly in Mineral Nanoconfinements of Water; **Andrea Greiner** and Frank Trixler; Early Earth and ExoEarths: origin and evolution of life; 3-7 April 2017; Warsaw, Poland

Adenosine Monophosphate Catalyzes Organic Nanostructure Self-Assembly; **Andrea Greiner;** <interact> 2016, 9th Munich Life Science Symposium for Young Scientists; 3-4 Nov. 2016; Munich, Germany

Biomedical Journal Publications

Identification of Stably Expressed lncRNAs as Valid Endogenous Controls for Profiling of Human Glioma; Theo F J Kraus, **Andrea Greiner**, Virginie Guibourt, Kristina Lisec, Hans A Kretzschmar; J Cancer 2015 Jan 1;6(2):111-9. doi: 10.7150/jca.10867

Genetic Characterization of Ten-Eleven-Translocation Methylcytosine Dioxygenase Alterations in Human Glioma; Kraus TF, **Greiner A**, Steinmaurer M, Dietinger V, Guibourt V, Kretzschmar HA. J Cancer. 2015 Jul 15;6(9):832-42. doi: 10.7150/jca.12010

Long non-coding RNA normalisers in human brain tissue; Kraus TF, **Greiner A**, Guibourt V, Kretzschmar HA. J Neural Transm (Vienna). 2015 Jul;122(7):1045-54. doi: 10.1007/s00702-014-1352-6

Loss of 5-hydroxymethylcytosine and intratumoral heterogeneity as an epigenomic hallmark of glioblastoma; Kraus TF, Kolck G, **Greiner A**, Schierl K, Guibourt V, Kretzschmar HA. Tumour Biol. 2015 Nov;36(11):8439-46. doi: 10.1007/s13277-015-3606-9